Experimental investigation of the dynamics in a strongly interacting Fermi gas: Collective modes and rotational properties

Dissertation
zur Erlangung des akademischen Grades
Doktor der Naturwissenschaften

eingereicht an der
Fakultät für Mathematik, Informatik und Physik
der Universität Innsbruck

von

Stefan Riedl

Betreuer der Dissertation:
Univ.-Prof. Dr. Rudolf Grimm,
Institut für Experimentalphysik

Innsbruck, Mai 2009

Abstract

This thesis explores the dynamic behavior of an ultracold strongly interacting Fermi gas. In particular measurements on collective excitation modes and the gas under rotation are performed. The strongly interacting gas is realized using an optically trapped Fermi gas of ^{6}Li atoms, where the interactions can be tuned using a broad Feshbach resonance. This tunability also allows us to control the coupling between two atoms and to explore the crossover from a molecular Bose-Einstein condensate (BEC) to a Bardeen-Cooper-Schrieffer (BCS) superfluid.

Performing precision measurements of the frequency of the radial compression mode, we test theoretical predictions for the equation of state in the BEC-BCS crossover. The experiment confirms recent quantum Monte-Carlo results and rule out simple mean-field BCS theory. Furthermore the results show the long-sought beyond-mean-field effects in the strongly interacting BEC regime.

We investigate the radial quadrupole mode to probe the dynamic behavior in the BEC-BCS crossover, without being influenced by changes in the equation of state. We find that in the unitarity limit and on the BEC side of the crossover, the observed oscillation frequencies of the mode agree with standard hydrodynamic theory. However, on the BCS side of the crossover, a striking down shift of the frequency is observed as a precursor to an abrupt transition to collisionless behavior. The interpretation of this behavior is still under debate.

A scissors mode excitation in an elliptical trap is used to characterize the temperature dependence of the dynamics of the strongly interacting gas in terms of hydrodynamic or near-collisionless behavior. We obtain a crossover phase diagram for the dynamic behavior, showing a large region where a non-superfluid strongly interacting gas shows hydrodynamic behavior. In addition we find a novel temperature-dependent damping peak, suggesting a relation to the superfluid phase transition, in a narrow interaction regime on the BCS side of the crossover.

To get a deeper insight into the dynamic behavior of the strongly interacting Fermi gas above the critical temperature, we perform detailed measurements of three different collective modes in the unitarity limit. The results are compared to theoretical calculations that take into account Pauli blocking and pair correlations in the normal state above the critical temperature for superfluidity. We

show that these two effects nearly compensate each other and the behavior of the gas is close to that of a classical gas.

As a first experiment on rotating strongly interacting Fermi gas we investigate the lifetime of the angular momentum. To determine the angular momentum we measure the precession of the radial quadrupole mode. We find that in the vicinity of the Feshbach resonance, the deeply hydrodynamic behavior in the normal phase leads to a very long lifetime of the angular momentum. Furthermore, we examine the dependence of the decay rate of the angular momentum on the ellipticity of the trapping potential and the interaction strength.

With the knowledge we gained from the previous experiment, we were able to study the moment of inertia of the gas. This allowed us to show superfluidity and to reveal the superfluid critical temperature for the strongly interacting Fermi gas, as the moment of inertia strongly depends on the superfluid fraction in the gas.

Zusammenfassung

Im Rahmen dieser Doktorarbeit wird das dynamische Verhalten eines stark wechselwirkenden Fermigases untersucht. Im speziellen werden Messungen von kollektiven Anregungen durchgeführt und das Verhalten des rotierenden Gases erforscht. Das Fermigas besteht aus optisch gefangenen ^{6}Li Atomen, die es erlauben die Wechselwirkung mit Hilfe einer breiten Feshbach-Resonanz zu kontrollieren. Des weiteren ist es dadurch möglich die Kopplung zwischen den Atomen zu beeinflussen und den Übergang von einem molekularen Bose-Einstein Kondensat (BEC) zu einem Bardeen-Cooper-Schrieffer (BCS) Superfluid zu untersuchen.

Mit Hilfe von Präzisionsmessungen der Frequenz der radialen Kompressionsmode testen wir theoretische Vorhersagen für die Zustandsgleichung im BEC-BCS Übergangsbereich. Unsere experimentellen Daten bestätigen ein aktuelle Quanten Monte-Carlo Vorhersage und schließen ein einfaches "mean-field" BCS Model aus. Weiters zeigen unsere experimentellen Ergebnisse im stark wechselwirkenden BEC Regime bereits vor langer Zeit vorhergesagte Effekte die über die "mean-field" Theorie hinausgehen.

Im weiteren untersuchen wir die radiale Quadrupolmode um das dynamisch Verhalten des Gases im BEC-BCS Übergangsbereich zu erforschen, ohne von der sich ändernden Zustandsgleichung beeinflusst zu werden. Unsere Ergebnisse zeigen, dass im Unitaritäts-Limit und auf der BEC Seite des Übergangsbereichs die beobachtete Oszillationsfrequenz der Mode mit den Vorhersagen der üblichen hydrodynamischen Theorie übereinstimmt. Auf der BCS Seite des Übergangsbereichs beobachten wir jedoch eine unerwartete deutlich Verringerung der Frequenz, gefolgt von einem Übergang zu stossfreiem Verhalten. Die genau Ursache für dieses Verhalten ist noch immer nicht geklärt.

Die Temperaturabhängigkeit des dynamischen Verhalten wird mit Hilfe der sogenannten Scissorsmode in einer elliptischen Falle untersucht. Durch unsere Messungen können wir ein Phasendiagramm, dass das dynamische Verhalten des Gases zeigt, erstellen. In diesem Phasendiagramm ist ein großer Bereich sichtbar in dem das stark wechselwirkende Gas hydrodynamisches Verhalten zeigt, obwohl es nicht superfluid ist. Zusätzlich dazu zeigen unsere Messungen einen neuartigen Peak in der Temperaturabhängigkeit der Dämpfung der Mode

auf der BCS Seite des Übergangsbereichs. Dieses Verhalten deutet auf einen Zusammenhang mit dem superfluiden Phasenübergang hin.

Um einen tieferen Einblick in das dynamische Verhalten des stark wechselwirkenden Gases oberhalb der kritischen Temperatur zu bekommen, untersuchen wir drei unterschiedliche Moden im Unitaritäts-Limit. Die erzielten Ergebnisse werden mit theoretischen Berechnungen verglichen die sowohl das Paulsche Ausschließungsprinzip als auch Paar Korrelationen für ein Gas oberhalb der kritischen Temperatur beinhalten. Unsere Ergebnisse zeigen, dass sich die beiden eben erwähnten Effekte gegenseitig kompensieren und somit das Verhalten des Gases vergleichbar dem eines klassischen Gases ist.

Als erstes Experiment zu rotierenden stark wechselwirkenden fermionischen Gasen untersuchen wir die Lebensdauer des Drehimpulses. Um den Drehimpuls zu bestimmen messen wir die Präzession der Quadrupolmode. Wir zeigen, dass in der unmittelbaren Nähe der Feshbach-Resonanz das tief hydrodynamische Verhalten in der normalen Phase zu einer besonders langen Lebensdauer des Drehmoments führt. Außerdem untersuchen wir die Abhängigkeit der Zerfallsrate des Drehimpulses von der Elliptizität des Fallenpotentials und der Wechselwirkungsstärke.

Mit dem Wissen über rotierende Gase aus dem vorhergehenden Experiment, war es möglich das Trägheitsmoment des Gases zu untersuchen. Messungen des Trägheitsmoments ermöglichten es uns Superfluidität nachzuweisen und die kritische Temperatur für Superfluidität im stark wechselwirkenden Gas zu bestimmen, da das Trägheitsmoment vom superfluiden Anteil im Gas abhängt.

CONTENTS

CHAPTER 1

Introduction

The experimental results presented in this thesis are part of a class of experiments which study the behavior of atomic strongly interacting Fermi gases. Systems of strongly interacting fermions can be found in many different areas of physics, like in condensed matter physics (high-temperature superconductors), in high-energy matter (quark-gluon plasma), and in astrophysics (neutron stars). In all these different areas, strongly interacting fermions pose great challenges for many-body quantum theories. The atomic ultracold Fermi gas, which is under investigation here, is a unique model systems to investigate strongly interacting fermions, because of their tunable interactions and controllable confinement. Thereby we can systematically explore this system and also test theoretical models which even have their origin in other areas of physics. In this thesis, we focus on the dynamic behavior of an ultracold strongly interacting Fermi gas consisting of ^{6}Li atoms to explore the rich physics of such a system.

The dynamic behavior of an ultracold atomic Fermi gas is an important source of information on the physical nature of the system. In an ultracold gas not only the scattering properties of single atoms influence the dynamic behavior but also the particle statistics. The dominant scattering process for an ultracold gas is s-wave scattering. But for a Fermi gas consisting of only a single atomic spin state the Pauli exclusion principle prohibits s-wave scattering. Therefore such a gas shows collisionless behavior, which means that the atoms freely move in the trap without scattering. A different dynamic behavior of the gas arises for bosonic atoms as s-wave scattering is allowed in this case. In a Bose gas both collisionless and hydrodynamic behavior can occur, depending on the scattering rate for the atoms. In contrast to collisionless behavior, hydrodynamic behavior means that the gas behaves like a fluid. This happens when the scattering rate is very high but also when the gas becomes superfluid. For a Bose gas a Bose-Einstein condensate (BEC) can form at sufficiently low temperature, which shows superfluid hydrodynamic behavior.

In our experiments, we use an equal mixture of two different spin states, which leads to a reacher dynamic behavior of the gas. It allows for s-wave

scattering between different spin states and furthermore to continuously tune the scattering length using a Feshbach resonance. Note that also in a mixture of two spin states the Pauli exclusion principal plays an important role. Although s-wave collisions are allowed between different atomic states the available phase space for scattering is reduced if the Fermi gas is degenerate. This reduces the scattering rate and eventually leads again to collisionless behavior of the gas.

The formation of pairs can lead to completely different dynamic behavior of the gas. One way of pairing the atoms is the formation of molecules. Here we consider a very weakly bound molecular state where the binding energy can be tuned using an external magnetic field; see Fig. 1.1. Close to a Feshbach resonance, the scattering length directly depends on the binding energy of this molecular state [Chi08]. Furthermore the center of the Feshbach resonance is at the magnetic field where the molecular state reaches the energy continuum of free atoms. Beyond the point where the molecular state reached the atom continuum, pairing is still possible via a mechanism described by Cooper [Coo56]; these pairs are therefore called Cooper pairs. In contrast to molecules, here pairing is a many-body effect. This means that pair formation is only possible in the presence of the Fermi gas itself. Note that close to the Feshbach resonance, where the gas cannot be considered as dilute, the nature of the pairs is more complex than simple molecules or Cooper pairs.

When decreasing the temperature one always ends up with superfluid behavior in the system. For a gas consisting of bosonic molecules a molecular BEC forms [Joc03a, Gre03, Zwi03]. For the case of many-body pairing the gas becomes superfluid at low temperature, which is called a Bardeen-Cooper-Schrieffer (BCS) superfluid [Bar57a, Bar57b]. Changing the magnetic field these to regimes are smoothly connected. The intermediate region between the BEC and the BCS regime is called the BEC-BCS crossover region [Eag69, Leg80, Noz85, Eng97]. In this region the scattering length exceeds the interparticle spacing and therefore the gas cannot be considered as dilute anymore. This region is thus called a strongly interacting Fermi gas.

Experiments in strongly interacting Fermi gases of atoms

Starting 2002 [O'H02], there was tremendous progress in experiments which investigate atomic strongly interacting Fermi gases[1]. The first experiments on strongly interacting Fermi gases focused on the realization of pair condensates both in the molecular regime [Joc03a, Gre03, Zwi03], which is the starting point for many of the experiments, and on the BCS side of the Feshbach resonance [Reg04, Zwi04, Zwi05b]. Measurements of the cloud size [Bar04b] and the expansion of the cloud [Bou04] showed that there is a smooth crossover from the BEC to the BCS regime. Using rf-spectroscopy several experiments were performed to study the pairing gap [Chi04, Shi07, Sch08a], the size of the pairs [Sch08b], and single-particle excitations [Ste08]. Pairing throughout the crossover was further

[1] Reviews on strongly interacting Fermi gases, including most of the experiments mentioned below, and a detailed theory description of the BEC-BCS crossover regime can be found in Refs. [Ing08, Gio08].

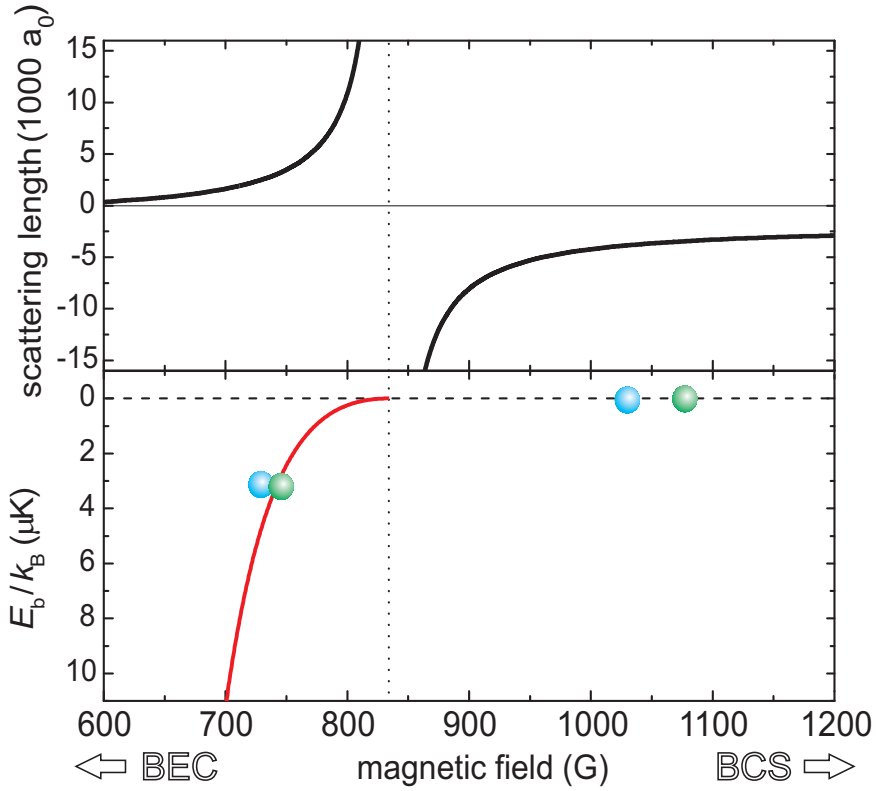

Fig. 1.1: The upper panel shows the s-wave scattering length between ^{6}Li atoms in the lowest two energy states for magnetic fields close to the Feshbach resonance at 834 G [Bar05b]. The resonant behavior of the scattering length comes along with a weakly bound molecular state which connects to the free atom continuum at the position of the Feshbach resonance. The lower panel shows the binding energy divided by the Boltzmann constant E_b/k_B of this molecular state. The fact that the molecular state is connected to the free atom continuum allows to adiabatically convert the fermionic atoms into bosonic molecules. Furthermore the Feshbach resonance smoothly connects the molecular BEC regime with the BCS regime.

studied using optical molecular spectroscopy [Par05] and the excitation spectrum was also investigated using a magnetic field modulation technique [Gre05]. Thermodynamic properties like the heat capacity [Kin05b] and the entropy [Luo07] were investigated. The momentum distribution of the gas in the crossover regime was studied using expansion measurements both in the low temperature limit [Reg05] and as a function of the temperature [Che06]. Expansion measurements were further used to determine the potential energy of the gas [Ste06]. Recent experiments using Bragg spectroscopy probe the dynamic and static structure factor [Vee08] and could determine the critical temperature using fast magnetic field ramps [Ina08]. Furthermore experiments on spin polarized strongly interacting Fermi gases attracted lots of attention as they showed new quantum phases [Par06a, Zwi06b, Zwi06a, Par06b, Shi06, Sch07a, Shi08b, Shi08a].

Recently experiments on Fermi gases consisting of a mixture of three different states investigated the collisional stability in the strongly interacting regime [Ott08, Huc09].

The dynamic behavior of the strongly interacting gas was first investigated looking at the expansion of the gas [O'H02, Bou03], which clearly showed hydrodynamic behavior. Soon after experiments on collective excitation modes have been performed as they can provide further insight into the dynamic behavior of degenerate quantum gases. Collective modes have been studied very early in atomic BEC research, both in experiments [Jin96, Mew96] and in theory [Str96a]. Measurements on collective oscillations have proven powerful tools for the investigation of various phenomena in atomic BECs [Jin97, SK98, Ono00, Mar00, Che02]. In the case of fermions, collective modes were first studied for weakly interacting gases [Gen01]. Building on this rich experience, collective modes attracted immediate attention to study strongly interacting Fermi gases [Kin04a, Bar04a, Kin04b, Kin05a]. These experiments already showed interesting hydrodynamic behavior and smooth or sudden transitions to collisionless dynamics, which are still not fully understood.

Beside measurements on collective modes the dynamic behavior of the strongly interacting gas was studied by measuring the sound velocity [Jos07] and investigating irrotational flow during expansion [Cla07]. Last but not least, superfluidity of the crossover gas was proven by the formation of a vortex lattice [Zwi05a]. In subsequent experiments the behavior of the superfluid under expansion [Sch07b] and critical velocity for superfluid flow was explored [Mil07].

Dynamics of the strongly interacting gas

In the following we will briefly discuss the special dynamic properties of a strongly interacting gas, including superfluidity, and the differences compared to dilute systems. Finally we will introduce the experiments performed in this thesis.

The strongly interacting Fermi gas has special properties concerning the dynamic behavior of the gas. When the interactions are strong the hydrodynamic behavior is not only restricted to the superfluid phase but also extends into the normal phase up to temperatures close to the Fermi temperature[2] [Cla07, Wri07, Rie08]. This is in contrast to dilute, ultracold atomic gases where hydrodynamic behavior is only reached below the superfluid critical temperature. The hydrodynamic behavior of the normal phase strongly depends on Pauli blocking and pairing which themselves depend on temperature and scattering length. At temperatures above the Fermi temperature also a gas in the strongly interacting region shows collisionless behavior as the scattering cross section decreases with increasing temperature [Chi08].

In a strongly interacting Fermi gas the center of the Feshbach resonance is a particularly interesting configuration. Here the scattering length, which is the only microscopic parameter that influences the gas, takes an infinite value.

[2]The Fermi temperature is defined as $T_F = E_F/k$, where E_F is the Fermi energy and k is the Boltzmann constant.

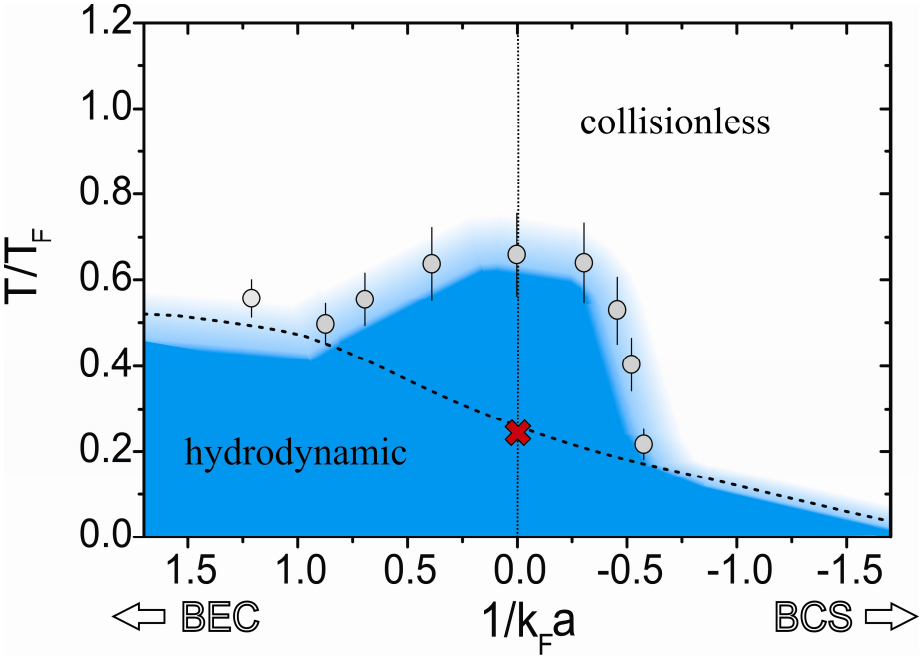

Fig. 1.2: Phase diagram for the dynamic behavior in a strongly interacting Fermi gas. The interaction parameter $1/k_F a$ is plotted on the horizontal axis and on the vertical axis the normalized temperature T/T_F is plotted. The parameter a is the s-wave scattering length. The blue color indicates where the gas shows hydrodynamic behavior. The transition from hydrodynamic to collisionless behavior as a function of the temperature is in general very smooth when the gas is strongly interacting. The dashed line shows the expected behavior for the superfluid critical temperature. When the interaction strength is very large, $|1/k_F a| < 0.5$, hydrodynamic behavior shows up clearly above the critical temperature. This is in contrast to the dilute BEC and BCS regimes, where hydrodynamic behavior only shows up together with superfluidity. The gray points with the errorbars are experimental data from measurements of the temperature dependent behavior of the scissors mode, see Chapter 4. They mark the transition from hydrodynamic to collisionless behavior. The red cross is the critical temperature obtained from measurements of the moment of inertia, see Chapter 7.

Therefore the scattering length is no longer a relevant quantity to describe the system and the behavior of such systems becomes totally independent of the microscopic details of the interparticle interactions. Consequently, k_F^{-1} and E_F alone define the relevant scales for length and energy[3], and the Fermi gas acquires universal properties. As a consequence the equation of state has the same density dependence as the ideal Fermi gas, apart from a dimensionless factor.

The strong interactions of the gas lead to distinct differences compared to dilute systems and in general complicate theoretical studies [Gio08]. As mentioned

[3]The parameter k_F is the Fermi wave number given by $E_F = \hbar^2 k_F^2/2M$, where M is the mass of the atom

above one difference is the dynamic behavior of the normal phase, which shows collisionless behavior in the BEC and BCS regime but hydrodynamic behavior in the crossover region. Furthermore, different to the dilute BEC regime, in the crossover region there is no bimodal density distribution for temperatures below the superfluid phase transition. Therefore the consequences of superfluidity cannot be seen from a major change in the appearance of the gas[4]. An important difference to the BCS regime is the formation of pairs already for temperatures above the phase transition. One often refers to the temperature range of these preformed pairs as the pseudogap regime. The differences mentioned above makes it in general more challenging to actually determine when the superfluid phase is reached.

The superfluid phase is of special interest in the crossover region as the strongly interacting gas is a new type of fermionic superfluid. It differs from ^{3}He, conventional and even High-T_c superconductors in its high critical temperature T_c when compared to T_F [Ing08]. To reveal superfluidity from its dynamic behavior one has to take care that in a strongly interacting Fermi gas both the superfluid but also the normal phase, which also has very low viscosity, show almost perfect hydrodynamic behavior. Therefore signatures that are unique to superfluids need to be addressed in an experiment. These are for example, frictionless flow, second sound, and the Josephson effect. Furthermore the behavior of a rotating gas can reveal superfluidity as rotational properties of a degenerate gas are quite different in the superfluid and normal phase. While the ground state of a superfluid gas with angular momentum contains quantized vortices[5], the normal gas rotates like a rigid body. In fact it was the formation of a vortex lattice provided first evidence for the superfluidity of a gas in the BEC-BCS crossover regime [Zwi05a]. Another striking consequence of superfluidity is the reduction of the moment of inertia with respect to its rigid-body value. The reduction (quenching) of the moment of inertia is again based on the fact that a superfluid cannot rotate like a rigid body. As a result, the apparent moment of inertia is smaller than that of a normal, rigid rotating system because the superfluid part does not rotate although the normal part is rotating. The observation of a quenched moment of inertia is part of the work presented in this thesis.

The studies of a strongly interacting Fermi gas performed in this thesis investigate the behavior of collective modes and the behavior of the gas under rotation. In this thesis systematic investigations of the radial compression mode, the radial quadrupole mode and the scissors mode are performed. Measurements on the compression mode serve as a sensitive probe for the equation of state of the gas in the low temperature limit throughout the BEC-BCS crossover regime. In contrast to the compression mode, the frequency of the radial quadrupole mode allows one to test the hydrodynamic behavior without being influenced by

[4] One exception is the strongly interacting gas with imbalanced spin population, where the phase transition leads to a change of the cloud shape due to phase separation [Zwi06a].

[5] If a superfluid is anisotropic in the plane perpendicular to the rotation axis also the irrotational flow of a superfluid contains angular momentum although there are no vortices.

the equation of state. This made it possible to investigate the transition from hydrodynamic to collisionless behavior with decreasing coupling strength of the atom pairs on the BCS side of the crossover. The investigation of the scissors mode focuses on the temperature dependence of the dynamic behavior in the crossover region. This measurement uncovers the range of temperatures and interaction strengths where hydrodynamic behavior of the normal phase appears. In addition a comparative study of all the three modes mentioned is performed to address open questions concerning the transition from hydrodynamic to collisionless behavior for a unitarity-limited gas.

Although collective modes allow to study the dynamic behavior of the gas they cannot directly reveal superfluid behavior of the gas. To show superfluid behavior of the strongly interacting Fermi gas we study the gas under rotation. We reveal superfluid behavior by demonstrating quenching of the moment of inertia. Quenching of the moment of inertia was first shown in liquid helium [Hes67] and also serves as a firm indicator for nucleon superfluidity [Rin80]. More recent a nonclassical moment of inertia in bulk solid helium was reported [Kim04a]. The reduction of the moment of inertia does not only serve as a proof for superfluidity but also contains information on the amount of the superfluid density in the system and thus allows to determine T_c.

In a preceding experiment on the rotating strongly interacting gas we investigate the lifetime of angular momentum, confined in a trap with controllable ellipticity. We find that in the vicinity of a Feshbach resonance the deeply hydrodynamic behavior in the normal phase leads to a very long lifetime of the angular momentum. Furthermore, we examine the dependence of the decay rate of the angular momentum on the ellipticity of the trapping potential and the interaction strength.

Overview

This thesis contains six articles, which are presented within separate chapters. At the beginning of each article, there is a short note indicating the primary contributions of the author of this thesis to that article.

A detailed description of the experimental setup can be found in the Ph.D. theses of S. Jochim [Joc04], M. Bartenstein [Bar05a], and A. Altmeyer [Alt07a] as well as in the diploma theses of G. Hendl [Hen03], C. Kohstall [Koh07], and myself [Rie04]. A detailed interpretation and additional information on the experiments published in the articles presented in Chapters 2 and 3 can be found in the PhD thesis of A. Altmeyer [Alt07a].

Chapter 2, *Precision Measurements of Collective Oscillations in the BEC-BCS Crossover*, deals with precision measurements of the frequency of the radial compression mode. The results allow for a test of theoretical predictions for the equation of state in the BEC-BCS crossover and show the long-sought beyond-mean-field effects in the strongly interacting BEC regime.

In Chapter 3, *Dynamics of a strongly interacting Fermi gas: the radial quadrupole mode*, we report on measurements of an elementary surface mode. The radial quadrupole mode allows us to probe hydrodynamic behavior in the BEC-BCS

crossover without being influenced by changes in the equation of state. The measurements show a striking down shift of the oscillation frequency on the BCS side of the crossover followed by an abrupt transition to collisionless behavior. The interpretation of this behavior is still under debate.

In Chapter 4, *Finite-Temperature Collective Dynamics of a Fermi Gas in the BEC-BCS Crossover*, we study the scissors mode to characterize the dynamics of the gas. We obtain a crossover phase diagram for collisional properties, showing a large region where a non-superfluid strongly interacting gas shows hydrodynamic behavior. Furthermore, in a narrow interaction regime on the BCS side of the crossover, we find a novel temperature-dependent damping peak, suggesting a relation to the superfluid phase transition.

In Chapter 5, *Collective oscillations of a Fermi gas in the unitarity limit: Temperature effects and the role of pair correlations*, we present detailed measurements of the frequency and damping of three different collective modes for a unitarity-limited gas. The results are compared to theoretical calculations that take into account Pauli blocking and pairing effects in the normal state above T_c. We show that these two effects nearly compensate each other and the behavior of the gas is close to the one of a classical gas.

In Chapter 6, *Lifetime of angular momentum in a rotating strongly interacting Fermi gas*, we investigate the lifetime of angular momentum in the strongly interacting Fermi gas, confined in a trap with controllable ellipticity. We find that in the vicinity of a Feshbach resonance, the deeply hydrodynamic behavior in the normal phase leads to a very long lifetime of the angular momentum. Furthermore, we examine the dependence of the decay rate of the angular momentum on the ellipticity of the trapping potential and the interaction strength.

In Chapter 7, *Quenching of the moment of inertia in a strongly interacting Fermi gas*, we report on the observation of a quenched moment of inertia as a consequence of superfluidity in a rotating, strongly interacting Fermi gas[6]. To determine the moment of inertia of the trapped, rotating gas we measure the precession of the radial quadrupole mode. Studying the moment of inertia as a function of the temperature reveals the superfluid phase transition.

In Chapter 8 we give an outlook for possible future directions of the experiment.

[6]At the time I handed in this thesis this article was still in preparation.

CHAPTER 2

Publication

Precision Measurements of Collective Oscillations in the BEC-BCS Crossover[†]

Phys. Rev. Lett. 98, 040401 (2007)

A. Altmeyer,[1] S. Riedl,[1,2] C. Kohstall,[1] M. J. Wright,[1] R. Geursen,[1] M. Bartenstein,[1] C. Chin,[3] J. Hecker Denschlag,[1] and R. Grimm[1,2]

[1] *Institut für Experimentalphysik und Zentrum für Quantenphysik, Universität Innsbruck, 6020 Innsbruck, Austria*

[2] *Institut für Quantenoptik und Quanteninformation, Österreichische Akademie der Wissenschaften, 6020 Innsbruck, Austria*

We report on precision measurements of the frequency of the radial compression mode in a strongly interacting, optically trapped Fermi gas of ^{6}Li atoms. Our results allow for a test of theoretical predictions for the equation of state in the BEC-BCS crossover. We confirm recent quantum Monte-Carlo results and rule out simple mean-field BCS theory. Our results show the long-sought beyond-mean-field effects in the strongly interacting BEC regime.

Ultracold, strongly interacting Fermi gases [O'H02, Bou03, Joc03a, Gre03, Zwi03, Bar04b, Reg04, Zwi04, Bou04, Kin04a, Bar04a, Kin04b, Chi04, Zwi05a, Par05] have attracted considerable attention over the past few years, serving as unique model systems to create, control, and investigate novel states of quantum matter. Experimentally, the availability of such systems has opened up exciting possibilities to study many-body quantum phenomena like molecular Bose-Einstein condensation (BEC) [Joc03a, Gre03, Zwi03] and the crossover from

[†] The primary contribution of the author of the present thesis to this publication is the setup of the new imaging system, together with the investigation of the effects of the residual trap ellipticity and the anharmonicity of the trapping potential on the compression mode frequency. This includes the development of a automated scheme to analysis the sloshing mode data. He also worked on maintaining and improving the experimental setup.

BEC to a Bardeen-Cooper-Schrieffer (BCS) type superfluid [Bar04b, Reg04, Zwi04, Bou04, Kin04a, Bar04a, Chi04, Kin04b, Zwi05a, Par05]. These experiments may also lead to a better understanding of strongly interacting quantum systems in different areas of physics, ranging from high-T_c superconductors to neutron stars and the quark-gluon plasma.

A degenerate two-component Fermi gas undergoes the BEC-BCS crossover [Eag69, Leg80, Noz85, Eng97] when the s-wave scattering length a is varied from positive to negative values across a scattering resonance. In the crossover region, where a is comparable with or larger than the interparticle spacing, the equation of state is governed by many-body effects. Understanding the equation of state is a fundamentally important challenge and constitutes a difficult task for many-body quantum theories, even in the zero-temperature limit. Mean-field BCS theory [Eag69, Leg80, Noz85, Eng97] provides a reasonable interpolation between the well-understood limits. More sophisticated crossover approaches [Pie05] yield quantitatively different results in certain regimes, none of them however providing a complete description of the problem. The most advanced theoretical results were obtained by numerical calculations based on a quantum Monte-Carlo (QMC) approach [Ast04].

On the BEC side of the crossover, there is an interesting competition in the equation of state between the strong interactions in a Bose gas and the onset of fermionic behavior. For a strongly interacting Bose gas, one can expect quantum depletion to increase the average energy per particle. To lowest order, this beyond-mean-field effect leads a correction to the equation of state predicted by Lee, Huang, and Yang (LHY) almost 50 years ago [Lee57b, Lee57a]. Beyond mean-field effects are expected to reduce the compressibility of a strongly interacting Bose gas as compared to the weakly interacting case. However, when approaching the resonance, fermionic behavior emerges and the system loses its purely bosonic character, which increases the compressibility of the strongly interacting gas. Mean-field BCS theory does not contain beyond-mean field effects and the LHY correction is absent there. However, the QMC results predict beyond-mean-field effects to be visible on the BEC-side of the crossover [Ast04].

In this Letter, we report on precision measurements of the radial compression mode in an optically trapped, strongly interacting Fermi gas of ^{6}Li atoms. The mode serves as a sensitive probe for the compressibility and thus the equation of state of a superfluid gas in the BEC-BCS crossover [Str04, Hei04, Hu04, Bul05, Kim04b, Man05, Ast05]. We reach a precision level that allows us to distinguish between the predictions resulting from mean field BCS theory and QMC calculations. Previous experiments on collective modes, performed at Duke University [Kin04a, Kin04b] and at Innsbruck University [Bar04a], showed frequency changes in the BEC-BCS crossover in both the slow axial mode and the fast radial compression mode of a cigar-shaped sample. The accuracy, however, was insufficient for a conclusive test of the different many-body theories in the strongly interacting regime.

We prepare a strongly interacting, degenerate gas of ^{6}Li atoms in the lowest two internal states as described in our previous publications [Bar04b, Bar04a,

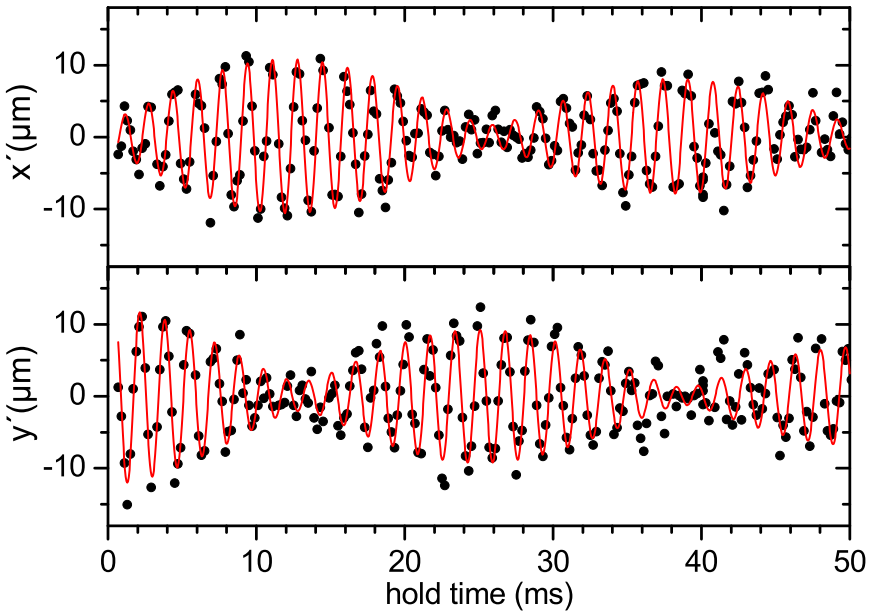

Fig. 2.1: Radial sloshing observed at a trap power of 540 mW and $B = 735$ G ($1/k_F a = 1.55$). The two-dimensional center-of-mass motion is represented in a coordinate system (x', y') rotated by 45° with respect to the principal axes of the trap. The beat signal between the two sloshing eigenmodes demonstrates the ellipticity of the trap with the two eigenfrequencies $\omega_x/2\pi = 570$ Hz and $\omega_y/2\pi = 608$ Hz (ellipticity $\epsilon = 0.066$).

.

Chi04]. The broad Feshbach resonance centered at a magnetic field of $B = 834$ G facilitates precise tuning of the scattering length a [Bar05b]. Forced evaporative cooling is performed in a 1030-nm near-infrared laser beam focussed to a waist of 54 μm at 764 G. This results in a deeply degenerate cloud of $N = 2.0(5) \times 10^5$ atoms. By adiabatically increasing the trap laser power after cooling, the sample is recompressed to achieve nearly harmonic confinement. In the axial direction the gas is magnetically confined in the curvature of the field used for Feshbach tuning with an axial trap frequency of $\omega_z/2\pi = 22.4$ Hz at 834 G. The experiments reported here are performed at two different final values of the laser power of the recompressed trap. At 135 mW (540 mW), the trap is 1.8μK (7.3μK) deep and the radial trap frequency is $\omega_r \approx 2\pi \times 290$ Hz (590 Hz). The Fermi energy of a non-interacting cloud is calculated to $E_F = \hbar^2 k_F^2/2m = \hbar(3\omega_r^2\omega_z N)^{1/3} = k_B \times 500$ nK (800 nK); here m is the mass of an atom and k_B is Boltzmann's constant.

Since our first measurements on collective excitation modes [Bar04a], we have upgraded our apparatus with a two-dimensional acousto-optical deflection system for the trapping beam and a new imaging system along the trapping beam axis. These two improvements provide us with full access to manipulate and observe the radial motion.

The trap beam profile is somewhat elliptic because of imperfections and aber-

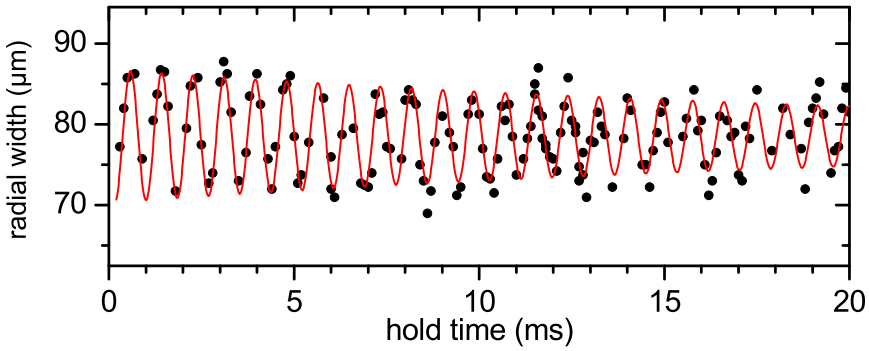

Fig. 2.2: Radial compression oscillation observed for the same conditions as the sloshing mode data in Fig. 2.1. The radial width is determined by averaging the horizontal and vertical Thomas-Fermi radii after expansion. Here we obtain $\omega_c/2\pi = 1185\,\mathrm{Hz}$.

rations in the optical set up. To simultaneously excite the two eigenmodes of the radial sloshing motion, we initially displace the trapped sample into a direction between the horizontal and vertical principal axes of the radial potential. After a variable hold time, during which the cloud oscillates freely, we turn off the optical trap. After a time of flight of typically 4 ms we take an absorption image of the released cloud. The center-of-mass position of the cloud then reflects its momentum at the instant of release. The experimental results in Fig. 2.1 demonstrate the sloshing with a beat between the two eigenmodes. A careful analysis of such data [Alt07a] allows us to determine the eigenfrequencies ω_x (horizontal sloshing) and ω_y (vertical sloshing) to within a relative uncertainty of typically 2×10^{-3}. We finally derive the mean sloshing frequency $\omega_\perp = \sqrt{\omega_x \omega_y}$ and the ellipticity parameter $\epsilon = (\omega_y - \omega_x)/\omega_\perp$.

To excite the radial compression oscillation we reduce the trap light power for a short time interval of $\sim$100μs, inducing an oscillation with a relative amplitude of typically 10%. After a variable hold time the cloud is released from the trap. From fits of two-dimensional Thomas-Fermi profiles to images of the expanding cloud taken 4ms after release, we determine the mean cloud radius. A typical set of measurements is shown in Fig. 2.2. A fit of a damped harmonic oscillation to such data yields the frequency ω_c and damping rate γ of the radial compression mode.

Our experiments are performed close to the limit of an elongated harmonic trap potential with cylindrical symmetry. This elementary case is of great general relevance for many quantum gas experiments in optical and magnetic traps (see, e.g., [Che02]), and collective excitations are conveniently normalized to the trap frequency ω_r [Str04, Hei04, Hu04, Bul05, Kim04b, Man05, Ast05]. The compression mode frequency can then be written as $\omega_c = f_c \omega_r$, where f_c is a dimensionless function of the interaction parameter $1/k_F a$ and is related to an effective polytropic index Γ [Str04, Hei04, Hu04, Bul05, Kim04b, Man05, Ast05] of the equation of state by $\omega_c^2 = 2(\Gamma + 1)\omega_r^2$.

In order to compare our experimental results with theory, we consider the quantity f_c, i.e. the normalized compression mode frequency of the ideal, cylindrically symmetric, elongated trap. We find, that for our experimental conditions, f_c is approximated by the ratio $\omega_c/\omega_\perp$ of the measured compression mode (ω_c) and mean sloshing mode ($\omega_\perp$) frequencies to better than one percent. On the desired accuracy level of 10^{-3}, however, two small effects have to be taken into account: the residual trap ellipticity and the anharmonicity of the radial potential in combination with the spatial extension of the trapped sample. We thus introduce two small corresponding corrections, expressing f_c in the form $f_c = (1 - \kappa\epsilon^2 + b\alpha)\,\omega_c/\omega_\perp$.

For the ellipticity correction $\kappa\epsilon^2$, a straightforward solution of the hydrodynamic eigenfrequency equation [Alt07a] yields $\kappa = (2+\Gamma)/4\Gamma$, where Γ can be approximated by $\Gamma = (\omega_c/\omega_\perp)^2/2 - 1$. For the anharmonicity correction, the parameter $\alpha = \frac{1}{2}m\omega_\perp^2 r_{\rm rms}^2/U_0$ relates the potential energy associated with the root-mean-square radius $r_{\rm rms}$ of the trapped cloud[1] to the trap depth. The coefficient b results from the differential anharmonicity shifts in the compression and sloshing modes and can be calculated according to [Str, Kin06, Alt07a]. We obtain [Alt07a] $b = 0.167$ and 0.280 in the limits of BEC and unitarity, respectively.

Our measurements on the sloshing and compression modes are summarized in Table 2.1, including the two small corrections. For the data in the strongly interacting BEC regime ($1/k_F a \gtrsim 1$) we used the weaker trap with $\omega_\perp/2\pi \approx 290\,\mathrm{Hz}$ to minimize unwanted heating by inelastic collisions. Closer to resonance ($1/k_F a \lesssim 1$) inelastic processes are strongly suppressed, but the increasing cloud size introduces larger anharmonicity shifts. Here we chose the deeper trap with $\omega_\perp/2\pi \approx 590\,\mathrm{Hz}$. On the BCS side of the resonance we observed increased damping as a precursor of the breakdown of hydrodynamics [Bar04a, Kin04b]. We thus restricted our measurements to magnetic fields below 850 G to ensure low damping rates ($\gamma/\omega_\perp < 0.01$) and superfluid hydrodynamics.

At a given magnetic field, a set of measurements on the sloshing and compression modes typically takes a few hours. To minimize uncertainties from slow drifts and day-to-day variations we always took the sloshing mode reference measurement right before or after the compression mode data. By repeating measurements under identical settings we found a typical remaining fractional uncertainty for the normalized compression mode frequencies of 5×10^{-3}, which is about 2-3 times larger than the fit errors of individual measurements.

In Fig. 6.6 we show our final results on the normalized compression mode frequency in the BEC-BCS crossover. The two theory curves [Ast05] correspond to the equation of state from mean-field BCS theory (lower curve) and the one from quantum Monte-Carlo calculations (upper curve). Our data confirm the quantum Monte-Carlo predictions and rule out the mean-field BCS theory. In the strongly interacting BEC regime ($1/k_F a \gtrsim 1$) our data are well above the value of 2. This highlights the presence of the long-sought beyond-mean-

[1] We obtain $r_{\rm rms}$ from in-situ measurements of axial profiles [Bar04b], using the relation $r_{\rm rms} = 2\omega_z^2/\omega_r^2 z_{\rm rms}$.

		sloshing		compression		corr.	
B (G)	$1/k_Fa$	$\omega_\perp/2\pi$ (Hz)	ϵ	$\omega_c/2\pi$ (Hz)	$\gamma/\omega_\perp$	$\kappa\epsilon^2$	$b\alpha$ (10^{-4})
727.8	2.21	292.7(5)	0.083(3)	596.3(6)	0.007(2)	48	20
735.1	1.96	298.6(5)	0.091(3)	602.8(8)	0.008(3)	60	26
742.5	1.75	294.5(5)	0.067(3)	593.2(7)	0.005(2)	33	28
749.8	1.55	296.3(4)	0.073(3)	599.0(7)	0.006(2)	38	28
760.9	1.27	296.0(4)	0.088(2)	592.3(7)	0.009(2)	58	24
771.9	1.03	293.6(7)	0.074(5)	586.2(8)	0.007(3)	41	27
834.1	0	287.5(7)	0.073(5)	519.4(9)	0.014(3)	55	94
757.2	1.07	605.0(9)	0.065(3)	1210.9(12)	0.010(2)	32	13
768.2	0.87	592.5(7)	0.069(2)	1186.6(12)	0.012(2)	36	16
775.6	0.75	590.2(4)	0.060(1)	1170.2(21)	0.007(4)	28	14
782.2	0.64	604.8(9)	0.061(3)	1187.1(16)	0.006(3)	29	16
801.3	0.38	586.8(7)	0.063(2)	1135.2(12)	0.010(2)	33	24
812.3	0.24	586.5(7)	0.058(2)	1106.9(16)	0.014(3)	30	33
834.1	0	596.3(9)	0.070(3)	1089.0(12)	0.010(2)	48	40
849.1	-0.14	583.2(7)	0.052(2)	1046.7(37)	0.007(2)	29	47

Table 2.1: Experimental data on radial collective modes in the BEC-BCS crossover. The data in the upper seven (lower eight) rows refer to the sets of measurements taken in the shallower (deeper) trap with $U_0 = 1.8\mu$K and $E_F = 500\,$nK ($U_0 = 7.3\mu$K and $E_F = 800\,$nK). The values in parentheses indicate 1σ fit uncertainties of individual measurements. Note that a systematic scaling uncertainty of $\sim$4% for $1/k_Fa$ results from the uncertainty in the atom number $N = 2.0(5) \times 10^5$.

field effects [Lee57b, Lee57a] in collective modes of a strongly interacting gas [Pit98, Str04, Hei04, Hu04, Bul05, Kim04b, Man05].

We finally address the question how non-zero temperatures influence the compression mode frequency. At unitarity, a recent experiment [Kin05a] has found small frequency upshifts with temperature. For a BEC, however, theory [Gio00] predicts temperature-induced down-shifts, which compete with the up-shifts from beyond-mean-field effects. We have performed a set of measurements on temperature shifts in the strongly interacting BEC regime ($1/k_Fa = 0.94$). Before exciting the collective oscillation, the evaporatively cooled gas was kept in the recompressed trap for a variable hold time of up to 1.5 s. During this time residual heating by inelastic processes slowly increased the temperature, which we observed as a substantial increase of damping with time. The damping rate γ thus serves us as a very sensitive, but uncalibrated thermometer [Kin04a, Kin05a]. Fig. 2.4, where we plot the normalized compression mode frequency versus damping rate, clearly shows a temperature-induced down-shift. We note that previous measurements in the strongly interacting BEC regime [Bar04a, Kin04b] were performed at relatively large damping rates in the range

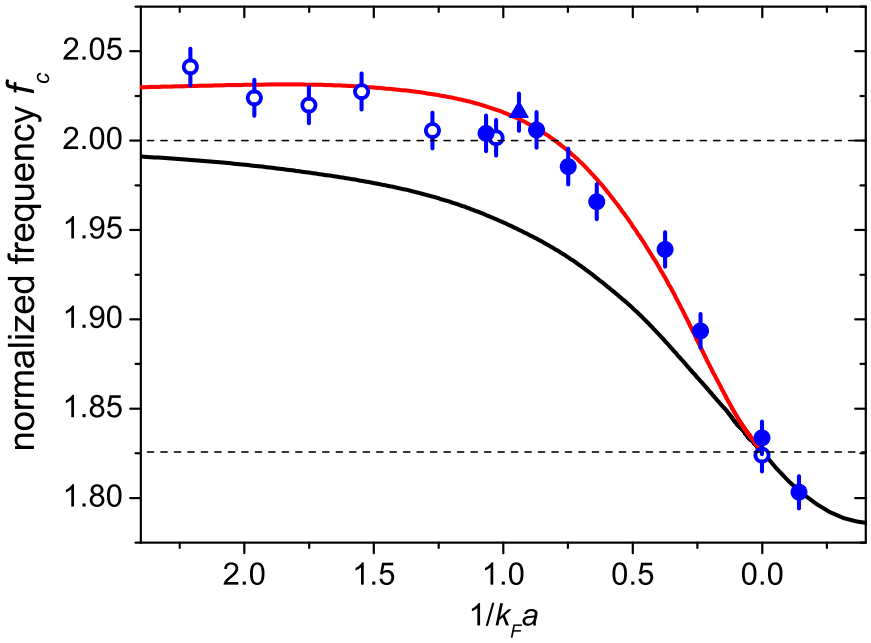

Fig. 2.3: Normalized compression mode frequency f_c versus interaction parameter $1/k_F a$. The experimental data include the small corrections for trap ellipticity and anharmonicity and can thus be directly compared to theory in the limit of an elongated harmonic trap with cylindrical symmetry. The open and filled circles refer to the measurements listed in Table 2.1 for $\omega_\perp/2\pi \approx 290\,\mathrm{Hz}$ and 590 Hz, respectively. The error bars indicate the typical scatter of the data points. The filled triangle shows a zero-temperature extrapolation of the measurements displayed in Fig. 2.4. The theory curves refer to mean-field BCS theory (lower curve) and QMC calculations (upper curve) and correspond to the data presented in Ref. [Ast05]. The horizontal dashed lines indicate the values for the BEC limit ($f_c = 2$) and the unitarity limit ($f_c = \sqrt{10/3} = 1.826$).

between 0.05 and 0.1, where frequency down-shifts are significant.

With our new knowledge on systematic frequency shifts in collective mode measurements, let us comment on the previous experiments performed in Innsbruck [Bar04a] and at Duke University [Kin04a, Kin04b]. We have reanalyzed our old data on the radial compression mode and identified a previously undetermined ellipticity of $\epsilon \approx 0.2$ as the main problem in our data interpretation [Alt06]. The fact that we had normalized the compression mode frequency to the vertical trap frequency (ω_c/ω_y) led to a substantial down shift in the hydrodynamic regime, but not in the collisionless regime. We furthermore believe that significant temperature shifts were present in the previous collective mode experiments. In particular for the strongly interacting BEC regime, temperature shifts in our old data on the axial mode [Bar04a] and the Duke data on the radial mode [Kin04b] provide a plausible explanation for these measurements being closer to the predictions of mean-field BCS theory than to the more advanced QMC results.

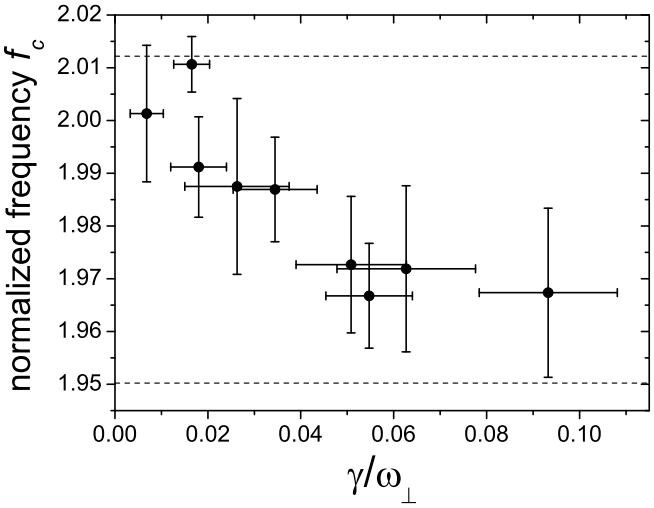

Fig. 2.4: Normalized compression mode frequency f_c versus damping rate for $1/k_F a = 0.94$ ($U_0 = 7.3\mu$K). The error bars represent 1σ fit uncertainties. The dashed lines indicate the zero-temperature values predicted by QMC calculations (upper line) and mean-field BCS theory (lower line).

In conclusion, our work shows that collective modes allow for precision tests of many-body theories in strongly interacting quantum gases. In future experiments, the observation of collective oscillation modes will serve as a powerful tool to investigate strongly interacting superfluids in a more general context, e.g. in mixtures of fermionic quantum gases.

We warmly thank S. Stringari for stimulating our interest in collective modes and for many useful discussions. We thank G. Astrakharchik for providing us with the theoretical data for Fig. 6.6, and R. Danielian for assistance in the experiments. We acknowledge support by the Austrian Science Fund (FWF) within SFB 15 (project part 21). S.R. is supported within the Doktorandenprogramm of the Austrian Academy of Sciences. C.C. acknowledges travel support from the NSF-MRSEC program under DMR-0213745.

CHAPTER 3

Publication

Dynamics of a strongly interacting Fermi gas: the radial quadrupole mode[†]

Phys. Rev. A 76, 033610 (2007)

A. Altmeyer,[1] S. Riedl,[1,2] M. J. Wright,[1] C. Kohstall,[1] J. Hecker Denschlag,[1] and R. Grimm[1,2]

[1] *Institut für Experimentalphysik und Zentrum für Quantenphysik, Universität Innsbruck, 6020 Innsbruck, Austria*

[2] *Institut für Quantenoptik und Quanteninformation, Österreichische Akademie der Wissenschaften, 6020 Innsbruck, Austria*

We report on measurements of an elementary surface mode in an ultracold, strongly interacting Fermi gas of ^{6}Li atoms. The radial quadrupole mode allows us to probe hydrodynamic behavior in the BEC-BCS crossover without being influenced by changes in the equation of state. We examine frequency and damping of this mode, along with its expansion dynamics. In the unitarity limit and on the BEC side of the resonance, the observed frequencies agree with standard hydrodynamic theory. However, on the BCS side of the crossover, a striking down shift of the oscillation frequency is observed in the hydrodynamic regime as a precursor to an abrupt transition to collisionless behavior; this indicates coupling of the oscillation to fermionic pairs.

[†]The primary contribution of the author of the present thesis to this publication is the construction of the scanning system together with C.K. and the development of the excitation scheme for the quadrupole mode. Together with M.J.W. he performed the data analysis with a special focus on the expansion effects. He also worked on maintaining the experimental setup.

3.1 Introduction

The advent of ultracold, strongly interacting Fermi gases [O'H02, Bou03], molecular Bose-Einstein condensates [Joc03a, Gre03, Zwi03], and fermionic condensates [Reg04, Zwi04] has opened up unique possibilities to study the fundamental physics of interacting fermions. The availability of controllable model systems with tunable interactions provides unprecedented experimental access to the many-body physics of fermionic quantum systems, which is of great fundamental importance for various branches of physics [Ing08].

A fundamental problem, which has been discussed in the theoretical literature for decades [Eag69, Leg80, Noz85, Eng97], is the crossover from Bose-Einstein condensation (BEC) to a macroscopic quantum state in the Bardeen-Cooper-Schrieffer (BCS) regime. In this crossover, the nature of pairing changes from the formation of bosonic molecules by fermionic atoms to pairing supported by many-body effects. With novel model systems now available in ultracold Fermi gases, the BEC-BCS crossover has recently stimulated a great deal of interest in both theory and experiment [Ing08].

Collective excitation modes in trapped ultracold Fermi gases provide powerful tools to investigate the macroscopic properties of a system in the BEC-BCS crossover [Vara]. For experiments of this class, ultracold ^{6}Li gases have excellent properties. This is because of their stability in the molecular regime [Cub03, Joc03b, Joc03a] and precise magnetic tunability of interactions based on a broad Feshbach resonance [Hou98, Bar05b]. Early experiments on collective modes in the BEC-BCS crossover provided evidence for superfluidity [Kin04a] and showed a striking transition from hydrodynamic to collisionless behavior [Bar04a]. More recent experiments yielded a precision test of the equation of state [Alt07b]. The previous experiments have focussed on collective modes with compression character, where both the hydrodynamic properties and the equation of state determine the mode frequency [Kin04a, Bar04a, Kin04b, Kin05a, Alt06, Alt07b].

In this Article, we report on measurements of a *pure surface mode* in the BEC-BCS crossover, which provides new insight into the dynamics of the system. The "radial quadrupole mode" in an elongated trap, the fundamentals of which are discussed in Sec. 5.3, allows for a test of hydrodynamic behavior without being influenced by changes in the equation of state. In Sec. 3.3, we present our experimental setup and the main procedures. We introduce a tool to excite collective oscillations with an acousto-optic scanning system. The results of our measurements, presented in Sec. 3.4, provide us with new insight on the abrupt transition from hydrodynamic to collisionless behavior, first observed in [Bar04a]. The present work provides strong evidence that quasi-static hydrodynamic theory [Varb] does not apply to collective modes of a strongly interacting fermionic superfluid, when the oscillation frequencies approach the pairing gap [Chi04].

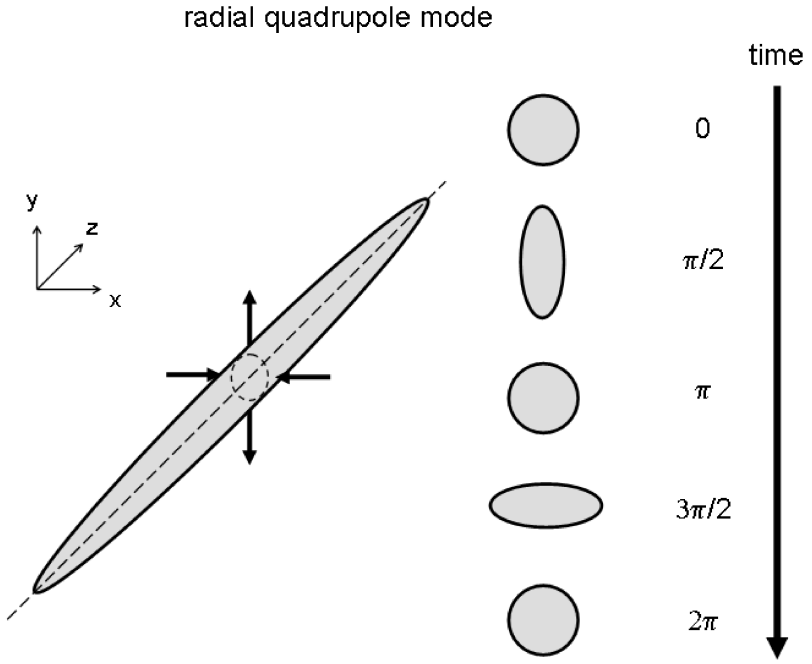

Fig. 3.1: Illustration of the radial quadrupole mode as an elementary collective excitation of an elongated, trapped atom cloud.

3.2 Radial Quadrupole Mode

The confining potential in our experiments is close to the limit of an elongated harmonic trap with cylindrical symmetry. In this case, we can consider purely radial collective oscillations, neglecting the axial motion. The frequencies of the radial modes can be expressed in units of the radial trap frequency ω_r. We note that our experiments are performed in a three-dimensional regime, where the energy $\hbar\omega_\mathrm{r}$ is typically a factor of 30 below the chemical potential and finite-size effects can be neglected.

In this situation, there are two elementary collective modes of the system, the radial compression mode and the radial quadrupole mode [Str96a, Vara]. We focus on the quadrupole mode, which is illustrated in Fig. 3.1. This mode corresponds to an oscillating radial deformation, which can be interpreted as a standing surface wave. The mode was first demonstrated in atomic BEC experiments [Ono00] and applied to investigate rotating systems [Bre03], but so far it has not been studied in strongly interacting Fermi gases.

Being a pure surface mode, the frequency ω_q of the radial quadrupole mode does not depend on the compressibility of the system. The frequency ω_q does not depend on the equation of state but on the collisional properties. In the hydrodynamic regime, whether the gas is a superfluid or a classical gas with a collision rate strongly exceeding the radial trap frequency, the frequency of this mode is given by [Str96a]

$$\omega_\mathrm{q} = \sqrt{2}\,\omega_\mathrm{r}. \tag{3.1}$$

In contrast, for a collisionless gas, where the atoms freely oscillate in the trap, the frequency is

$$\omega_{\mathrm{q}} = 2\,\omega_{\mathrm{r}}. \tag{3.2}$$

Because ω_{q} is insensitive to the compressibility of the gas and the difference between the collisonless and the hydrodynamic frequencies is large, the radial quadrupole mode can serve as an excellent tool to probe pure hydrodynamics. Particularly interesting is the transition from hydrodynamic to collisionless behavior at lowest temperatures. Such a change occurs in a strongly interacting Fermi gas on the BCS side of the resonance [Bar04a, Kin04b, Alt06]. Near this transition, measurements on the compression mode indicated frequency down shifts, which raised questions concerning the validity of standard hydrodynamic theory in this interaction regime [Com04, Com06]. Previous experiments could not unambiguously identify the origin of frequency shifts near the hydrodynamic-to-collisionless transition, which is a particular motivation for probing the crossover gas with the radial quadrupole mode.

3.3 Experimental Procedure

The apparatus and the basic preparation methods for experiments with a strongly interacting Fermi gas of ^{6}Li atoms have been described in our previous work [Joc03a, Bar04b, Bar04a, Chi04]. As a starting point, we produce a molecular BEC of $^6\mathrm{Li}_2$ [Joc03a, Bar04b]. By changing an external magnetic field, we can control the inter-particle interactions in the vicinity of a Feshbach resonance, which is centered at 834G [Hou98, Bar05b]. The interactions are characterized by the atomic s-wave scattering length a.

We start our experiments with an ensemble of about $N = 4 \times 10^5$ atoms in an almost pure BEC at a magnetic field of 764 G. In order to change the properties of the system adiabatically, we slowly ramp to the final magnetic field, where the measurements are performed [Bar04b]. The temperature of the gas is typically below 0.1 T_{F}, unless stated otherwise.

In order to observe the collective oscillations, we take absorption images of the cloud in the x-y-plane after release from the trap. We illuminate the atoms with a probe beam along the z-direction of the cigar-shaped cloud. The probe light causes a resonant excitation of the D2-line, at a wavelength of 671nm. We use dichroic mirrors for combining and separating the probe and the dipole trapping beam. The frequency of the probe beam can be tuned over a range of more than 1GHz, which enables resonant imaging over the whole range of magnetic fields that we create in our experiments.

The gas is confined in a nearly harmonic trapping potential, which has an axially symmetric, cigar-shaped trap geometry. Optical confinement in the radial direction is created by a focused 1030-nm near-infrared laser beam with a waist of ~ 58 μm. The potential in the axial direction consists of a combination of optical and magnetic confinement [Joc03a]; the magnetic confinement is dominant under the conditions of the present experiments. We set the laser

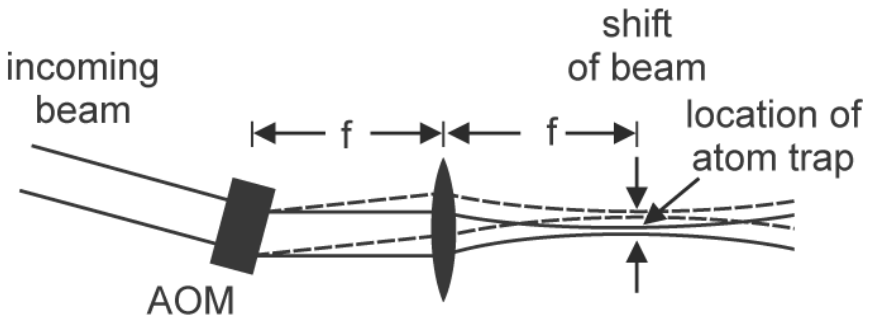

Fig. 3.2: Schematic illustration of the scanning system. A wide collimated beam passes through an AOM. The resulting deflection angle depends on the driving frequency of the AOM. The beam passes through a lens at the distance of one focal length behind the AOM. The lens focuses the beam for atom trapping. A change in deflection angle results in a parallel shift of the beam position in the focal plane. The solid and dashed lines show the beam path for different deflection angles. The zeroth order beam is not shown.

power to 270 mW, which results in a radial trap frequency of $\omega_\mathrm{r} \approx 2\pi \times 370$ Hz and an axial trap frequency of $\omega_\mathrm{z} \approx 2\pi \times 22$ Hz at a magnetic field of 764 G. The trap frequencies correspond to a Fermi energy of a noninteracting cloud $E_\mathrm{F} = \hbar(\omega_\mathrm{r}^2\omega_\mathrm{z}3N)^{1/3} = k_\mathrm{B} \times 740\mathrm{nK}$.

In order to excite collective oscillations, we suddenly change the optical trapping potential. The position and shape of our trapping potential in the x-y-plane can be manipulated through the use of a two-dimensional scanning system. One feature of the system is that we can rapidly displace the trap laterally. Fast modulation of the beam position enables us to create time-averaged potentials [Mil01, Fri01].

The scanning system is constructed by use of two acousto-optic modulators (AOMs), which are aligned for vertical and horizontal deflections. Fig. 3.2 illustrates the principle of our scanning system for one direction. A collimated beam passes through an AOM and is deflected depending on the driving frequency. A lens is placed at a distance of one focal length behind the AOM, so that the deflection results in a parallel displacement of the beam. By changing the driving frequency of the AOM, the lateral position of the focus is shifted. This system enables us to displace the focus of the trapping beam in the horizontal and the vertical direction by up to four times the beam waist in all directions. Furthermore, the deflection can be modulated by frequencies of up to $\sim$ 1MHz within 3dB bandwidth. In our trap configuration, we use modulation frequencies of 100kHz, which greatly exceeds the trap frequency. We create elliptic potentials, i.e. potentials with $\omega_\mathrm{x} \neq \omega_\mathrm{y}$, by modulating the trap position along a specific direction. We use this for the excitation of the quadrupole mode. By choosing a suited modulation function[1], these elliptic potentials are nearly harmonic.

[1]We use a periodic modulation with an arc sine-like function. This results in much better harmonic potentials than a simple sawtooth modulation ramp [Koh07].

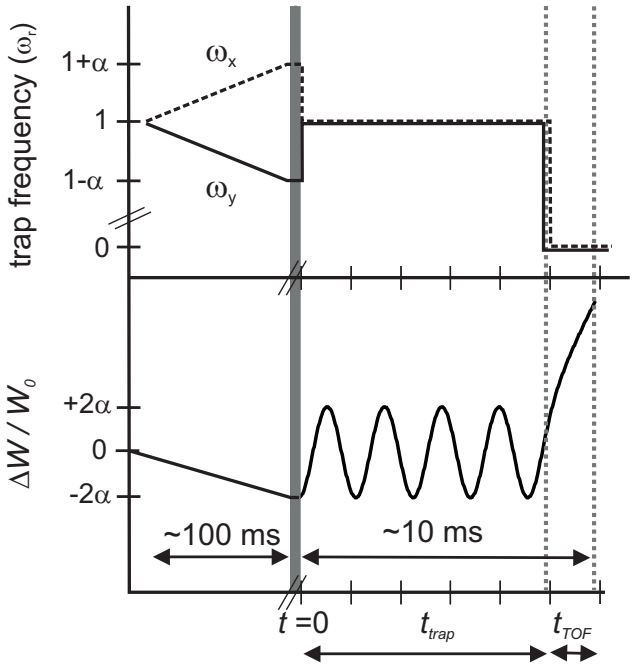

Fig. 3.3: Timing scheme for the excitation of the radial quadrupole mode. The ellipticity of the trap is slowly ramped up within 100 ms. This results in a change of α in the trap frequencies, where α characterizes the ellipticity, and sets the initial, normalized deformation $\Delta W/W_0 = -2\alpha$. W_0 is defined as the width of the cloud in the trap without excitation. At $t = 0$, the elliptic deformation is switched off and the oscillation in the trap begins. (Shown here is an oscillation in the hydrodynamic regime.) The oscillation continues until the trap is turned off at $t = t_{\mathrm{trap}}$, which is usually between 0 and 10 ms. At $t = t_{\mathrm{trap}}$, the cloud is released from the trap and expands for the time t_{TOF}, which is typically 2 ms.

When we excite the quadrupole mode, we first adiabatically deform the trapping potential in ~ 100 ms to an elliptic shape. This slow deformation ensures that the cloud stays in thermal equilibrium even in the near-collisionless regime and no excitations occur. We suddenly switch off the deformation leading to an oscillation in the x-y-plane of the elliptic cloud in the originally round trap.

The initial deformation corresponds to different trap frequencies in horizontal and vertical direction where $\omega_{0\mathrm{x}} = (1+\alpha)\omega_{\mathrm{r}}$ and $\omega_{0\mathrm{y}} = (1-\alpha)\omega_{\mathrm{r}}$. The parameter α determines the amplitude of the emerging oscillation; we choose it for most of our measurements (unless stated otherwise) to be $\alpha \approx 0.05$. We increase α by increasing the modulation for the time averaged potential along the y-direction. As the modulation decreases the confinement strength of the dipole trap, we simultaneously ramp up the trap power to ensure that the mean trap frequency $\omega_{\mathrm{r}} = \sqrt{\omega_{0\mathrm{x}}\omega_{0\mathrm{y}}}$ remains constant. This avoids excitation of the compression mode.

Fig. 3.3 shows the timing scheme for the excitation of the radial quadrupole mode. At $t = 0$, the collective oscillation is excited and the cloud starts oscillating in the trap for a variable time t_{trap}. Horizontal and vertical widths of the

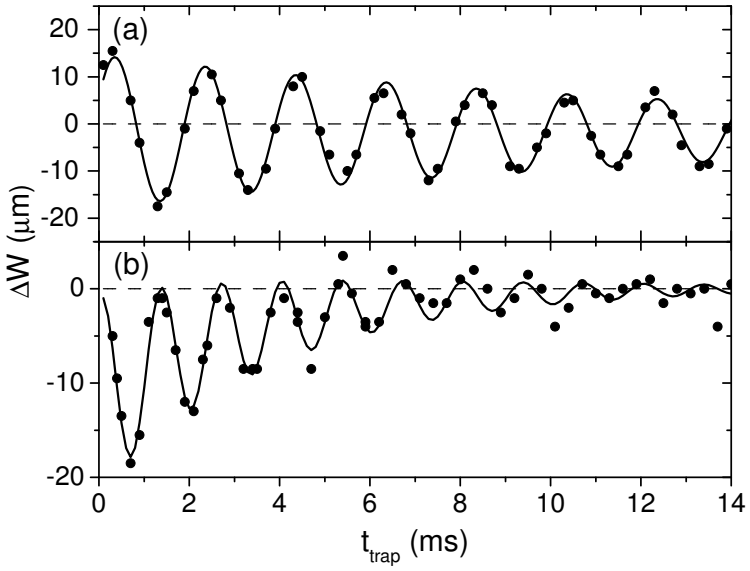

Fig. 3.4: Typical radial quadrupole oscillations in the hydrodynamic (a) and collisionless (b) regimes. The solid lines show fits to our data according to Eq.(3.3). The dashed lines indicate $\Delta W = 0$. The expansion time t_{TOF} is 2 ms. In (a), the oscillation in the unitarity limit ($B = 834$G) is shown, whereas (b) shows the oscillations for $B = 1132$G ($1/k_{\mathrm{F}}a \approx -1.34$).

cloud, W_{x} and W_{y}, oscillate in the trap out of phase with a relative phase shift of π. As an observable, we choose the difference in widths $\Delta W = W_{\mathrm{x}} - W_{\mathrm{y}}$, which cancels out small effects of residual compression oscillations. For normalization, we introduce the width W_0 of the cloud in the trap without excitation.

Experimentally, we determine the collective quadrupole oscillations after suddenly switching off the trap and a subsequent expansion time t_{TOF}. We then take an absorption image of the cloud and determine its horizontal and vertical widths W_{x} and W_{y} via a two-dimensional Thomas-Fermi profile fit. From these measurements after expansion, we can determine the in-trap behavior.

Typical data sets of radial quadrupole oscillations are shown in Fig. 3.4. Fig. 3.4(a) shows an oscillation in the hydrodynamic regime; here we observe a weakly damped harmonic oscillation centered about a small constant offset. Fig. 3.4(b) shows the typical behavior in the collisionless regime. The frequency of the oscillation is clearly higher than in the hydrodynamic regime. The oscillation shows stronger damping and has an exponentially time-varying offset.

We find that, for both regimes, the dependence of ΔW on t_{trap} can be well described by the fit function

$$\begin{aligned} \Delta W = \; & A\, e^{-\kappa t_{\mathrm{trap}}} \cos\left(\omega_{\mathrm{q}} t_{\mathrm{trap}} + \phi\right) \\ & + C\, e^{-\xi t_{\mathrm{trap}}} + y_0, \end{aligned} \tag{3.3}$$

which is explained in detail in Appendix B.

Note that the frequency ω_q and the damping constant κ are independent of the expansion during t_{TOF} and characterize the behavior of the trapped oscillating atom cloud. In contrast, the amplitude A and the phase shift ϕ depend on the expansion time and provide further information on the dynamics of the gas. The offset function $C\ e^{-\xi t_{trap}}$ with amplitude C and damping constant ξ results from thermalization effects and is only relevant in the collisionless regime (see discussion in Appendix B). The constant offset y_0 results from a slight inhomogeneity of the magnetic field, which gives rise to a weak saddle potential. This increases (decreases) the cloud size in y-direction (x-direction) during expansion.

3.4 Experimental Results

Here we first discuss our measurements of the frequency ω_q and the damping rate κ of the in-trap oscillation (Sec. 3.4.1). We then present the data for the phase offset ϕ and the amplitude A (Sec. 3.4.2). Finally, we explore the hydrodynamic-to-collisionless transition (Sec. 3.4.3). As commonly used in the field of BEC-BCS crossover physics [Ing08], the dimensionless parameter $1/k_F a$ is introduced to characterize the interaction regime. The parameter $k_F = \sqrt{2mE_F}/\hbar$ is the Fermi wave number and m is the mass of an atom.

3.4.1 Frequency and damping

In Fig. 3.5, we show the results for the frequency ω_q and the damping rate κ of the radial quadrupole mode throughout the BEC-BCS crossover. Both ω_q and κ are normalized to the trap frequency ω_r, which we determine by a sloshing mode measurement [Alt07b]. We include small corrections resulting from anharmonicity of the trapping potential and the residual ellipticity of the trap (see Appendix C).

The data confirm the expected transition between the hydrodynamic and the collisionless regime on the BCS side of the resonance (see Sec. 5.3). The transition is qualitatively different from the hydrodynamic-to-collisionless crossover in a classical gas [Bug05] or in a Fermi gas without superfluidity [Vic00]. Instead of a continuous and monotonous variation of the frequency between the two limits ($\sqrt{2}\,\omega_r$ and $2\,\omega_r$), an abrupt change occurs. When this transition is approached from the hydrodynamic side, a striking frequency downshift shows up as a precursor of the transition to higher frequencies. In the transition region (shaded area in Fig. 3.5), no data points are shown because of the large damping and correspondingly very large uncertainties for the measured frequency.

The damping rate shows similar behavior as in our previous measurements on the radial compression mode [Bar04a, Alt06]. Maximum damping occurs near the hydrodynamic-to-collisionless transition, whereas minimum damping is observed slightly below the resonance. In general, we find that damping is roughly two times larger for the quadrupole mode than for the compression

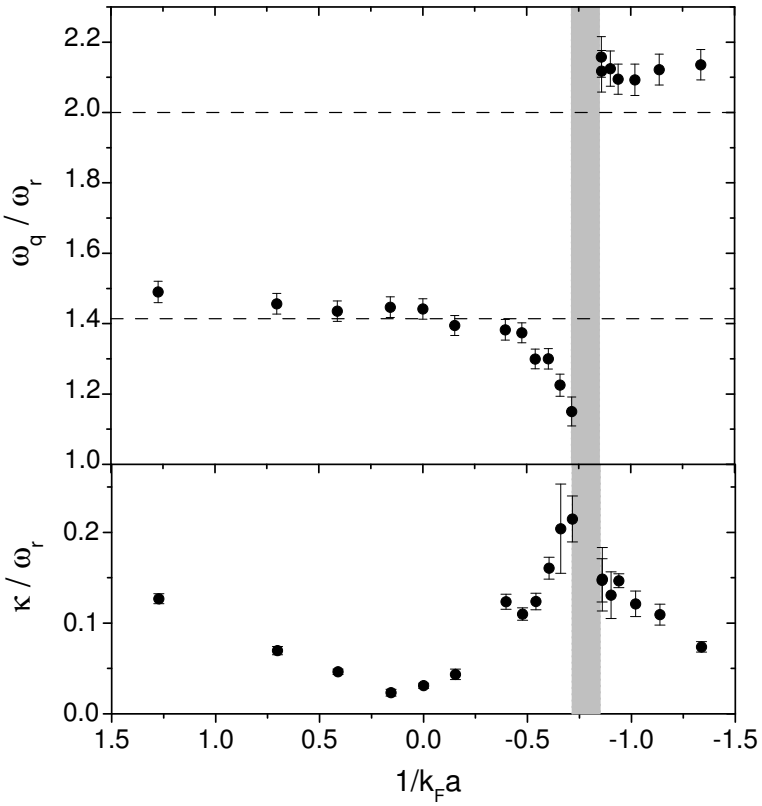

Fig. 3.5: Frequency ω_q (upper plot) and damping rate κ (lower plot) of the radial quadrupole mode. Both quantities are normalized to the radial trap frequency ω_r and plotted versus the interaction parameter $1/k_\mathrm{F}a$. The dashed lines indicate the theoretical predictions in the hydrodynamic ($\omega_\mathrm{q}/\omega_\mathrm{r} = \sqrt{2}$) and in the collisionless limit ($\omega_\mathrm{q}/\omega_\mathrm{r} = 2$). The shaded area marks the transition from hydrodynamic to collisionless behavior between $1/k_\mathrm{F}a \approx -0.72$ ($B \approx 930\,\mathrm{G}$) and $1/k_\mathrm{F}a \approx -0.85$ ($B \approx 960\,\mathrm{G}$).

mode at the same temperature[2]. The faster damping of the quadrupole mode is plausible in view of the larger frequency change at the transition.

We now discuss the behavior in different regions in more detail:

$1/k_\mathrm{F}a \approx 0$: In the unitarity limit, the normalized frequency agrees well with the theoretically expected value of $\omega_\mathrm{q}/\omega_\mathrm{r} = \sqrt{2}$ for a hydrodynamic gas, see Eq. (3.1). To check for consistency with previous experiments [Alt07b],

[2]Note that in the present measurements, the temperatures are somewhat higher than in our recent compression mode measurements [Alt07b]. There are essentially two reasons for the higher temperatures. First, the atoms stay longer in the recompressed trap because of the longer excitation scheme of the quadrupole mode. Second, for the quadrupole measurements we optimized our evaporative cooling scheme regarding particle number and not temperature.

we here also reproduced the frequency $\sqrt{10/3}\,\omega_\mathrm{r}$ of the radial compression mode on the 10^{-3} accuracy level. The damping is low for the Fermi gas in the unitarity limit. In contrast to the compression mode, the quadrupole mode frequency stays constant throughout the crossover, indicating that it is independent of the equation of state.

$1/k_\mathrm{F}a > 0$: In the strongly interacting BEC regime, there is an increase in the damping and a slight increase in the frequency for increasing $1/k_\mathrm{F}a$. As the gas is more susceptible to heating by inelastic processes in the deep molecular regime [Vara], both effects may be due to a thermal component in this region.

$1/k_\mathrm{F}a \approx -0.8$: The frequency exhibits the pronounced "jump" from the hydrodynamic to the collisionless frequency. This transition is accompanied by a pronounced maximum of the damping rate.

$1/k_\mathrm{F}a \lesssim -0.8$: The frequency stays almost constant about 5% above the theoretically expected value of $\omega_\mathrm{q} = 2\omega_\mathrm{r}$. Interaction effects in the attractive Fermi gas are likely to cause this significant upshift [Ped03, Urb07]. As we cannot experimentally realize a non-interacting Fermi gas above the resonance, we could not perform further experimental checks.

$1/k_\mathrm{F}a \lesssim 0$ and $1/k_\mathrm{F}a \gtrsim -0.8$: In this regime, we detect a substantial down shift in the quadrupole mode frequency. The effect begins to show up already slightly above the resonance ($1/k_\mathrm{F}a = 0$) and increases to a magnitude of almost 20% ($\omega_\mathrm{q}/\omega_\mathrm{r} \approx 1.15$ at $1/k_\mathrm{F}a = -0.72$), before the transition to collisionless behavior occurs. Indications of a similar down shift have been observed already in compression mode experiments [Bar04a, Alt06, Kin04b], but here the down shift is considerably larger and not blurred by changes in the equation of state.

A plausible explanation for the curious behavior of the collective mode frequency on the BCS side of the resonance is provided by coupling of the oscillation to the pairing gap [Com04, Chi04, Vara]. If we assume that the abrupt transition is caused by pair breaking resulting from resonant coupling of the oscillation to the gap, then the down shift may be interpreted as a coupling effect when the gap is not much larger than the oscillation frequency [Com06]. A similar shift may also arise from coupling of hydrodynamics and quasiparticle motion [Urb07]. The observed phenomenon still awaits a full theoretical interpretation.

3.4.2 Phase shift and amplitude

Additional information on the interaction regime is provided by the phase shift ϕ and the amplitude A of the observed oscillation (see Eq.(3.3)). This is useful since extremely high damping in the transition region makes a meaningful determination of frequency and damping practically impossible. We find that both amplitude and phase shift, however, can be determined with reasonable

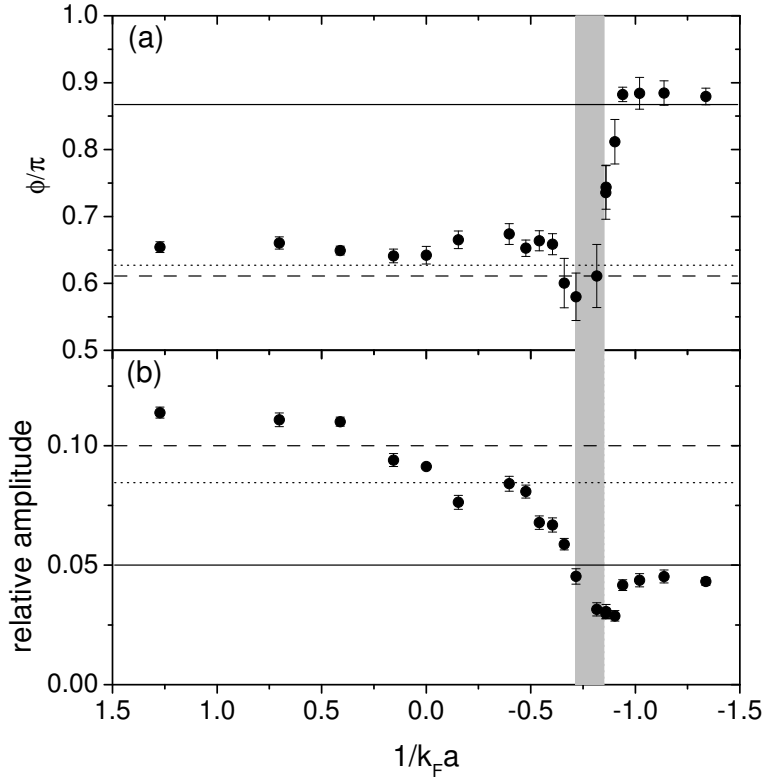

Fig. 3.6: (a) Phase shift ϕ and (b) relative amplitude of the quadrupole mode versus interaction parameter $1/k_{\mathrm{F}}a$ after $t_{\mathrm{TOF}} = 2$ms expansion. The horizontal lines show calculations from our theoretical model: the solid lines in the collisionless limit, the dotted lines in the hydrodynamic regime at unitarity ($\gamma = 2/3$) and the dashed lines in the hydrodynamic regime in the BEC limit ($\gamma = 1$). These calculated values can be read off from Fig. 3.10 for the phase and Fig. 3.9 for the amplitude. The shaded area marks the transition between hydrodynamic and collisionless behavior between $1/k_{\mathrm{F}}a \approx -0.72$ and $1/k_{\mathrm{F}}a \approx -0.85$ (see also Fig. 3.5).

uncertainties even in the transition regime.

In the following, we present measurements of phase shift and amplitude. These are compared to model calculations, which are described in detail in Appendix A.

In Fig. 3.6, the phase ϕ and the relative amplitude are plotted versus the interaction parameter $1/k_{\mathrm{F}}a$. The relative amplitude is given by the amplitude A (definition see Eq.(3.3)) divided by the average width of the cloud after expansion. The average width is obtained by averaging $(W_{\mathrm{x}} + W_{\mathrm{y}})/2$ over one oscillation period using the same data set from which we extract A.

In the transition area around $1/k_{\mathrm{F}}a = -0.8$, the phase shift ϕ shows the steplike change at the transition from the hydrodynamic to the collisionless regime.

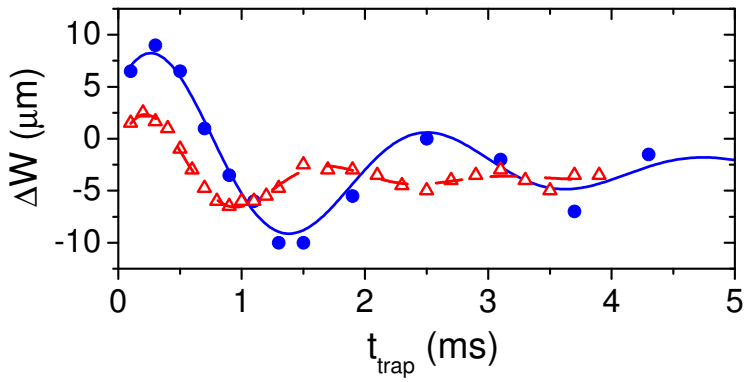

Fig. 3.7: (color online) Oscillations of the quadrupole surface mode at a magnetic field of 920 G and $1/k_{\mathrm{F}}a = -0.66$. The filled circles correspond to a cold ensemble, whereas the open triangles correspond to a heated ensemble. The solid lines are fits to the data according to Eq.(3.3).

This is similar to the jump in frequency in Fig. 3.5. In the collisionless and unitary regimes, the phase agrees with the theoretically expected values (solid line and dotted line, respectively).

As a general trend, the relative amplitude is larger in the hydrodynamic and smaller in the collisionless regime. In the hydrodynamic regime, the relative amplitude decreases for decreasing $1/k_{\mathrm{F}}a$, which is explained by the change of γ from 1 to 2/3; γ is the polytropic index of the equation of state (see Appendix A). At unitarity, the relative amplitude agrees well with the numerically calculated value for $\gamma = 2/3$ (dotted line). In the collisionless limit, the relative amplitude is half of the value at unitarity, which is also consistent with our calculations in App. A 3. We note that at the transition from the hydrodynamic to the collisionless regime, the value of the relative amplitude decreases even below the collisionless value.

In summary, the behavior of the phase shift and the amplitude agrees with our model presented in Appendix A (see also Fig. 3.9 and Fig. 3.10), in particular the prominent change in the phase offset is confirmed.

3.4.3 Further observations

The measurements presented in the preceding subsections were taken under fixed experimental conditions, where only the scattering length a was varied. In this subsection we investigate how the transition from hydrodynamic to collisionless behavior depends on the experimental parameters excitation amplitude, trap depth and temperature. In a first set of experiments, we explored whether the position of the transition depends on the excitation amplitude. We increase or decrease the amplitude by a factor of 2. This allows us to compare the

oscillations where the amplitude is ~ 20 %, ~ 10 % and ~ 5 % of the averaged width. We do not observe any significant change in the position of the transition.

In general, we find that the transition always occurs when the mode frequency is similar to the pairing gap. This is supported by the fact that when we vary the trap depth the transition occurs at a constant scattering length ($a \approx -5000a_0$, B $\approx$ 960G) and does not depend on $1/k_\mathrm{F}a$ [3]. A change in laser power of our trapping laser influences both Fermi energy E_F and the frequency ω_q. As we increase the trap power by a factor of 10, we also increase the radial trap frequencies by a factor of $\sqrt{10} \approx 3.2$. This changes the Fermi energy by a factor of 2.2 and the pairing gap, which scales like the trap frequencies, by roughly a factor of 3 [Chi04]. These findings suggest that the transition is linked to a coupling of the collective oscillation to the pairing gap. This is also in agreement with earlier results on the radial compression mode [Bar04a, Vara].

To explore the temperature dependence of the transition between the hydrodynamic and the collisionless phase, we use a controlled heating scheme similar to the one described in [Alt07b], where we hold the gas in a recompressed trap and let it heat up. We set the magnetic field to 920G ($1/k_\mathrm{F}a = -0.66$), i.e. slightly below the hydrodynamic-to-collisionless transition, where the regime is still clearly hydrodynamic. We observe the oscillations in a gas at the lowest temperature we can achieve in our experiments (filled circles) and in a "hotter" gas (open triangles) in Fig. 3.7. The temperature of the cold gas is $\lesssim 0.1\,T_\mathrm{F}$ and we believe the temperature of the heated gas to be $\lesssim 0.2\,T_\mathrm{F}$. Figure 3.7 clearly shows that the frequency for the colder ensemble is lower than that of the heated one and the amplitude is lower by roughly a factor of 2. Using our model in Appendix A this indicates a temperature driven transfer of the ensemble from the hydrodynamic to the collisionless regime.

Thus we find that the radial quadrupole mode is suited to detect temperature induced changes of the collisional regime of the gas. An exploration of the phase diagram of our system depending on temperature is possible, but beyond the scope of this article. In our lab, work is currently in progress on the radial scissors mode, which turns out to be an even better tool for the exploration of temperature effects.

3.5 Conclusions

We have presented measurements on the radial quadrupole mode of an ultracold ^{6}Li Fermi gas in the BEC-BCS crossover. As a pure surface excitation, this elementary mode probes hydrodynamic behavior without being affected by changes in the equation of state. We have measured the characteristic properties of this collective mode in a wide range of interaction strengths.

Our observations provide new insight into the dynamics of the gas, in particular on the BCS side of the crossover, where the character of the oscillations

[3] Due to the increased Fermi wave number k_F for the deeper trap configuration, the transition in terms of the interaction parameter shifts from $1/k_\mathrm{F}a \approx -0.8$ to $1/k_\mathrm{F}a \approx -0.5$.

abruptly changes from hydrodynamic to collisionless behavior. Our measurements presented in this paper show the phenomenon much clearer than in the radial compression mode [Bar04a, Kin04b, Alt06] and provide quantitative data on the behavior near the transition. In particular, the data show that a substantial down shift of the collective mode frequency occurs in the hydrodynamic regime as a precursor of the transition.

The experimental results support the interpretation that the coupling of oscillation mode and pairing gap [Com04, Chi04, Vara] plays a crucial role for the collective excitation dynamics on the BCS side of the crossover. We anticipate that our new quantitative data on the hydrodynamic-to-collisionless transition will stimulate further theoretical investigations on this intriguing phenomenon.

Acknowledgments
We thank S. Stringari and M. Urban for stimulating discussions. We thank E. R. Sánchez Guajardo for helpful discussions during the process of writing this paper. We acknowledge support by the Austrian Science Fund (FWF) within SFB 15 (project part 21). S.R. is supported within the Doktorandenprogramm of the Austrian Academy of Sciences. M.J.W. is supported by a Marie Curie Incoming International Fellowship within the 6th European Community Framework Program (40333).

3.6 Appendix A: Scaling approach and expansion effects

Here we present a theoretical model to describe the oscillation of the cloud in the trap as well as its expansion after release; the model adopts the scaling approach applied in [Bru00, Men02, Kin06]. The interplay between the dynamics of the collective mode and the expansion behavior is of particular interest as it introduces novel methods to investigate the collisional regime. We use a scaling approach for both the hydrodynamic and the collisionless regime [Bru00, Men02, Kin06]. In App. A 1, the limit of a hydrodynamic gas is presented, whereas in App. A 2, the model in the collisionless regime is discussed. Based on these models, we show calculated results for the amplitude and the phase after expansion in App. A 3.

The scaling approach describes the cloud at the time t after excitation [Bru00, Men02, Kin06]. Using the scaling function $b_i(t)$ for $i = x, y$, the width $W_i(t)$ for all times $t > 0$ can be written as

$$W_i(t) = b_i(t) W_i(0), \tag{3.4}$$

where $W_x(0) = (1 - \alpha)W_0$ and $W_y(0) = (1 + \alpha)W_0$ are the initial widths at excitation and W_0 is the width of the cloud without excitation. The initial conditions for the scaling function are $b_i(0) = 1$ and $\dot{b}_i(0) = 0$.

3.6.1 Dynamic behavior in the hydrodynamic limit

In the hydrodynamic limit, the equations of hydrodynamics lead to the following differential equations for b_x and b_y [Men02]

$$\begin{aligned} \ddot{b}_x &= \frac{\omega_{0x}^2}{b_x\,(b_x b_y)^\gamma} - b_x\,\omega_x^2, \\ \ddot{b}_y &= \frac{\omega_{0y}^2}{b_y\,(b_x b_y)^\gamma} - b_y\,\omega_y^2, \end{aligned} \tag{3.5}$$

where γ is the polytropic index of the equation of state and $b_z(t) = 1$ for our elongated trap geometry. The parameters ω_{0x} and ω_{0y} are the trap frequencies at the moment of excitation ($t = 0$), when the cloud has no further excitation and is in thermal equilibrium. In contrast to this, $\omega_{\mathrm{x}}(t)$ and $\omega_{\mathrm{y}}(t)$ are the time dependent trap frequencies. The timing scheme is illustrated in Fig. 3.3. The following equation summarizes the behavior of the trap frequencies $\omega_i(t)$:

$$\omega_i(t) = \begin{cases} \omega_{0i} & , t = 0 \\ \omega_{\mathrm{r}} & , 0 < t < t_{\mathrm{trap}} \\ 0 & , t > t_{\mathrm{trap}}. \end{cases} \tag{3.6}$$

This enables us to calculate the scaling functions b_x and b_y as solutions of Eq.(3.5) for the in-trap oscillation. In the limit of small amplitudes ($\alpha \ll 1$) solutions are

$$\begin{aligned} b_x &= 1 + \alpha(1 - \cos\omega_{\mathrm{q}} t), \\ b_y &= 1 - \alpha(1 - \cos\omega_{\mathrm{q}} t), \end{aligned} \tag{3.7}$$

where $\omega_{\mathrm{q}} = \sqrt{2}\,\omega_{\mathrm{r}}$ is the radial quadrupole oscillation frequency. Together with Eq.(3.4), we are able to determine the difference in widths of the cloud to be

$$\Delta W = -2\,\alpha W_0 \cos\omega_{\mathrm{q}} t. \tag{3.8}$$

3.6.2 Dynamic behavior in the collisionless limit

In the collisionless limit, the following set of two uncoupled equations characterizes b_i, where i stands for x, y, [Bru00]

$$\ddot{b}_i = \frac{\omega_{0i}^2}{b_i^3} - b_i\omega_i^2. \tag{3.9}$$

In the limit of small amplitudes ($\alpha \ll 1$) solutions of the in-trap oscillation are

$$\begin{aligned} b_x &= 1 + \frac{\alpha}{2}(1 - \cos\omega_{\mathrm{q}} t), \\ b_y &= 1 - \frac{\alpha}{2}(1 - \cos\omega_{\mathrm{q}} t), \end{aligned} \tag{3.10}$$

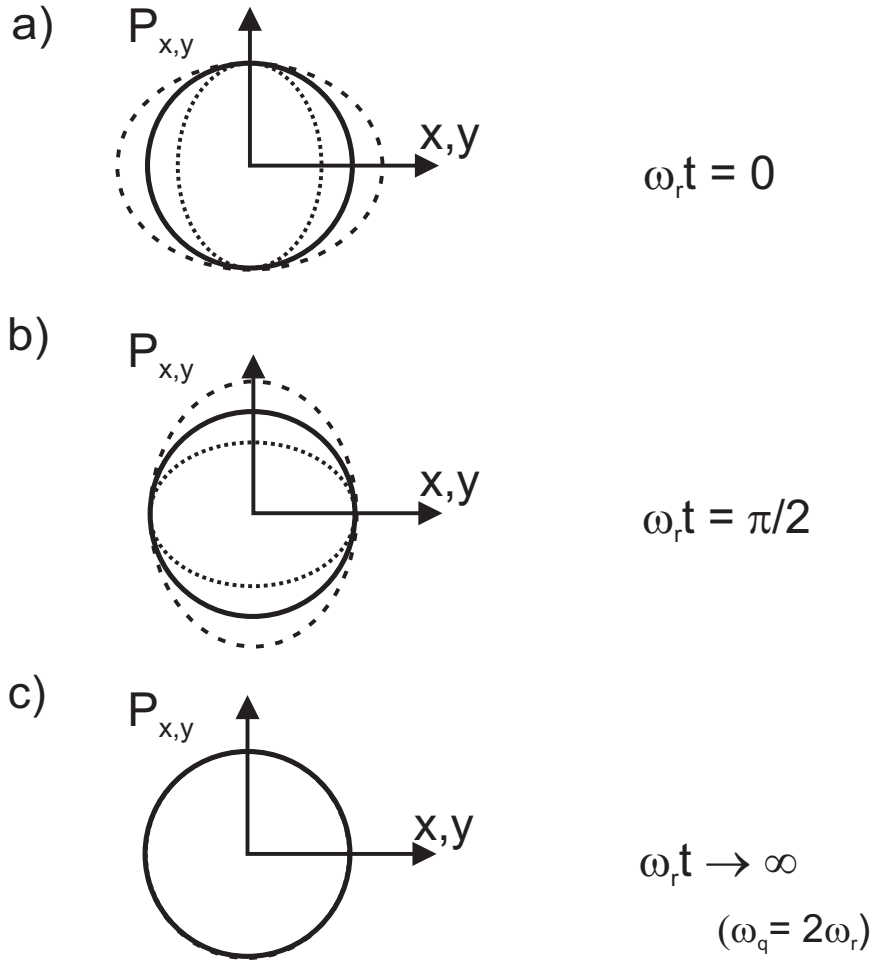

Fig. 3.8: Phase space dynamics for the quadrupole mode in the collisionless regime. Shown are phase space contours of an ensemble of particles which is held in a round trap (i.e. $\omega_x = \omega_y = \omega_\mathrm{r}$). In (a) and (b) the situation during the oscillation in the trap is shown for two different times t. The solid line indicates the equilibrium phase space contour (without excitation), whereas the dotted (dashed) line shows the contour in the x (y) direction after excitation of the oscillation mode. (c) After long times, residual thermalization finally damps out the oscillations and leads to a circular phase space contour.

where $\omega_\mathrm{q} = 2\,\omega_\mathrm{r}$ is the radial quadrupole oscillation frequency. Together with Eq.(3.4), we are able to determine the difference in widths of the cloud to be

$$\Delta W = -\alpha W_0 \left(1 + \cos \omega_\mathrm{q} t\right). \tag{3.11}$$

In contrast to the hydrodynamic limit, the oscillation is initially not centered around $\Delta W = 0$. Furthermore the oscillation has an amplitude 1/2 of the amplitude in the hydrodynamic gas.

Besides the finding of analytical solutions, it is enlightning to understand the collective oscillations in the collisionless limit by considering the phase space dynamics of the cloud. In Fig. 3.8, we show the contours of phase space dis-

tributions in the x- and y- directions. The axes are scaled such that for the round trap, i.e. $\omega_x = \omega_y = \omega_r$, the dynamics of any point in phase space is a simple circular rotation about the origin with frequency ω_r. Thus, the solid circle in Fig. 3.8 (a) indicates an equilibrium phase space contour for the round trap. Right after applying the excitation scheme as described in Sec. 3.3 the phase space contours in the x- and y- direction are given by the dashed and dotted ellipses in Fig. 3.8 (a). Since the gas is fully thermalized at the instant of excitation, the initial momentum distribution in x- and y- direction is the same. As time progresses, the elliptic contours will rotate with frequency ω_r (see Fig. 3.8 (b)), which corresponds to oscillations in the trap. We note that both the spatial and the momentum distribution in the x-direction are never larger than the ones in the y-direction. Therefore, ΔW oscillates between $2\alpha W_0$ and zero and the aspect ratio of the cloud never inverts. This is to be compared to the hydrodynamic case where ΔW oscillates between $\pm 2\alpha W_0$.

Residual thermalization effects in a near collisionless gas will damp out the initial oscillation amplitude of αW_0 and one will eventually end up again with a circular phase space contour (see Fig. 3.8 (c)). This is studied in detail in Appendix B.

3.6.3 Amplitude and phase on expansion

Here we present our calculated results based on the models in App. 3.6.1 and App. 3.6.2 for the hydrodynamic and the collisionless limit, respectively. We show the relative amplitude that is given by the amplitude A (definition see Eq.(3.3)) divided by the average width of the cloud after expansion (for definition details see Sec. 3.4.2). Calculations of this relative amplitude are shown in Fig. 3.9, whereas calculations and measurements for the phase offset ϕ are shown in Fig. 3.10.

Fig. 3.9 shows the calculated relative amplitude of a surface mode oscillation in the hydrodynamic (dashed and dotted curves) and in the collisionless (solid curve) regime as function of the reduced expansion time $\omega_r t_{TOF}$. The hydrodynamic curves are calculated for the BEC limit of $\gamma = 1$ (upper, dashed curve) and in the unitarity limit of $\gamma = 2/3$ (lower, dotted curve). The amplitude in the collisionless regime is smaller than in the hydrodynamic regime. Initially the amplitude of the excitation is half as large in the collisionless as in the hydrodynamic regime, as already explained in App. 3.6.2. In expansion the normalized amplitude stays constant in the collisionless regime and in the hydrodynamic regime for $\gamma = 1$. For $\gamma = 2/3$ in the hydrodynamic regime it decreases for longer expansion times.

In Fig. 3.10 we compare experimental data for the phase shift ϕ with numerical simulations. The data have been taken at unitarity where $1/k_F a = 0$ (hydrodynamic, open circles), and on the BCS-side of the resonance at $1/k_F a = -1.34$ (collisionless, closed triangles). The dashed line is based on a model for the hydrodynamic interaction regime and the solid line on a model for the collisionless regime. The data agree with the theoretical model where no free fit parameters

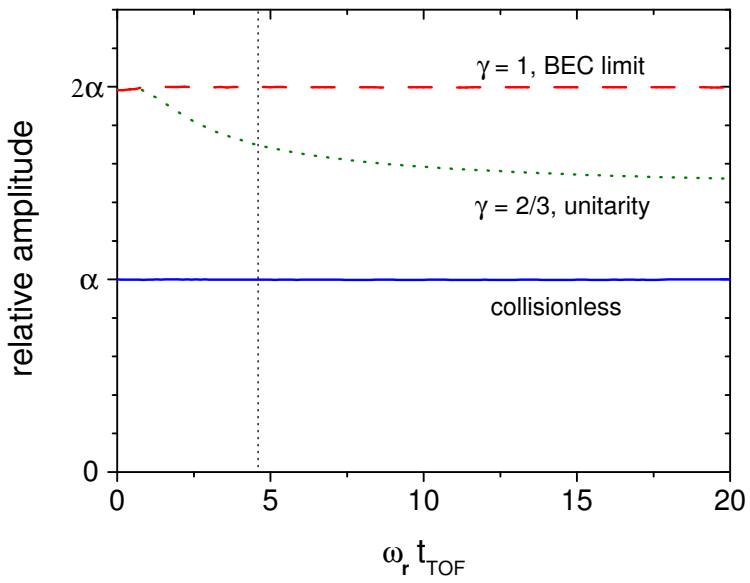

Fig. 3.9: (color online). Calculated relative amplitude of a surface mode oscillation versus reduced time of flight $\omega_r t_{TOF}$ after release from the trapping potential. The values are calculated for the hydrodynamic (dashed curve: $\gamma = 1$, dotted curve: $\gamma = 2/3$) and collisionless regime (solid curve). The vertical dotted line marks the typical expansion time in our experiments.

are used. This confirms our approach presented above.

3.7 Appendix B: Thermalization effects in a near-collisionless gas

Here we describe thermalization effects in a near-collisionless gas that are not included in the model for the collisionless limit in App. 3.6.2. Despite the word "collisionless", collisions play a crucial role for thermalization for our experimental parameters. A typical time scale for thermalization processes is only a few oscillation cycles long. By analyzing the theory, we are able to introduce a universal fit function, as given by Eq.(3.3), which describes the oscillation both in the hydrodynamic and in the near-collisionless regime.

The measured behavior of the nearly collisionless quadrupole oscillation (see Fig. 3.4) has two characteristics: after excitation the oscillation is centered around $\Delta W = (W_x(0) - W_y(0))/2$, then after some time it is centered around $\Delta W = 0$. These two limits are consistent with thermalization of the gas on a relevant time scale greater than the period of the oscillation.

In order to model these effects, we follow a theory based on a classical gas

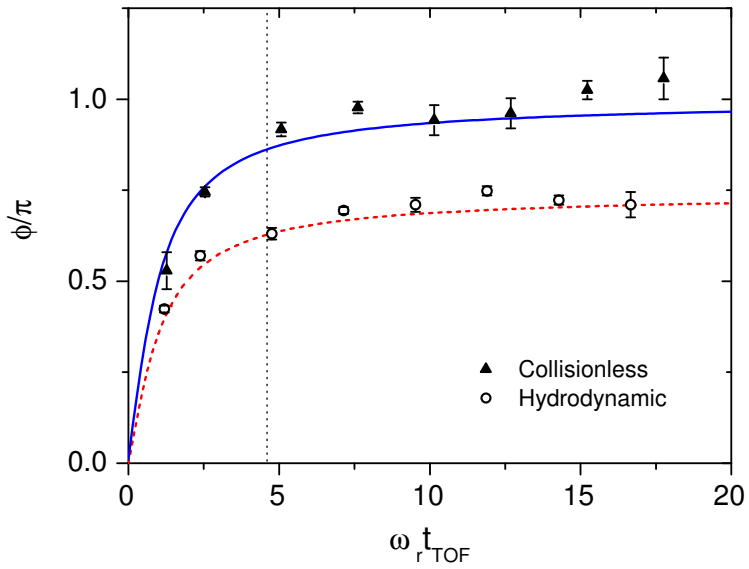

Fig. 3.10: (color online) Phase ϕ of the collective surface mode as detected by fits according to Eq.(3.3) versus reduced expansion time $\omega_r t_{TOF}$ at unitarity (open circles) and at $1/k_F a = -1.34$ (filled triangles). The lines are numerical simulations for the hydrodynamic (dashed line) and collisionless regime (solid line). The vertical dotted line marks the typical expansion time in our experiments.

in the transition between the hydrodynamic and the collisionless behavior described in [Ped03]. An application of this theory for the compression mode in the hydrodynamic regime has been used in [Kin06]. Here we will handle thermalization effects of the quadrupole mode in the near-collisionless regime.

Using the classical Boltzmann-Vlasov kinetic equation in the relaxation-time approximation and ignoring mean field effects one can derive the following coupled differential equations [Ped03]

$$\ddot{b}_i = \omega_{0i}^2 \frac{\theta_i}{b_i} - \omega_i^2 b_i \tag{3.12}$$

and

$$\dot{\theta}_i = \frac{1}{\tau_R}(\theta_i - \bar{\theta}) - 2\frac{\dot{b}_i}{b_i}\theta_i. \tag{3.13}$$

The parameter b_i is the scaling function described earlier in Appendix A; θ_i is a scaling parameter directly related to the temperature and $\bar{\theta} = \frac{1}{3}\Sigma_k \theta_k$. The initial condition for θ_i is $\theta_i(0) = 1$, as long as the gas is in thermal equilibrium at the moment of the excitation. The parameter τ_R is the relaxation time which describes the time scale of collisions. In the collisionless limit, when $\tau_R \to \infty$,

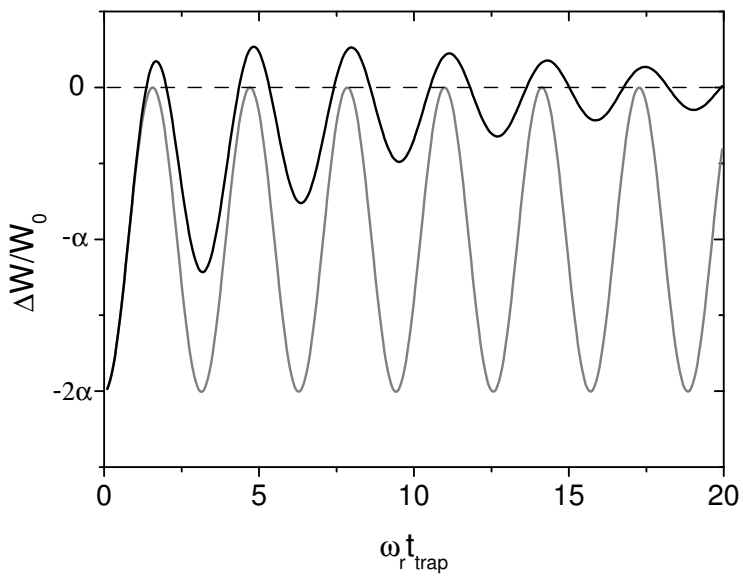

Fig. 3.11: Calculated quadrupole oscillations in the near-collisionless regime. The lines show the relative difference in width ΔW as a function of the reduced time $\omega_{\mathrm{r}} t_{\mathrm{trap}}$. The oscillation is modeled according to Eq.(3.12) and (3.13). The dark line shows the result of the calculation when $\omega_{\mathrm{r}}\tau_R = 2.3$ and the grey line shows the coscillation in the collisionless limit at $\omega_{\mathrm{r}}\tau_R = 1000$.

the differential equations (3.12) simplify to the simple form in Eq. (3.9). For the hydrodynamic limit ($\tau_R \to 0$), we find Eq. (3.5).

The solutions to these equations depend on the parameter τ_R as can be seen in Fig. 3.11. Our measured data in the collisionless regime are well described by $\omega_{\mathrm{r}}\tau_R \sim 2.3$ (compare to Fig. 3.4).

The universal fit function

We find that the model calculations from (3.12) and (3.13) can be well described with the following fit function

$$\begin{aligned} \Delta W = \; & A\, e^{-\kappa t_{\mathrm{trap}}} \; \cos\left(\omega_{\mathrm{q}} t_{\mathrm{trap}} + \phi\right) \\ & + C\, e^{-\xi t_{\mathrm{trap}}} + y_0. \end{aligned} \tag{3.14}$$

The first term describes the exponentially damped oscillations. The second term describes the shift of the center of the oscillation in the collisionless regime. The third term y_0 is a constant offset which will be discussed later.

We have used Eq.(3.14) to fit our experimental measurements. We find that the free fit parameters ξ and κ are related through $\xi/\kappa \approx 1.5$ for all our measurements in the near-collisionless regime. In the hydrodynamic regime $C = 0$, and therefore ξ becomes irrelevant.

The constant offset y_0 is due to an experimental artifact that results from a slight inhomogeneity of the magnetic field. At the location of the atoms the inhomogeneous magnetic field leads to a weak saddle potential which causes a slight anisotropic expansion during time of flight. This anisotropy is responsible for a slight offset in ΔW.

3.8 Appendix C: Corrections to the normalized frequency

The theoretical normalized frequencies $\omega_\mathrm{q}/\omega_\mathrm{r}$ are calculated for perfectly harmonic trapping potentials in an idealized symmetric trap geometry. There are small derivations from this conditions in real experiments. In order to compare the experimental data to the idealized theoretical case, we have to correct our data. The measured normalized frequency $\omega_\mathrm{q}/\omega_\mathrm{r}$ of the radial quadrupole mode has to be increased because of two small corrections. The larger correction is based upon a slight anharmonicity of the trapping potential and the spatial extension of the cloud in the trap. The smaller correction is caused by a small residual ellipticity of the trapping potential.

The potential created by our trapping beam has a Gaussian shape. This results in a nearly harmonic potential in the center of the trap; however, for higher precision one must take into account higher order terms of the potential. Anharmonicity effects influence both our measurements of the sloshing mode frequency, where we determine ω_r, and our measurements of the quadrupole mode frequency ω_q. As we evaluate the normalized frequency $\omega_\mathrm{q}/\omega_\mathrm{r}$, the anharmonicity effects on sloshing and quadrupole mode almost cancel out each other. The small remaining correction to the normalized frequency is included by multiplying with a prefactor $1+b\sigma$ [Alt07b, Alt07a]. The anharmonicity parameter σ relates the energy of the oscillation to the total potential depth and is defined by $\sigma = \frac{1}{2}m\omega_r^2 r_\mathrm{rms}^2/V_0$, where r_rms is the root-mean-square radius of the trapped cloud and V_0 is the potential depth. The parameter b depends on the interaction regime. In the hydrodynamic regime, it is given by $(4+10\gamma)/(2+7\gamma)$, whereas in the collisionless regime b is determined by $6/5$ [Alt07a]. Here, γ is the polytropic index of the equation of state. In our experiments, typically $b\sigma \approx 0.014$, but $b\sigma$ can rise to an upper limit of $b\sigma < 0.027$.

In the hydrodynamic regime, there is also a correction due to residual ellipticity effects. This correction takes into account that we compare our measurements with a theory for non-elliptic geometries. The ellipticity ϵ of the trap is defined by $\epsilon = (\omega_\mathrm{y} - \omega_\mathrm{x})/\omega_\mathrm{r}$. In our experiments, the ellipticity is small and given by $\epsilon \approx 0.07$. Therefore, we can apply the ellipticity correction by multiplication of a prefactor $1+\lambda\epsilon^2$ [Alt07b, Alt07a], where the interaction dependent factor λ is given by $(\gamma+2)/(4\gamma)$. Altogether, $\lambda\epsilon^2$ is smaller than 0.006 for all data points.

CHAPTER 4

Publication

Finite-Temperature Collective Dynamics of a Fermi Gas in the BEC-BCS Crossover[†]

Phys. Rev. Lett. 99, 150403 (2007)

M. J. Wright,[1] S. Riedl,[1,2] A. Altmeyer,[1,2] C. Kohstall,[1] E. R. Sánchez Guajardo,[1]
J. Hecker Denschlag,[1] and R. Grimm[1,2]

[1] *Institut für Experimentalphysik und Zentrum für Quantenphysik, Universität Innsbruck, 6020 Innsbruck, Austria*

[2] *Institut für Quantenoptik und Quanteninformation, Österreichische Akademie der Wissenschaften, 6020 Innsbruck, Austria*

We report on experimental studies on the collective behavior of a strongly interacting Fermi gas with tunable interactions and variable temperature. A scissors mode excitation in an elliptical trap is used to characterize the dynamics of the quantum gas in terms of hydrodynamic or near-collisionless behavior. We obtain a crossover phase diagram for collisional properties, showing a large region where a non-superfluid strongly interacting gas shows hydrodynamic behavior. In a narrow interaction regime on the BCS side of the crossover, we find a novel temperature-dependent damping peak, suggesting a relation to the superfluid phase transition.

Ultracold Fermi gases with tunable interactions have opened up intriguing possibilities to study the crossover from bosonic to fermionic behavior in strongly interacting many-body quantum systems [Ing08]. In the zero-temperature limit, a Bose-Einstein condensate (BEC) of molecules is smoothly connected with a

[†]The primary contribution of the author of the present thesis to this publication is the development of the experimental procedure to excite and detect the scissors mode oscillation. Together with M.J.W. he recorded and analysed the data for this publication. The temperature measurement was implemented by M.J.W..

superfluid of paired fermions in the Bardeen-Cooper-Schrieffer (BCS) regime. In recent years, great progress has been achieved in the theoretical description of the ground state at zero temperature, and fundamental properties have been experimentally tested with considerable accuracy [Gio08]. Finite-temperature phenomena in the BEC-BCS crossover, however, pose great challenges for their theoretical description. Experimental observations of finite-temperature behavior in the crossover have focussed on the measurement of condensate fractions [Reg04, Zwi04], on the spectroscopic investigation of pairing phenomena [Chi04], or on the special case of unitarity-limited interactions [Kin05a, Ste06, Cla07].

To understand the collective dynamics of an ultracold quantum gas, it is crucial to study the conditions for hydrodynamic behavior. Collective mode experiments have probed the dynamics of strongly interacting Fermi gases for variable interaction strength near zero temperature [Bar04a, Kin04b, Alt07b, Alt07c]. The results show the existence of both a hydrodynamic regime of collective motion and a near-collisionless regime with independent motion of the trapped particles. The role of temperature, however, remained essentially unexplored.

In this Letter, we explore the collective behavior of a finite-temperature, strongly interacting Fermi gas of ^{6}Li atoms throughout the BEC-BCS crossover. In order to characterize the transition from hydrodynamic to collisionless behavior, we analyze scissors mode oscillations at different temperatures. With varying temperature, the oscillations show a smooth transition between the two collisional regimes along with a broad maximum in the damping rate. We discover an unexpected second peak in the damping rate at lower temperatures in a narrow region on the BCS side of the crossover, where the gas remains hydrodynamic. This suggests the lower-temperature damping peak to be connected to the transition from a superfluid to a normal hydrodynamic gas.

The scissors mode in ultracold quantum gas experiments [GO99a, Mar00] is an angular oscillation of the cloud about a principle axis of an elliptical trap, see Fig. 4.1(a). In our experiments, we confine the atoms in a harmonic, triaxial optical dipole trap. We choose the geometry of the trap to produce an elliptically shaped gas in the x-y plane with very weak confinement along the z axis. The scissors mode experiments are done in the x-y plane. In terms of trap frequencies, the standard configuration is $\omega_x > \omega_y \gg \omega_z$, where these trap frequencies are defined along the principle axes of the trap. If the gas is hydrodynamic, the angle of the gas oscillates collectively with a single frequency of $(\omega_x^2 + \omega_y^2)^{1/2}$. If the gas is collisionless, the trapped atoms oscillate independently, resulting in a two-frequency oscillation. The larger frequency is given by $\omega_x + \omega_y$. When the collisional regime is changed this frequency is adiabatically connected to the hydrodynamic frequency. The smaller frequency is given by $\omega_x - \omega_y$ and is absent in the hydrodynamic limit [GO99a].

The preparation of a strongly interacting Fermi gas of ^{6}Li proceeds in the same way as described in our previous work [Joc03a, Alt07c]. The result is a deeply degenerate, balanced two-component spin mixture of typically $N = 4 \times 10^5$ atoms with tunable s-wave interactions near a broad Feshbach resonance, which

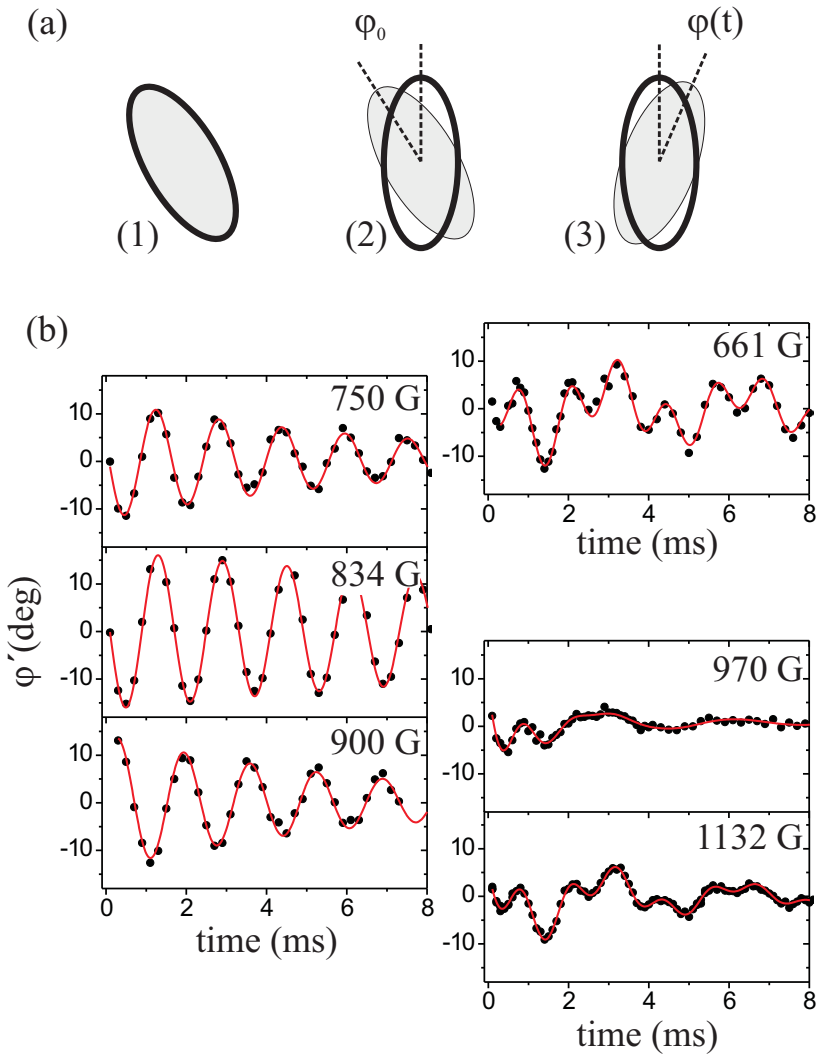

Fig. 4.1: (a) Schematic showing the excitation of the scissors mode. (1) The gas (shaded region) is at rest, in equilibrium with the trap (heavy solid line). (2) The trap is suddenly rotated. (3) The gas oscillates around the new equilibrium position. (b) Scissors mode oscillations observed at the lowest obtainable temperature ($T \approx 0.1 T_F$ at 834 G) for various magnetic fields. On the left side, where B = 750 G, 834 G, and 900 G ($1/k_F a$ = 1.4, 0.0, and −0.6), the gas is hydrodynamic. On the right side, where B = 661 G, 970 G, and 1132 G ($1/k_F a$ = 5.0, −1.0, and −1.44), the gas is nearly collisionless and exhibits the characteristic two-frequency oscillation. Here $\omega_x = 2\pi \times 580\,\mathrm{Hz}$, $\omega_y = 2\pi \times 270\,\mathrm{Hz}$, and $T_F = 0.69\,\mu\mathrm{K}$.

is centered at a magnetic field $B = 834\,\mathrm{G}$. Rapid spatial modulation of the trapping beam by two acousto-optical deflectors is used to create a time-averaged elliptical trapping potential for the scissors mode [Alt07c]. The aspect ratio is set to $\omega_x/\omega_y \approx 2.0$. We employ a trap with frequencies $\omega_x = 2\pi \times 830$ Hz and $\omega_y = 2\pi \times 415$ Hz ($\omega_z = 2\pi \times 22\,\mathrm{Hz}$), if not indicated otherwise. This results in a Fermi temperature $T_F = (\hbar\bar{\omega}/k_B)\,(3N)^{1/3} = 0.94\mu\mathrm{K}$, where $\bar{\omega} = (\omega_x\omega_y\omega_z)^{1/3}$. The trap depth corresponds to about $12\,T_F$. To excite the scissors mode, we suddenly rotate the angle of the trap by ~ 5 degrees, see Fig. 1(a).

The angle of the oscillating cloud is determined by processing absorption images, taken after a short expansion time of $400\,\mu$s. A two-dimensional Thomas-Fermi profile is fit to the images, where the tilt of the principle axes of the cloud is a free parameter, see Fig. 4.1(a). Note that the short expansion somewhat decreases the ellipticity of the cloud, but increases the amplitude of the scissors mode oscillation [Mod03]. In the hydrodynamic regime, we fit a damped cosine function to the experimental data. In the collisionless regime, we fit the oscillation to a sum of two damped cosine functions each with their own free parameters. In the region between these two limits, we find that a single damped cosine function fits the data reasonably well, as the lower-frequency component damps out very quickly [GO99a].

First, we examine the collective behavior of the gas at our lowest obtainable temperatures. We compare scissors mode oscillations at different settings of the magnetic field, i.e. different values of $1/k_F a$. Typical scissors mode oscillations are shown in Fig. 4.1(b). At $B = 661$ G, far on the BEC side of resonance, the gas exhibits nearly collisionless behavior. Here inelastic collisions result in heating the gas above the critical temperature for BEC. In the regime where the gas is strongly interacting, $B = 750$ G, 834 G, and 900 G, the gas oscillates collectively. High precision measurements taken at $B = 834$ G show the scissors mode oscillation yields a frequency that agrees with theory within one percent. Far on the BCS side, at $B = 970$ G and 1132 G, the gas exhibits behavior that is nearly collisionless. The abrupt transition between the hydrodynamic and collisionless regimes at low temperature occurs at essentially the same magnetic field, $B \approx 950$ G, as in other collective mode experiments [Bar04a, Kin04b, Alt07c].

To explore finite-temperature collisional behavior, we extend the scissors mode measurements. To set the temperature, we use a controlled heating scheme. Here, we suddenly compress the trap and allow for subsequent equilibration[1]. We control the temperature of the gas by adjusting the amount of compression.

The determination of the temperature T in an ultracold, strongly interacting Fermi gas is in general difficult [Kin05b]. We can measure an effective temperature (or entropy) parameter $\tilde{T}$ at the center of the Feshbach resonance, $B = 834$ G. We determine $\tilde{T}$ by fitting integrated, one-dimensional, density

[1]Sudden compression of the trap excites the axial mode which is long lived. Since the frequency is much smaller than the scissors mode frequency, it can be neglected. Nonetheless, we carried out a direct comparison without the axial mode present and found the same behavior.

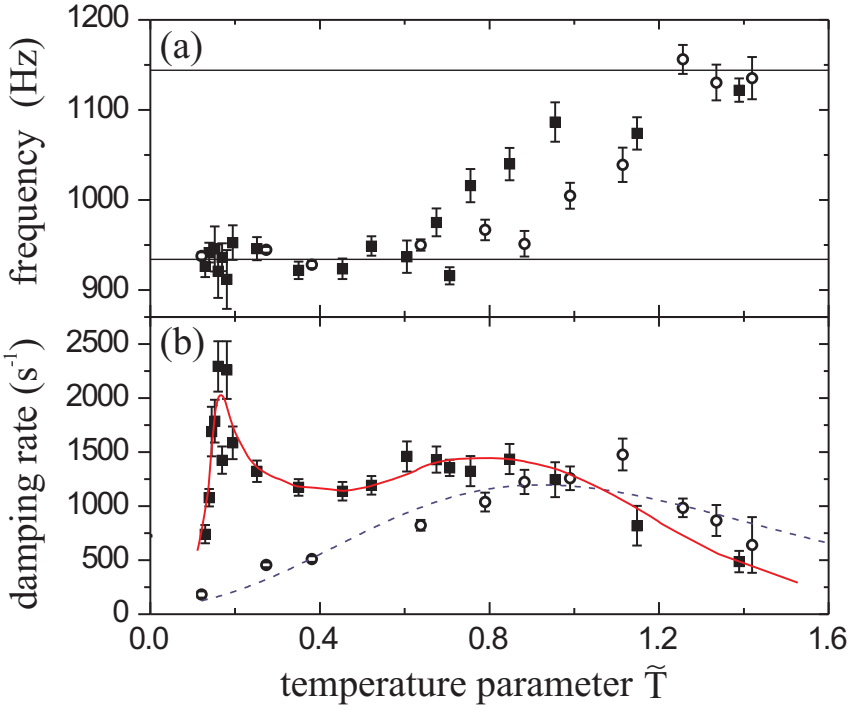

Fig. 4.2: Frequency and damping rate for the scissors mode oscillation for B = 895 G ($1/k_Fa = -0.45$, solid squares) and at B = 834 G ($1/k_Fa = 0$, open circles). The frequency limits in the hydrodynamic and collisionless regimes are shown by the horizontal lines in (a), including small corrections for the anharmonicity of the trap [Rie08]. The lines in (b) are introduced as guides to the eye. For $\tilde{T}$ greater than 1.14, the scissors mode oscillations are fit by a two-frequency cosine function (for details see text).

profiles in the manner described in [Kin05b, Kin06, Sta05]. At B = 834 G, for $T/T_F > 0.3$, the parameter $\tilde{T}$ is proportional to the real temperature with $T/T_F \approx \tilde{T}/1.5$. For lower temperatures, an empirical conversion has been determined[2] [Kin05b, Kin06, Sta05]. The parameter $\tilde{T}$, measured in the unitarity limit at 834 G, can be used also as a temperature scale for other interaction regimes under the condition that entropy is conserved in adiabatic sweeps of the magnetic field [Che05a].

In Figure 4.2, we show the frequency and damping rate as a function of $\tilde{T}$ for two cases, in the unitarity limit ($1/k_Fa = 0.00$) and at the BCS side of the crossover ($1/k_Fa = -0.45$). The frequency behavior in Fig. 4.2(a) is qualitatively the same for both cases. At low temperatures, the gas shows the hydrodynamic frequency and, at the highest temperatures, we observe the behavior characteristic for the collisionless gas. With varying temperature, the changing frequency smoothly connects the hydrodynamic with the collisionless regime. Quantitatively, the transition occurs at somewhat higher $\tilde{T}$ in the unitarity limit. In

[2] $\tilde{T} \approx 1.2(T/T_F)^{1.49}$ for $(T/T_F) < 0.3$.

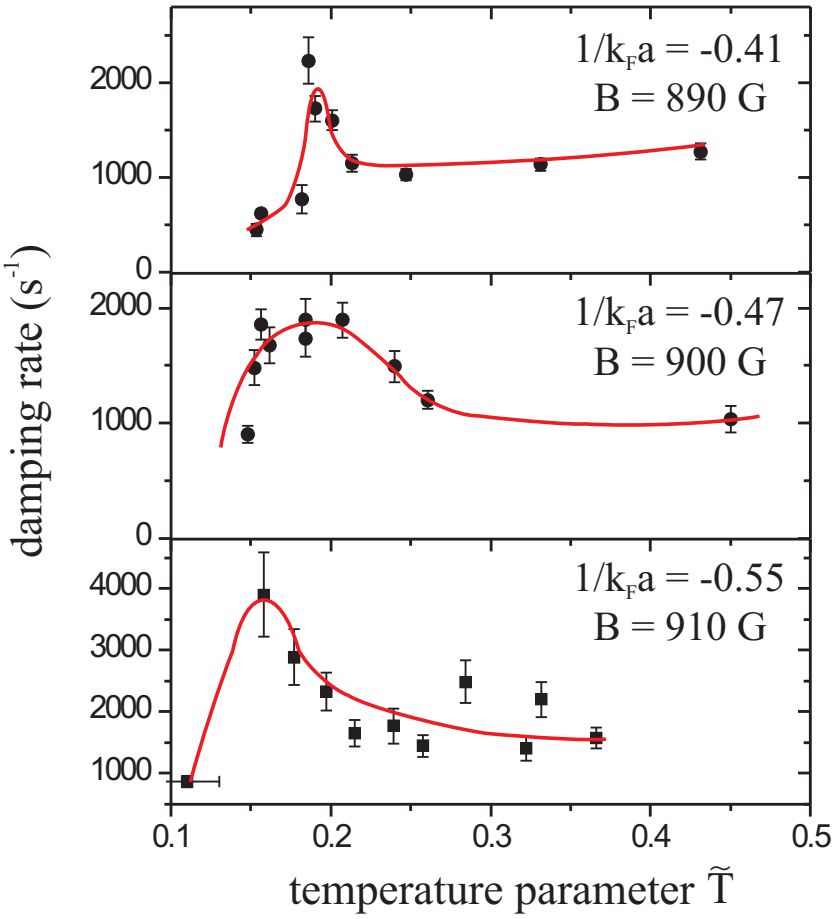

Fig. 4.3: Low-temperature damping peak observed in a narrow magnetic-field region at the BCS side of the resonance ($1/k_F a \approx -0.5$). The solid lines are introduced as guides to the eye.

the transition region, the damping rate shows a maximum that accompanies the change in frequency, see Fig. 4.2(b). We introduce the temperature parameter $\tilde{T}_H$ for this damping maximum, marking the transition between hydrodynamic and collisionless behavior.

The temperature dependence of the damping rate in Fig. 4.2(b) reveals a qualitatively different behavior between the two interaction regimes. An additional peak shows up at lower temperatures for the BCS side of the crossover, while this peak is absent in the unitarity limit. Remarkably, this novel feature is not associated with a change in the frequency.

We could detect the low-temperature damping peak only in a very narrow range at the BCS side of the crossover. This feature was found between magnetic fields of 890 G and 920 G, corresponding to interaction parameters $1/k_F a$ between -0.6 and -0.4. In Fig. 4.3, we show the low-temperature damping peak as it changes in this narrow region. Closer to resonance, the peak becomes very narrow, shifts toward higher temperatures, and finally seems to disappear.

To mark the location of this peak, we introduce the temperature parameter $\tilde{T}_S$.

We now discuss our observations in terms of a crossover phase diagram for the scissors mode excitation[3]. In Fig. 4.4(a), we plot $\tilde{T}_H$ (closed circles) and $\tilde{T}_S$ (open squares) as a function of the interaction parameter. The data points for $\tilde{T}_H$ show a pronounced maximum at the center of the resonance. To facilitate an interpretation of the experimental data, we convert $\tilde{T}_H$ and $\tilde{T}_S$ into real temperatures T_H and T_S, following the theory of Ref. [Che05a]. Fig. 4.4(b) shows the resulting phase diagram, including a theoretical prediction [Per04] (see also [Che05b]) of the temperature T_C for the phase transition to a superfluid state.

Near the center of the Feshbach resonance, hydrodynamic behavior is observed far above the superfluid transition temperature. The large difference between T_H and T_C confirms the existence of a non-superfluid hydrodynamic region above T_C [Min01, Kin05a, Cla07]. Our measurements show that this normal-gas hydrodynamic regime is restricted to the narrow, strongly interacting region near resonance where $1/k_F a$ stays well below unity. On the BEC side, T_H is close to the expected value for T_C. Here one can assume that hydrodynamic behavior essentially results from the formation of a molecular BEC. A surrounding non-condensed molecular gas would exhibit near-collisionless properties, similar to what has been measured in atomic BEC experiments [Mar01]. On the BCS side of resonance, T_H falls off very rapidly. In this region, collective modes may couple to the weakly bound fermion pairs [Bar04a, Alt07c]. We did not observe hydrodynamic behavior beyond that point.

For the low-temperature damping peak found at the BCS side of the crossover near $1/k_F a \approx -0.5$, our phase diagram in Fig. 4.4(b) suggests a close relation to the superfluid phase transition. The peak occurs at roughly $0.6\,T_C$, and it follows the general behavior of the superfluid transition to move toward higher temperature as it approaches the resonance. This points to a scenario where a substantial superfluid core in the center of the trap is surrounded by a non-superfluid, but still hydrodynamic fraction in the outer region of the trap. Whether damping results from the coupling of these two components or whether other mechanisms are responsible for this phenomenon remains an open question. We note that the low-temperature damping peak is not specific to the scissors mode. We have also found a corresponding, but less pronounced peak in measurements of the radial breathing mode. Further investigations and better theoretical understanding will be required to answer the intriguing question whether the novel damping peak does indeed mark the transition from the normal hydrodynamic to the superfluid state.

In conclusion, we have investigated hydrodynamic behavior at finite temperatures in the BEC-BCS crossover using scissors mode excitations. Our measurements highlight the existence of a region of non-superfluid hydrodynamics

[3] In a comparative study of different collective modes [Rie08] we found the scissors mode to behave very similar to the radial quadrupole mode [Alt07c], which is also a surface mode. The radial compression mode behaves quite differently [Kin05a, Rie08]. The axial mode [Bar04a] shows in general hydrodynamic behavior in a much wider parameter range because of its much lower frequency.

in the strongly interacting regime where $|k_F a| \gtrsim 1$. In the unitarity limit, predominant hydrodynamic behavior is found up to $\sim 0.6\, T_F$, which substantially exceeds the superfluid transition temperature of $\sim 0.3\, T_F$. With increasing temperature, the transition from hydrodynamic to collisionless behavior proceeds in general smoothly and is accompanied by a local maximum of damping. In addition, we have discovered a novel low-temperature damping peak at the BCS side of the crossover, which suggests a relation to the superfluid phase transition. With this observation, experiments on collective oscillation modes of Fermi gases in the BEC-BCS crossover continue to produce puzzling observations [Bar04a, Kin05a, Alt07c] with the potential to stimulate deeper theoretical understanding of the physics of strongly interacting Fermi gases.

We thank S. Stringari for stimulating discussions. We also thank Q. Chen, K. Levin, and J. E. Thomas for discussions concerning determination of the temperature. We acknowledge support by the Austrian Science Fund (FWF) within SFB 15 (project part 21). M.J.W. is supported by a Marie Curie Incoming International Fellowship within the 6th European Community Framework Program.

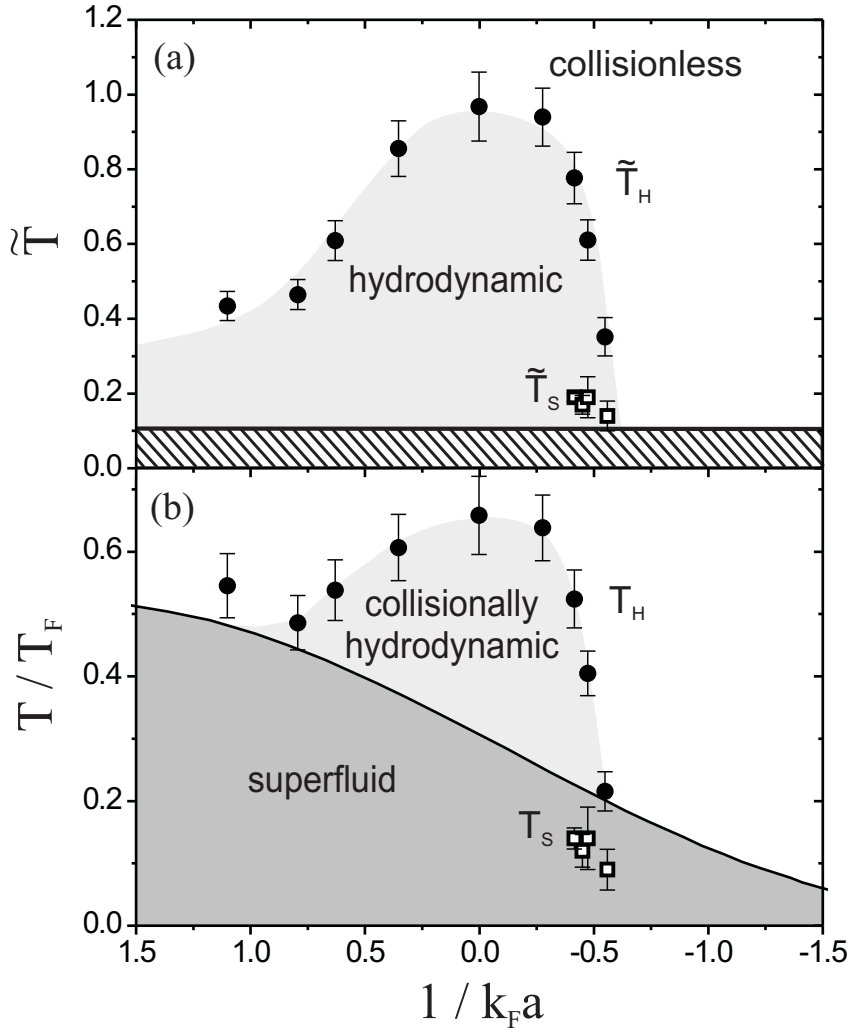

Fig. 4.4: Phase diagram for the hydrodynamic behavior of the scissors mode in terms of (a) the temperature parameter $\tilde{T}$ and (b) the real temperature T. The smooth transition from hydrodynamic to collisionless is characterized by the temperature parameter $\tilde{T}_H$ (temperature T_H). The second damping peak near $1/k_F a \approx -0.5$ is marked by $\tilde{T}_S$ (T_S). In (a) the hatched region indicates the region ($\tilde{T} < 0.1$) where our thermometry does not produce reliable results. In (b) the solid line shows a theoretical curve for the phase transition to superfluidity [Per04].

CHAPTER 5

Publication

Collective oscillations of a Fermi gas in the unitarity limit: Temperature effects and the role of pair correlations[†]

Phys. Rev. A 78, 053609 (2008)

S. Riedl,[1,2] E. R. Sánchez Guajardo,[1] C. Kohstall,[1] A. Altmeyer,[1,2] M. J. Wright,[1] J. Hecker Denschlag,[1] and R. Grimm[1,2]

[1] *Institut für Experimentalphysik und Zentrum für Quantenphysik, Universität Innsbruck, 6020 Innsbruck, Austria*

[2] *Institut für Quantenoptik und Quanteninformation, Österreichische Akademie der Wissenschaften, 6020 Innsbruck, Austria*

G. M. Bruun[3,4] and H. Smith[4]

[3] *Dipartimento di Fisica, Università di Trento and CNR-INFM BEC Center, I-38050 Povo, Trento, Italy*

[4] *Niels Bohr Institute, University of Copenhagen, DK-2100 Copenhagen Ø, Denmark*

We present detailed measurements of the frequency and damping of three different collective modes in an ultracold trapped Fermi gas of ^{6}Li atoms with resonantly tuned interactions. The measurements are carried out over a wide range of temperatures. We focus on the unitarity limit, where the scattering length is much greater than all other relevant length scales. The results are compared to theoretical calculations that take into account Pauli blocking and pair correlations in the normal state above the critical temperature for superfluidity. We show that these two effects nearly compensate each other and the behavior of the gas is close to that of a classical gas.

[†]The author of the present thesis performed all the measurements in this publication and analyzed the effect of anharmonicity on the collective modes. The theory part of this publication was done by G.M.B. and H.S.

5.1 Introduction

The study of collective oscillations in quantum liquids and gases has yielded a wealth of insights into the properties of strongly correlated systems. An early example concerning strongly correlated Fermions is the observed transition from ordinary first sound to zero sound in the normal state of liquid ^{3}He as the temperature is lowered [Abe66]. In this Article we explore related phenomena in an ultracold quantum gas of fermions in the unitarity limit [Ing08] by measuring three different collective modes under similar conditions. The frequency and damping of the modes exhibit the characteristic transition from hydrodynamic behavior at low temperature to collisionless behavior at higher temperature. The experimental observations are compared to theoretical model calculations that apply to the normal state of the gas above the critical temperature T_c for superfluidity. In the unitarity limit, the strongly correlated normal state between T_c and the Fermi temperature T_F is arguably not as well understood as the $T = 0$ superfluid phase [Gio08]. It is shown that the combined effects of temperature and pair correlations account for most of the observed features in this interesting temperature regime.

Our measurements of the collective modes are carried out for an elongated trap geometry, which has previously been shown to be well suited for studying the dynamical behavior of a strongly interacting Fermi gas [Bar04a, Kin04a, Kin04b, Kin05a, Alt07b, Alt07c, Wri07]. We focus on two collective excitations of a cylindrically symmetric cigar-shaped cloud, namely the radial compression mode and the radial quadrupole mode. In addition we study the scissors mode under conditions where the cloud exhibits pronounced ellipticity in the plane perpendicular to the direction of the cigar-shaped cloud. In all three modes, the cloud oscillates mainly in the plane normal to the direction of the cigar-shaped cloud. For a sketch of the modes see Fig. 5.1.

Previous experiments on collective modes in a strongly interacting Fermi gas studied the effect of the interaction strength in the zero-temperature limit. [Bar04a, Kin04a, Kin04b, Alt07b, Alt07c]. Systematic investigations were performed studying the radial compression mode [Bar04a, Kin04a, Alt07b] and the radial quadrupole mode [Alt07c]. Measurements on the compression mode served as a sensitive probe for the equation of state of the gas in the zero temperature limit throughout the BEC-BCS crossover regime. In contrast to the compression mode, the frequency of the radial quadrupole mode allows one to test the hydrodynamic behavior without being influenced by the equation of state. This made it possible to investigate the transition from hydrodynamic to collisionless behavior with decreasing coupling strength of the atom pairs on the BCS side of the crossover.

While the hydrodynamic behavior in the zero-temperature limit is now well understood as a result of superfluidity, an understanding of the effects of temperature on the collective modes has remained a challenge. Only few experiments have so far addressed this problem [Alt07b, Kin05a, Wri07, Kin04a]. Previously, the temperature dependence of the radial compression mode [Kin05a] and the

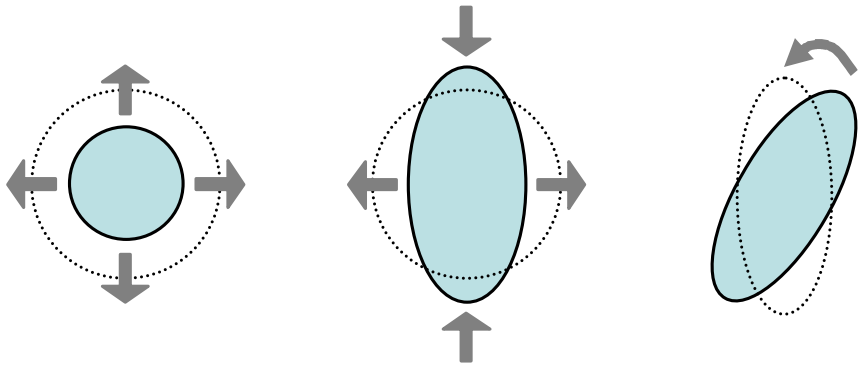

Fig. 5.1: Sketch of the three collective modes investigated in this work: the compression mode, the quadrupole mode and the scissors mode (from left to right). The oscillations take place in the plane of tight confinement, perpendicular to the direction of the elongated, cigar-shaped cloud. While the compression mode represents an oscillation of the overall cloud volume, the other two modes only involve surface deformations. Exciting the quadrupole mode leads to an oscillating elliptic shape. The scissors mode appears as an angular oscillation of an elliptic cloud about a principal axis of an elliptic trap geometry.

scissors mode was studied [Wri07]. Our present experiments aim at addressing the open questions raised by the different results obtained in these experiments: The frequency and damping of the radial compression mode was studied as function of the temperature in an experiment performed at Duke University [Kin05a]. There the mode frequency appeared to stay close to the hydrodynamic value even for temperatures exceeding the Fermi temperature. This surprising finding stands in contrast to scissors mode measurements, performed later at Innsbruck University [Wri07], which clearly showed a transition to collisionless behavior in the same temperature range. Furthermore the Duke data on the damping of the compression mode did not show a maximum as it was seen in the Innsbruck data on the scissors mode measurement. These apparent discrepancies are a particular motivation for our present study of different collective modes under similar experimental conditions.

5.2 Experimental Procedure

The apparatus and the basic preparation methods for experiments with a strongly interacting Fermi gas of ^{6}Li atoms have been described in our previous work [Joc03a, Bar04b]. As a starting point, we produce a molecular BEC of $^6Li_2$. By changing an external magnetic field, we can control the interparticle interactions in the vicinity of a Feshbach resonance, which is centered at 834 G [Bar05b]. The measurements of the collective modes are performed at the center of the Feshbach resonance, where the interactions are unitarity limited.

The atoms are confined in an elongated, nearly harmonic trapping potential, where the trap frequencies ω_x and ω_y in the transverse direction are much

	compression	quadrupole	scissors
$\omega_x/2\pi$ (Hz)	1100	1800	1600
$\omega_y/2\pi$ (Hz)	1100	1800	700
$\omega_z/2\pi$ (Hz)	26	32	30
T_F (μK)	1.8	2.7	1.9
V_0/k (μK)	19	50	40

Table 5.1: Trap parameters for the different modes.

larger then the axial trap frequency ω_z. The confinement in the transverse direction is created by an optical dipole trap using a focused 1030 nm laser beam with a waist of 47 μm. Note that the Gaussian shape of the laser beam leads to significant anharmonicities in the trapping potential. The potential in the axial direction consists of a combination of optical and magnetic confinement; the magnetic confinement is dominant under the conditions of the present experiments. The trap parameters, given in Table 5.1, represent a compromise between trap stability and anharmonic effects[1]. The Fermi temperature is given by $T_F = E_F/k$, where the Fermi energy $E_F = \hbar(3N\omega_x\omega_y\omega_z)^{1/3} = \hbar^2k_F^2/2m$, k_F is the Fermi wavenumber and k is the Boltzmann constant. The parameter V_0 is the trap depth, and N is the total number of atoms, given by $N = 6 \times 10^5$. The interactions are characterized by the dimensionless parameter $1/k_Fa$, where a is the s-wave scattering length.

To control the aspect ratio ω_x/ω_y, we use rapid spatial modulation of the trapping beam by two acousto-optical deflectors, resulting in the creation of time-averaged trapping potentials [Alt07c]. This on one hand allows us to compensate for residual ellipticity of the trapping potential on the percent level and thus to realize a cylindrical symmetric trap ($\omega_x = \omega_y$). On the other hand it allows for the excitation of surface modes by deliberately introducing elliptic trapping potentials ($\omega_x \neq \omega_y$). The procedures used to excite the modes are outlined in Appendix A. To change the temperature we apply a controlled heating scheme via sudden compression of the gas as described in [Wri07]. Detection of the cloud is done by absorption imaging which displays the shape of the cloud in the x-y plane after expansion. For each mode under investigation we determine the frequency and damping following the procedures of our previous work [Alt07c, Wri07, Alt07b]; see also Appendix A.

Because of the Gaussian shape of the trapping potential, corrections are needed for a precise comparison of the experimental observation to the idealized case of perfect harmonic trapping. Especially for higher temperatures, when the size of the cloud is larger, anharmonic corrections become important. This

[1] Anharmonic effects depend on the ratio between the Fermi energy and trap depth E_F/V_0 [Str]. Reducing this ratio decreases the anharmonic effects. This can be done by increasing the power of the trapping beam since the E_F increases slower then V_0 because of the magnetic trapping along the axial direction. On the other hand we find larger heating rates and larger drifts in the trap depth with increasing power.

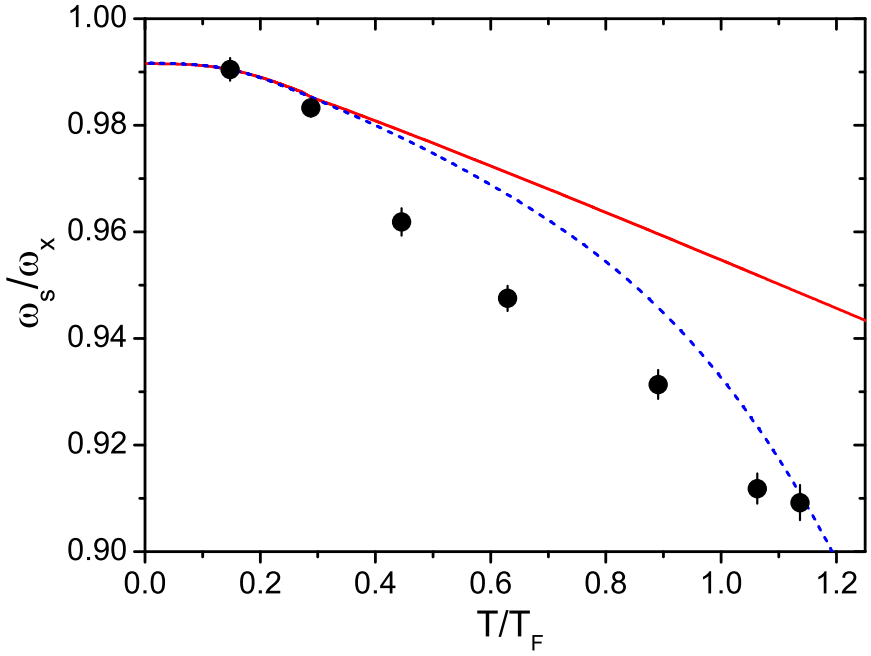

Fig. 5.2: Sloshing mode frequency ω_s normalized by the trap frequency ω_x as a function of temperature. The measured frequency shows a decrease with increasing temperature, (dots) which is due to the increase in the size of the cloud. The lines show the expected frequency from a first-order anharmonic correction; see Appendix B. To determine the cloud size for different temperatures we assume a harmonic potential (solid line) and a Gaussian potential (dashed line), respectively. The calculation of $\langle x^2 \rangle$ is based on density profiles derived by Q. Chen, J. Stajic, and K. Levin; see Ref. [Che05a]

is demonstrated by measurements of the transverse sloshing mode frequency ω_s (Fig. 5.2), which clearly show a substantial decrease with increasing temperature. To reduce the anharmonic effects on the frequencies of the collective modes under investigation, we normalize the compression and quadrupole collective mode frequencies to the sloshing mode frequency in the transverse direction. This normalization reduces the anharmonic effects to a large extent since the decrease of the sloshing mode frequency with increasing cloud size is of the same order as the corresponding decrease of the frequency of the transverse modes [Str]. To normalize the scissors mode frequency we take the geometric average of the two different sloshing mode frequencies in the transverse direction.

For each of the trap parameters of the different modes we determine the sloshing mode frequency as a function of the temperature. As an example we show ω_s for the trap parameters used for the compression mode measurement; see Fig. 5.2. We compare ω_s/ω_x (dots) to a theoretical model which allows us to calculate the sloshing frequency as a function of the cloud size; see Appendix B. Assuming a harmonic potential to derive the mean squared size $\langle x^2 \rangle$ underestimates the anharmonic effects (solid line) in particular for higher temperatures. Taking into account a Gaussian potential[1] to determine $\langle x^2 \rangle$ (dashed line) gives

results that agree much better with the measured sloshing frequency.

Since the purpose of this article is a comparative study of different collective modes and not the precision measurement of a single mode as in previous work [Alt07b], we follow a faster yet simpler procedure to normalize the frequencies. We measure the sloshing mode frequency only on particular temperatures of interest. From these points we determine the temperature dependence of the sloshing frequency by interpolation. Even though the normalization takes into account the temperature dependence of the anharmonicity, it does not reduce effects due to drifts in the power of the trapping beam. We believe this to be the main source for the scatter of the data in Fig. 5.4.

To determine the temperature of the gas we first adiabatically change the magnetic field to 1132 G [2], where $1/k_F a \approx -1$, to reduce the effect of interactions on the density distribution [Luo07]. Under this condition, for $T > 0.2T_F$, the interaction effect on the density distribution is sufficiently weak to treat the gas as a non-interacting one to determine the temperature from time-of-flight images. We fit the density distribution after 2 ms release from the trap to a finite-temperature Thomas-Fermi profile. The temperature measured at 1132 G is converted to the temperature in the unitarity regime under the assumption that the conversion takes place isentropically, following the approach of Ref. [Che05a]. Statistical uncertainties for the temperature stay well below $0.05T_F$.

5.3 Theory

We shall compare our experimental findings to the results of model calculations that apply to the normal state of the gas, i.e. at temperatures above T_c. In this Section, we outline our theoretical approach to the calculation of mode frequencies for $T > T_c$. A more detailed description can be found in Refs. [Mas05] and [Bru05]. We assume that single-particle excitations are reasonably well defined in the sense that most of the spectral weight of the single-particle spectral function is located at a peak corresponding to that of non-interacting particles. The low-energy dynamics of the gas can then be described by a semiclassical distribution function $f(\mathbf{r}, \mathbf{p}, t)$ which satisfies the Boltzmann equation. A collective mode corresponds to a deviation $\delta f = f - f^0$ away from the equilibrium distribution $f^0(\mathbf{r}, \mathbf{p})$. Writing $\delta f(\mathbf{r}, \mathbf{p}, t) = f^0(\mathbf{r}, \mathbf{p})[1 - f^0(\mathbf{r}, \mathbf{p})]\Phi(\mathbf{r}, \mathbf{p}, t)$ and linearizing the Boltzmann equation in $\delta f(\mathbf{r}, \mathbf{p}, t)$ yields

$$f^0(1 - f^0)\left(\frac{\partial \Phi}{\partial t} + \dot{\mathbf{r}} \cdot \frac{\partial \Phi}{\partial \mathbf{r}} + \dot{\mathbf{p}} \cdot \frac{\partial \Phi}{\partial \mathbf{p}}\right) = -I[\Phi], \tag{5.1}$$

where $\dot{\mathbf{r}} = \mathbf{v} = \mathbf{p}/m$, $\dot{\mathbf{p}} = -\partial V/\partial \mathbf{r}$ and I is the collision integral. We take the potential $V(\mathbf{r})$ to be harmonic and given by $V(\mathbf{r}) = m(\omega_x^2 x^2 + \omega_y^2 y^2 + \omega_z^2 z^2)/2$.

To describe the collective modes we expand the deviation function in a set of basis functions ϕ_i according to

$$\Phi(\mathbf{r}, \mathbf{p}, t) = e^{-i\omega t} \sum_i c_i \phi_i(\mathbf{r}, \mathbf{p}), \tag{5.2}$$

[2] This is the largest magnetic field where absorption images can be taken.

where ω is the mode frequency. For the compression mode with a velocity field $\mathbf{v} \propto (x, y, z)$, we use the functions

$$\phi_1 = x^2 + y^2,\ \phi_2 = xp_x + yp_y,\ \phi_3 = p_x^2 + p_y^2,\ \phi_4 = p_z^2. \tag{5.3}$$

For the quadrupole mode with a velocity field $\mathbf{v} \propto (y, x, 0)$ (ignoring the small velocity along the axial direction), we use

$$\phi_1 = x^2 - y^2,\ \phi_2 = xp_x - yp_y,\ \phi_3 = p_x^2 - p_y^2, \tag{5.4}$$

whereas the basis functions for the scissors mode are given in Ref. [Bru07]. Our choice of basis functions is physically motivated by the characteristic features of the three different modes illustrated in Fig. 5.1. Since we limit ourselves to a few simple functions, the basis sets are not complete, but we do not expect qualitative changes to occur as a result of including more basis functions in our calculation.

We now insert the expansion (5.2) into (5.1) and take moments by multiplying with the functions ϕ_i and integrating over both $\mathbf{r}$ and $\mathbf{p}$. This yields a set of linear equations for the coefficients c_i for each of the collective modes. The corresponding determinants give the mode frequencies. For the compression mode, we obtain

$$i\omega(\omega^2 - 4\omega_\perp^2) + \frac{1}{\tau}\left(\frac{10}{3}\omega_\perp^2 - \omega^2\right) = 0, \tag{5.5}$$

and for the quadrupole mode, we get

$$i\omega(\omega^2 - 4\omega_\perp^2) + \frac{1}{\tau}\left(2\omega_\perp^2 - \omega^2\right) = 0. \tag{5.6}$$

The equation for the scissors mode is given in Ref. [Bru07].

The effective collision rate $1/\tau$ in (5.5) and (5.6) is given by

$$\frac{1}{\tau} = \frac{\int d^3r d^3p p_x p_y I[p_x p_y]}{\int d^3r d^3p p_x^2 p_y^2 f^0(1 - f^0)}. \tag{5.7}$$

Note that this expression for $1/\tau$ involves a spatial average over the cloud. In the collisionless limit, $\omega\tau \gg 1$, the two equations (5.5) and (5.6) both yield $\omega = 2\omega_\perp$, where $\omega_\perp = \omega_x = \omega_y$, while in the hydrodynamic limit, $\omega\tau \ll 1$, they result in $\omega = \sqrt{10/3}\omega_\perp$ for the compression mode and $\omega = \sqrt{2}\omega_\perp$ for the quadrupole mode.

The dependence on temperature T and scattering length a enters through τ. In particular, Pauli blocking and pair correlations strongly depend on T and a, and we now examine their role on the effective collision rate. In Fig. 5.3, we plot $1/\tau$ as a function of temperature for a gas in the unitarity limit $|a| \to \infty$ using three different approximations for the collision integral. First, the dashed curve gives the effective collision rate in the classical regime using the vacuum expression $\mathcal{T}_{\rm vac} = \mathcal{T}_0/(1 + iqa)$ for the scattering matrix with $\mathcal{T}_0 = 4\pi\hbar^2 a/m$.

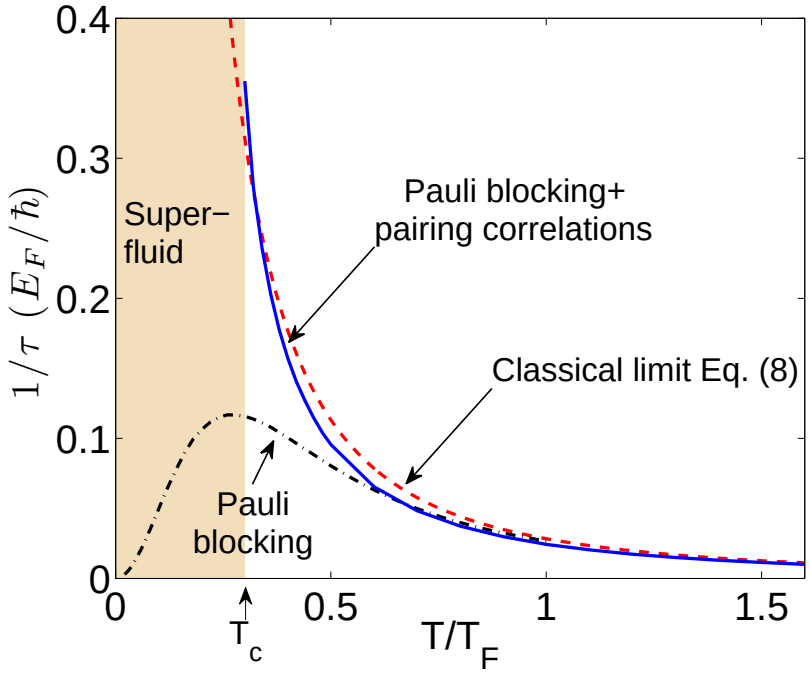

Fig. 5.3: (Color online) The effective collision rate for a gas in the unitarity limit. The dashed curve is the classical result, the dash-dotted includes Pauli blocking, and the solid line includes pairing correlations in the scattering matrix. The superfluid region for $T < T_c$ is indicated.

The s-wave differential cross section $d\sigma/d\Omega$ which enters in the collision integral I is related to the scattering $\mathcal{T}$ matrix by $d\sigma/d\Omega = m^2|\mathcal{T}|^2/(4\pi\hbar^2)^2$. In the classical regime, we then get from (5.7)

$$\frac{1}{\tau_{\rm class}} = \frac{4}{45\pi}\frac{kT_F}{\hbar}\frac{T_F^2}{T^2} \tag{5.8}$$

for a gas in the unitarity limit [Bru07]. The small prefactor $4/(45\pi) \approx 0.028$ in (5.8) implies that the effective collision rate is significantly smaller than what one would expect from simple estimates or dimensional analysis at unitarity. Second, the dash-dotted curve gives the effective collision rate when Pauli blocking effects are included as in [Mas05], while we still use the vacuum expression $\mathcal{T}_{\rm vac}$ for the scattering matrix. Pauli blocking effects reduce the available phase space for scattering thereby reducing the scattering rate. For $T \ll T_F$ Pauli blocking in a normal Fermi system gives $1/\tau \propto T^2$. Finally, we plot as a solid curve in Fig. 5.3 the effective collision rate taking into account both Pauli blocking and many-body effects for $\mathcal{T}$ in the ladder approximation which includes the Cooper (pairing) instability. This gives $\mathcal{T} = \mathcal{T}_0/(1-\mathcal{T}_0\Pi)$ where Π is the pair propagator. Since our treatment of the pair correlations only apply to the normal state of the gas, we plot this curve for temperatures greater than the critical temperature T_c, which within the ladder approximation used here is given by $T_c \approx 0.3T_F$ for

a trap [Bru05].

We see that $1/\tau$ is increased by the pairing correlations for the $\mathcal{T}$-matrix. The pairing correlations significantly increase the effective collision rate for temperatures $(T-T_c)/T_c \lesssim 1$ [Bru05]. One often refers to this temperature range as the pseudogap regime. In fact, pairing correlations almost cancel the Pauli blocking effect in the collision integral above T_c and $1/\tau$ is fairly accurately given by the classical value as can be seen from Fig. 5.3. At high temperatures, this cancelation can be demonstrated analytically by carrying out a high-temperature expansion of (5.7). We obtain after some algebra the simple expression

$$\frac{1}{\tau} = \frac{1}{\tau_{\rm class}} \left[1 + \frac{1}{32} \left(\frac{T_F}{T} \right)^3 \right] . \tag{5.9}$$

The presence of the small prefactor 1/32 in (5.9) shows that the leading correction to the classical limit is less than 3% at temperatures above the Fermi temperature T_F.

5.4 Results and Discussion

The theoretical results of the previous section were all obtained for a purely harmonic potential. Since anharmonicity plays an important role in our experiments, as discussed in Sec. 5.2, we normalize the measured frequencies and damping rates for the collective modes to the measured temperature-dependent sloshing frequencies, for which an example is shown in Fig. 5.2. In the following we compare our observations to the theoretical results. It should be emphasized that the theoretical expressions for the frequency and damping contain no free parameters to fit theory and experiment.

First we discuss the frequency for the three modes under investigation as a function of the temperature, as plotted in Fig. 5.4. In all three cases the theoretical expression for the frequency (the full lines in Fig. 5.4) smoothly changes from the hydrodynamic value at the lowest temperature considered to the collisionless value at high temperatures. The normalized frequencies in the hydrodynamic limit for the quadrupole mode and compression mode are $\sqrt{2} \approx 1.41$ and $\sqrt{10/3} \approx 1.83$, respectively. The normalized frequency in the collisionless limit for both these modes is 2. Using the geometric average of the trap frequencies to normalize the scissors mode frequency, one gets, using the ratio $\omega_x/\omega_y = 16/7$ from Table I, that $\sqrt{(\omega_x^2+\omega_y^2)/(\omega_x\omega_y)} \approx 1.64$ in the hydrodynamic limit and $(\omega_x+\omega_y)/\sqrt{\omega_x\omega_y} \approx 2.17$ in the collisionless limit. Note that the scissors mode consists of a two-frequency oscillation in the collisionless limit. Here we only consider the larger frequency component. The lower frequency component exhibits increasing damping toward lower temperatures and disappears in the hydrodynamic limit [GO99a].

Figure 5.4 illustrates that there is a reasonable overall agreement between experiment and theory, although some differences exist. The agreement is best for

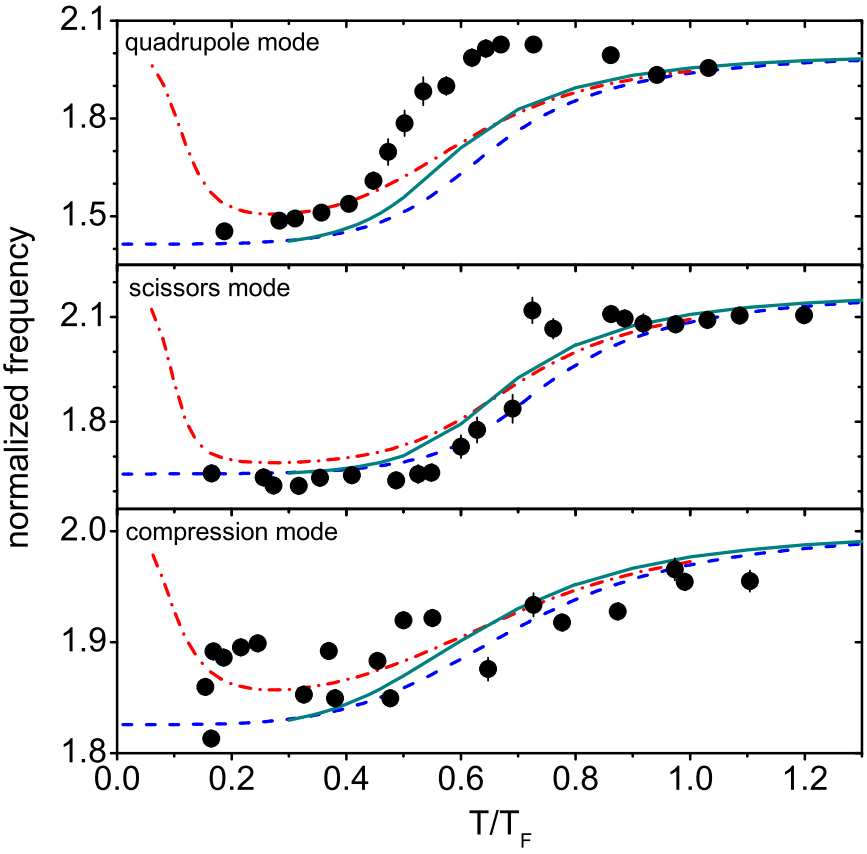

Fig. 5.4: Observed normalized mode frequencies versus temperature for the quadrupole mode, the scissors mode and the compression mode. The error bars indicate the statistical error of a single frequency measurement. The full lines are the result of the theory for the normal state described in section 5.3, which includes the combined effects of Pauli blocking and pair correlations; note that these curves start at $T = 0.3T_F$, which in the ladder approximation used here is the transition temperature to the superfluid state. For illustrative purposes we also show the theoretical results when only Pauli blocking is taken into account (dash-dotted lines) and those for a classical gas (dashed lines).

the scissors mode, while for the quadrupole mode the changeover from hydrodynamic to collisionless behavior happens at a lower temperature than the one found theoretically. The measured compression mode frequency, which shows considerable scatter, increases with increasing temperature and is close to the collisionless value at the highest temperature measured.

The observed change from the hydrodynamic to the collisionless frequency for the compression mode is in contrast to Ref. [Kin05a], where the frequency remains close to the hydrodynamic value for the same temperature range. We attribute this discrepancy to different treatments of anharmonic effects, which are particularly important for this mode since the difference between the hydrodynamic and collisionless frequency is of the same order as the frequency shift due to anharmonic effects. In Ref. [Kin05a] the data are corrected by including

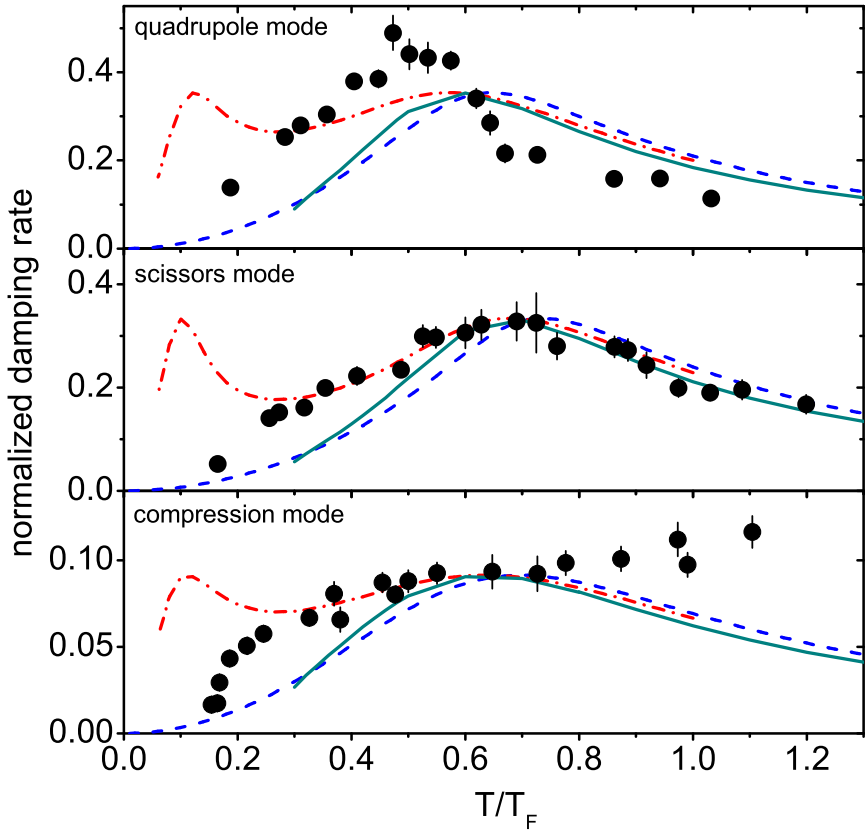

Fig. 5.5: Normalized mode damping versus temperature for the quadrupole mode, the scissors mode and the compression mode. The points are experimental values, while the full lines represent our calculated values, taking into account both Pauli blocking and pairing effects. The dash-dotted line only takes Pauli blocking into account, while the dashed line is the classical (high-temperature) result.

anharmonic effects to first order, while we adopt the point of view that the main anharmonic effects can be taken into account by normalizing the measured oscillation frequencies to the measured temperature-dependent sloshing frequencies. Figure 5.2 illustrates that a simple first-order treatment of anharmonic effects on the sloshing frequency does not account quantitatively for the observed variation with temperature.

At very low temperatures the measured frequencies are close to the hydrodynamic values because the gas is in the superfluid phase [Alt07b, Alt07c]. Without pair correlations, but with Pauli blocking, at these low temperatures the frequencies would assume their collisionless values as illustrated by the dash-dotted lines in Fig. 5.4.

We now proceed to consider the damping of the oscillations. The experimental values for the normalized damping rate are shown in Fig. 5.5. Theoretically, one expects the damping to vanish in the hydrodynamic and collisionless limits and exhibit a maximum in between, as brought out by the calculations in

Sec. 5.3. Experimentally, both the quadrupole and the scissors mode exhibit the expected maximum in damping in the transition region. For the compression mode, however, the damping does not decrease at higher temperatures. This surprising behavior for the compression mode has already been found in [Kin05a]. A possible reason for the increasing damping is dephasing-induced damping due to anharmonicity. Anharmonic effects are more important for the compression mode as the intrinsic damping is relatively small due to the small difference between the frequencies in the collisionless and hydrodynamic limits [GO99b]. In contrast to the case of frequency discussed above, we cannot expect to take into account the main effects of anharmonicity by normalizing the measured damping rate to the temperature-dependent sloshing mode frequencies. This makes it delicate to compare our experimental results to those of a theory based on a purely harmonic potential. The damping of the quadrupole mode shows the expected qualitative behavior, although the maximum in damping happens at a lower temperature compared to theory. This is consistent with the frequency data for this mode, since the transition there also happens at lower temperature. For the scissors mode the experimental data agree fairly well with theory, although some discrepancy exists at the lowest temperatures.

We can relate the frequency and damping of the quadrupole mode directly to each other by eliminating the collision rate $1/\tau$ in (5.6). Writing $\omega = \omega_Q - i\Gamma_Q$ for the solution of (5.6) with ω_Q and Γ_Q being the quadrupole frequency and damping, we obtain

$$\Gamma_Q = \sqrt{-\omega_\perp^2 - \omega_Q^2 + \sqrt{8\omega_Q^2 - 7\omega_\perp^2}}. \tag{5.10}$$

A similar relation holds for the two other modes. This allows us to compare theory and experiment independently of any approximations involved in the evaluation of $1/\tau$. Figure 5.6 shows the normalized damping rate versus the normalized frequency of the quadrupole and the scissors mode; we do not show the data for the compression mode because of the apparent problems discussed before. We find that the maximum damping of the quadrupole mode is larger than expected. For the scissors mode the damping is larger only at low frequencies. This suggests that the difference between theory and experiment is not a consequence of the approximations entering the calculation of the relaxation rate but could be due to anharmonic effects or the need for larger basis sets to describe the modes [see (5.3) and (5.4)].

5.5 Conclusion

In this work we have presented measurements of the frequency and damping of three different collective modes under similar conditions for an ultracold Fermi gas of ^{6}Li atoms in the unitarity limit. The experimental results obtained in the normal state of the gas are in reasonable agreement with our theoretical calculations, which take into account Pauli blocking and pair correlations. The

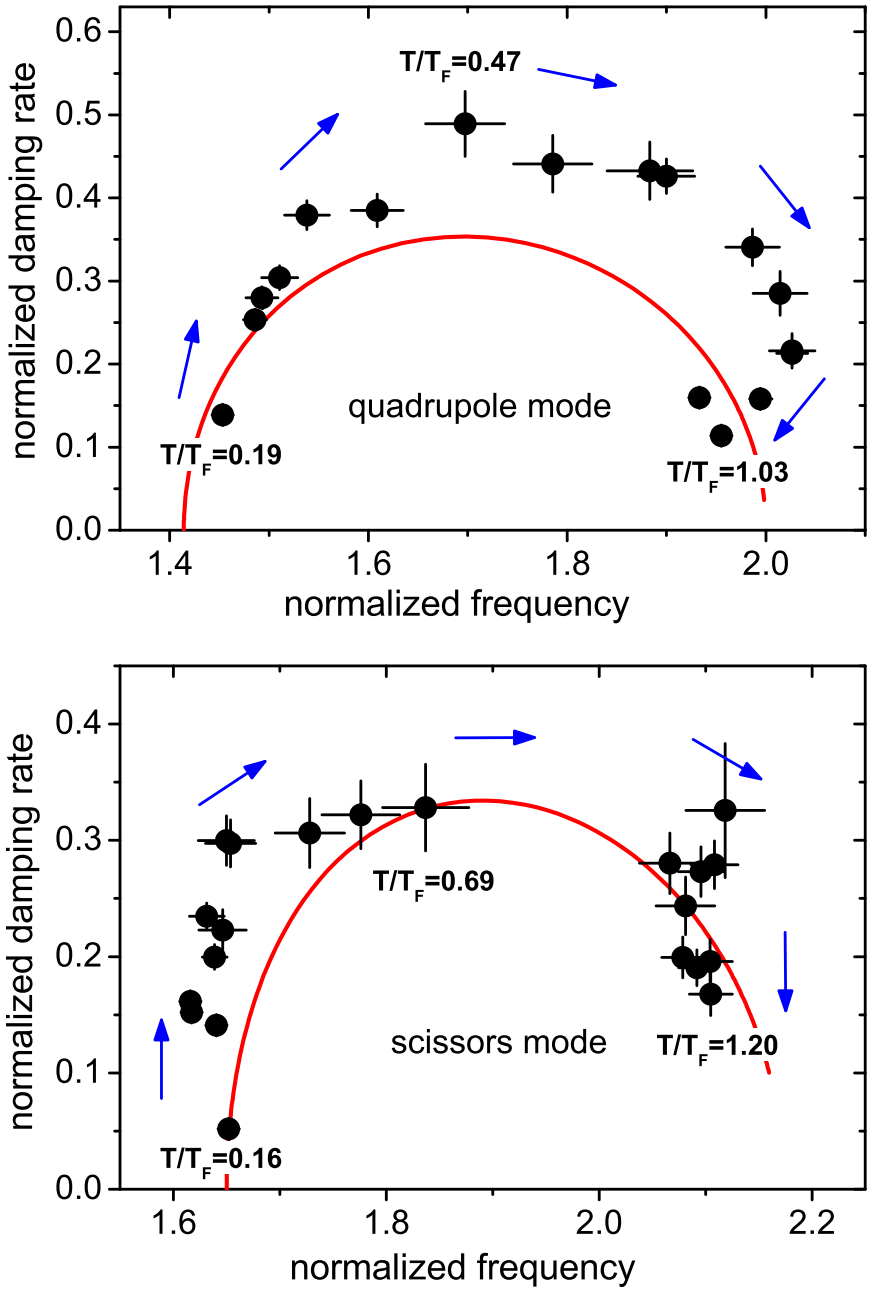

Fig. 5.6: Normalized mode damping versus normalized frequency for the quadrupole and scissors mode. The solid line shows the expected behavior for a harmonic trap. The arrows point toward the direction of increasing temperature.

remaining discrepancies may originate in a variety of sources such as our treatment of anharmonic effects, the temperature calibration, and the use of a restricted basis for solving the Boltzmann equation. Also they may reflect the need to incorporate further interaction effects in the kinetic equation, which forms the starting point for the theoretical calculations. For instance, there are self-energy shifts on the left-hand side of the kinetic equation which could be important. The study of collective modes is a sensitive probe of the properties of strongly interacting particles such as the gas of ^{6}Li atoms under investigation, and further work on temperature-dependent phenomena will undoubtedly shed more light on these interesting many-body systems.

Acknowledgments
We acknowledge support by the Austrian Science Fund (FWF) within SFB 15 (project part 21). M.J.W. was supported by a Marie Curie Incoming International Fellowship within the 6th European Community Framework Program. Fruitful discussions with S. Stringari are appreciated. We thank Q. Chen and K. Levin for providing us with density profiles and temperature calibration curves.

5.6 Appendix A

Here we present more details of the experimental procedures used to excite the three collective modes.

To excite the radial quadrupole mode we adiabatically deform the radially symmetric trap to an elliptic shape while keeping the average trap frequency constant before turning off the deformation suddenly [Alt07c]. The deformation is chosen such that the amplitude of the mode oscillation relative to the cloud size is below 10%. A two-dimensional Thomas-Fermi profile is fitted to the images, taken after a short expansion time of 0.5 ms. The difference in the width of the main axes is determined for different hold times and fitted to a damped sine function, from which we determine the frequency and damping of the mode.

The excitation of the radial compression mode is done by a sudden compression of the cloud. To determine the frequency and damping of the compression mode we follow the same procedure as for the quadrupole mode but fitting to the sum of the widths. Here we use an expansion time of 2 ms before taking the image.

The scissors mode appears as an angular oscillation of an elliptic cloud about a principal axis of an elliptic trap. To excite this oscillation we create an elliptic trap in the $x - y$ plane and suddenly rotate the angle of the principal axes by 5 degrees [Wri07]. The tilt of the principal axes of the cloud is determined 0.8 ms after releasing the cloud from the trap for different hold time. If the gas is hydrodynamic, we fit a single damped sine function to the oscillation of the angle. However, for a collisionless gas, the oscillation exhibits two frequencies. Thus we fit a sum of two damped sine functions each with their own free parameters. When the behavior changes from hydrodynamic to collisionless the single damped sine function fits the data reasonably well, as discussed in [Wri07].

Since the larger of the two frequencies in the collisionless regime smoothly connects to the hydrodynamic frequency at low temperatures we only consider this frequency in the paper.

5.7 Appendix B

Here we briefly discuss the calculation of the transverse sloshing modes including anharmonic corrections to lowest order. The transverse trapping potential is

$$V(x,y) = V_0(1 - e^{-x^2/a^2 - y^2/b^2}) \simeq$$
$$V_0\left(\frac{x^2}{a^2} + \frac{y^2}{b^2} - \frac{x^4}{2a^4} - \frac{y^4}{2b^4} - \frac{x^2y^2}{a^2b^2}\right). \tag{5.11}$$

Concentrating without loss of generality on the sloshing mode in the x-direction, we choose the function $\Phi = c_1 x + c_2 p_x$. Putting this into the linearized Boltzmann equation (5.1), eliminating c_2, and taking the moment $\int dxdyn(x,y)$ with $n(x,y)$ the density (we ignore the axial direction), we obtain for the sloshing frequency

$$\omega_s^2 = \omega_x^2\left(1 - \frac{m\omega_x^2\langle x^2\rangle + m\omega_y^2\langle y^2\rangle}{2V_0}\right). \tag{5.12}$$

Here $\langle x^2\rangle = \int n(x,y)x^2dxdy/\int n(x,y)dxdy$ and we have used $\omega_x^2 = 2V_0/ma^2$ together with $\omega_y^2 = 2V_0/mb^2$.

CHAPTER 6

Publication

Lifetime of angular momentum in a rotating strongly interacting Fermi gas[†]

Phys. Rev. A 79, 053628 (2009)

S. Riedl,[1,2] E. R. Sánchez Guajardo,[1,2] C. Kohstall,[1,2] J. Hecker Denschlag,[1] and R. Grimm[1,2]

[1] *Institut für Experimentalphysik und Zentrum für Quantenphysik, Universität Innsbruck, 6020 Innsbruck, Austria*

[2] *Institut für Quantenoptik und Quanteninformation, Österreichische Akademie der Wissenschaften, 6020 Innsbruck, Austria*

We investigate the lifetime of angular momentum in an ultracold strongly interacting Fermi gas, confined in a trap with controllable ellipticity. To determine the angular momentum we measure the precession of the radial quadrupole mode. We find that in the vicinity of a Feshbach resonance, the deeply hydrodynamic behavior in the normal phase leads to a very long lifetime of the angular momentum. Furthermore, we examine the dependence of the decay rate of the angular momentum on the ellipticity of the trapping potential and the interaction strength. The results are in general agreement with the theoretically expected behavior for a Boltzmann gas.

6.1 Introduction

The dynamics of an ultracold quantum gas is an important source of information on the physical nature of the system. A particularly interesting situation is an atomic Fermi gas in the vicinity of a Feshbach resonance [Ing08, Gio08]. The

[†]The author of the present thesis developed the experimental procedure, performed the measurements and made the data analysis for this publication. Thereby he was supported by E.R.S.G. and C.K..

Feshbach resonance allows us to tune the two-body interaction and thus to control the coupling between the atoms. It connects a molecular Bose-Einstein condensate (BEC) with a Bardeen-Cooper-Schrieffer (BCS) superfluid. In the crossover region between these two limiting cases, the center of the Feshbach resonance is of special interest. Here the unitarity-limited interactions lead to universal behavior of the Fermi gas.

The strong two-body interactions close to the Feshbach resonance lead to very low viscosity and hydrodynamic behavior in the normal phase, similar to the properties of a superfluid [Cla07, Wri07]. The coexistence of normal and superfluid hydrodynamic behavior is a special property of the strongly interacting Fermi gas, which stands in contrast to ultracold Bose gases, where deep hydrodynamic behavior is usually restricted to the superfluid condensate fraction. The low-viscosity hydrodynamic behavior leads to a long lifetime of collective motion in the system. Using collective modes the dynamics has been investigated in a broad range of temperatures and interaction strengths in the crossover region [Cla07, Wri07, Bar04a, Kin04a, Kin04b, Kin05a, Alt07b, Alt07c, Rie08], including the hydrodynamic regime in the normal phase. Another important collective motion is the rotation of the gas, which is of particular interest in relation to superfluidity [Zwi05a].

In this Article, we study the lifetime of the angular momentum of a rotating strongly interacting Fermi gas. We determine the angular momentum using the precession of the radial quadrupole mode. This method is well established to study the angular momentum in experiments with BEC [Che00, Hal01a, Lea02]. We observe that the unique hydrodynamic behavior of the strongly interacting Fermi gas leads to particularly long lifetimes of the angular momentum. We perform a quantitative analysis of the dissipation of the angular momentum caused by the trap anisotropy for a gas in the unitarity limit. The measurements show general agreement with the expected behavior for a Boltzmann gas [GO00]. As shown in a previous study comparing experiment and theory [Rie08], a Boltzmann gas describes the behavior of a gas in the normal state with unitarity-limited interactions reasonably well. Finally we study the dependence of the lifetime on the interaction strength of the gas in the crossover region between the BEC and BCS regime.

6.2 Experimental procedure

To realize an ultracold strongly interacting Fermi gas we trap and cool an equal mixture of ^{6}Li atoms in the lowest two atomic states as described in our previous work [Joc03a, Alt07c]. We control the interparticle interaction by changing the external magnetic field in the vicinity of a broad Feshbach resonance centered at 834 G [Bar05b]. The atoms are held by an optical dipole trap using a red-detuned single focused laser beam and an additional magnetic trap along the beam; this magnetic confinement dominates over the optical confinement along the beam under the conditions of the present experiments. The resulting trap provides weak confinement along the beam (z axis) and stronger transverse confinement

(x-y plane), leading to a cigar-shaped cloud. The trap is well approximated by a harmonic potential with trap frequencies $\omega_x \approx \omega_y \approx 2\pi \times 800\,\mathrm{Hz}$ and $\omega_z = 2\pi \times 25\,\mathrm{Hz}$. The trap, in general, also has a small transverse ellipticity, which can be controlled during the experiments. We define an average transverse trap frequency as $\omega_r = \sqrt{\omega_x \omega_y}$. The Fermi energy of the noninteracting gas is given by $E_F = \hbar(3N\omega_x\omega_y\omega_z)^{1/3} = \hbar^2 k_F^2/2M$ where $N = 5\times10^5$ is the total atom number, M is the atomic mass, and k_F is the Fermi wave number. The corresponding Fermi temperature is $T_F = E_F/k = 1.3\,\mu\mathrm{K}$, with k as the Boltzmann constant. The interaction strength is characterized by the dimensionless parameter $1/k_F a$, where a is the atomic s-wave scattering length.

To dynamically control the shape of the trapping potential in the transverse plane, we use a rapid spatial modulation of the trapping laser beam by two acousto-optical deflectors, which allows us to create time-averaged trapping potentials [Alt07c]. The control over the potential shape has two different applications for the measurements. As a first application we use it to adjust the static ellipticity $\epsilon = (\omega_x^2 - \omega_y^2)/(\omega_x^2 + \omega_y^2)$ of the trap in the x-y plane. This allows us to compensate for residual ellipticity of the trapping potential, i.e., of the trapping laser beam, and also to induce a well defined ellipticity. The second application is the creation of a rotating elliptic potential with a constant ellipticity ϵ' [1]. This is needed to spin up the gas. Both the static ellipticity in the x-y plane and the rotating elliptic potential can be controlled independently. To determine the ellipticity we measure the frequency of the sloshing mode along the two principal axes of the elliptic potential. This allows controlling the ellipticity with an accuracy down to typically 0.005.

To measure the angular momentum of the cloud, we exploit the fact that collective excitation modes are sensitive to the rotation of the cloud. Here we use the precession of the radial quadrupole mode to determine the angular momentum of the rotating cloud; see Fig. 6.1. This method works under the general condition that the gas behaves hydrodynamically [Che03]. In our case of a strongly interacting Fermi gas, this method probes both the superfluid and the classically hydrodynamic part and does not distinguish between these two components. For the case of atomic BEC, the precession has been well studied in theory [Sin97, Dod97, Svi98, Zam98] and used in experiments to determine the angular momentum of the BEC [Che00, Hal01a, Lea02]. For an atomic BEC the non-condensed part is usually collisionless and does not contribute to the mode precession.

The radial quadrupole mode consists of two collective excitations with angular quantum numbers $m = +2$ and $m = -2$ and frequencies ω_+ and ω_-, respectively. These two excitations correspond to an elliptic deformation of the cloud rotating in opposite directions. The superposition of the excitations results in the radial quadrupole mode. For a gas at rest the two excitations are degenerate, while for a gas carrying angular momentum the frequencies are different, which causes a precession of the mode, see Fig. 6.1. The mode precesses with a frequency

[1] $\epsilon' = (\omega_x'^2 - \omega_y'^2)/(\omega_x'^2 + \omega_y'^2)$, where ω_x' and ω_y' are the trap frequencies in the frame of the rotating potential.

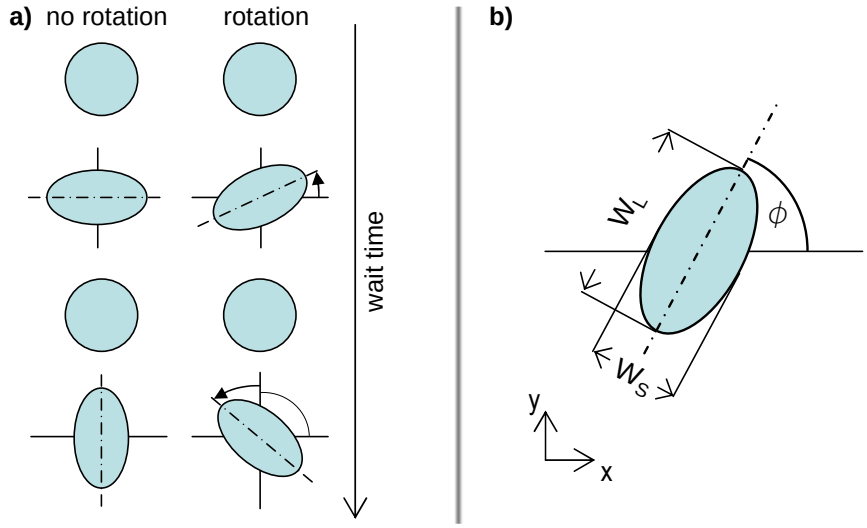

Fig. 6.1: Oscillation of the cloud after excitation of the radial quadrupole mode. For a rotating hydrodynamic gas the principal axes of the quadrupole mode oscillation precess with a frequency determined by the angular momentum of the gas. To follow the precession we measure the angle of the long axis of the cloud. Note that every half oscillation period this angle changes by $\pi/2$ because of the mode oscillation; see also Fig. 6.2. The oscillation of the cloud shape is determined by measuring the widths along the short (W_S) and the long axis (W_L) of the cloud.

$\Omega_\phi = (\omega_+ - \omega_-)/4$. The angular momentum itself can be calculated from the precession frequency [Zam98] using

$$\Omega_\phi = L_z/(2Mr_{\mathrm{rms}}^2). \tag{6.1}$$

Here L_z is the average angular momentum per atom and r_{rms}^2 is the mean value of $x^2 + y^2$ of the density distribution[2].

To excite the quadrupole mode we switch on an elliptic potential for $50\,\mu$s; this short elliptic deformation does not affect the angular momentum of the gas. For the excitation we make sure that ω_r does not change. This ensures that no compression mode is excited and only an equal superposition of the $m = \pm 2$ modes is created [Alt07c].

To follow the quadrupole oscillation we determine the angle of the long axis, ϕ, and the difference of the widths along the principle axes of the cloud, $\Delta W = W_L - W_S$, after a variable wait time in the trap; see Fig. 6.1. Therefore we fit a zero-temperature two-dimensional Thomas-Fermi profile to absorption images[3].

[2]We determine r_{rms} at unitarity from the trap parameters using $E_F = 2M\omega_r^2 r_{\mathrm{rms}}^2\sqrt{1+\beta}$ where we used the universal scaling parameter $\beta = -0.56$ [Gio08]. Note that this underestimates r_{rms} by a few percent because it does not take into account the finite temperature and the rotation of the gas. This does not effect the measurement of the lifetime of rotation as this depends on the relative change of L_z.

[3]For the parameters used in the experiment a zero temperature Thomas-Fermi profile fits the density distribution reasonably well.

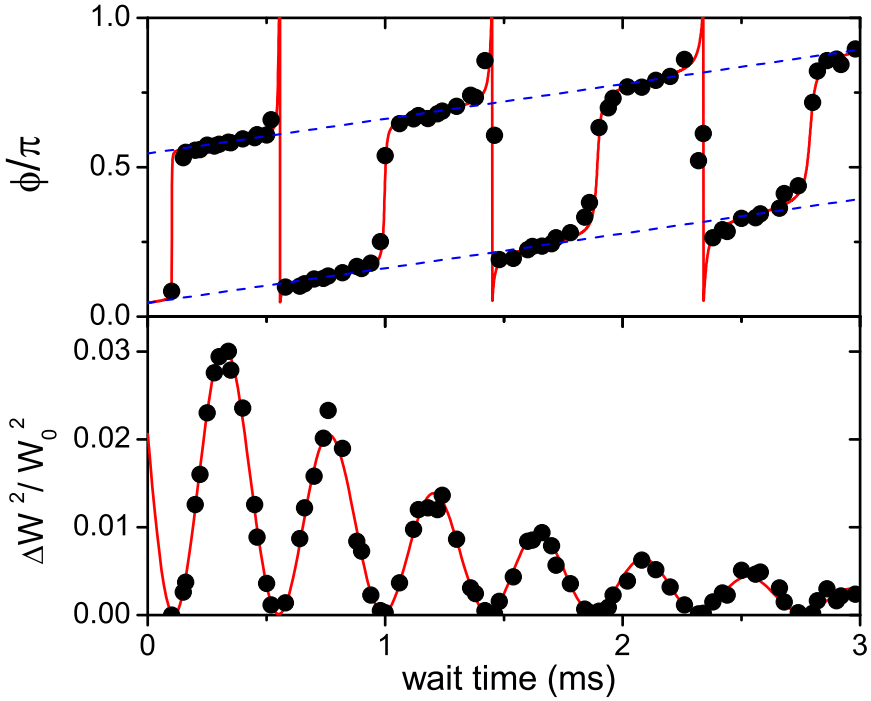

Fig. 6.2: Evolution of the quadrupole mode in a rotating Fermi gas in the unitarity limit. The upper panel shows the precession of the principal axes of the mode. The experimental data are shown by the dots. The solid line represents a fit according to Eq. 6.2. The dashed lines correspond to the idealized precession of the angle when there is no damping present in the mode. Whenever the oscillation of the difference in widths $\Delta W^2/W_0^2$ (lower panel) has a local maximum the observed precession angle coincides with the idealized precession. The parameter W_0 is the average width of the cloud. The finite value of ϕ at zero wait time results from the precession of the cloud during expansion. Here $L_z = 1.7\hbar$ and $T/T_F \approx 0.2$.

We also keep the angle of the long axis a free fit parameter. The width of the cloud is defined as twice the Thomas-Fermi radius.

To resolve the density distribution in the x-y plane, we let the cloud expand for 0.8 ms before taking the image. The expansion does not only increase the width of the cloud but also leads to an increase in the precession angle as a consequence of the angular momentum. A quantitative analysis of the small contribution to the total precession angle that results from the expansion is given in Appendix B.

Figure 6.2 shows the evolution of the precessing quadrupole mode. The upper part shows the precession angle. The finite value of ϕ at zero wait time results from the expansion. The periodic jumps of the precession angle reflect the alternation between the long and the short axis while the quadrupole mode evolves. As the precession proceeds, these jumps become more and more smooth. This is caused by stronger damping of the $m = -2$ excitation compared to the $m = +2$ excitation. Similar behavior has been observed in Ref. [Bre03] for the case of

a BEC. There the authors discussed two possible mechanisms where the difference in damping is due to either a rotating thermal cloud [Wil02] or Kelvin mode excitations [Che03]. From our measurements we cannot discriminate between these two mechanisms.

To fit the observed precession of the quadrupole mode, we use the function given in Appendix A. We find very good agreement between the data and the expected behavior. For the data set shown in Fig. 6.2 the angular momentum is $1.7\hbar$. The average damping rate is $(\Gamma_- + \Gamma_+)/2 = (460 \pm 30)\,\mathrm{s}^{-1}$, while the difference in the damping rate of the $m = -2$ compared to the $m = +2$ excitation is $\Gamma_- - \Gamma_+ = (80 \pm 40)\,\mathrm{s}^{-1}$.

We find that a simplified procedure can be used to determine the angular momentum from a single measurement, instead of fitting the whole precession curve. If the measurement is taken at a time when ΔW^2 has a local maximum, the precession angle ϕ is independent of the distortion caused by the difference in the damping rates between the two excitations; see Fig. 6.2. This allows us to determine the difference $\omega_+ - \omega_- = 4\,\phi/\Delta t$ and therefore to determine L_z with a single measurement. The duration Δt is the sum of the wait time in the trap and an effective precession time t_e, which accounts for the precession of the quadrupole mode during expansion as discussed in Appendix B. Depending on the damping of the mode oscillation, we measure the precession angle at the first or second maximum[4] of ΔW^2.

To determine the temperature of the gas in the unitarity limit, we first adiabatically change the magnetic field to 1132 G [5], where $1/k_F a \approx -1$, to reduce the effect of interactions on the density distribution [Luo07]. Under this condition, for $T > 0.2T_F$, the interaction effect on the density distribution is sufficiently weak to treat the gas as a noninteracting one and to determine the temperature from time-of-flight images. We fit the density distribution after 2 ms release from the trap to a finite-temperature Thomas-Fermi profile. The temperature measured at 1132 G is converted to the temperature in the unitarity limit under the assumption that the conversion takes place isentropically, following the approach of Ref. [Che05a].

6.3 Spinning up the gas

To spin up the gas we introduce a rotating anisotropy into the initially round trap in the x-y plane. More specifically, we suddenly switch to a rotating elliptic trap potential with a rotation frequency Ω_t and ellipticity $\epsilon' = 0.03$, rotate for a time t_{rot} on the order of 100 ms, and then ramp down the ellipticity in 50 ms while the trap is still rotating.

In the case of hydrodynamic behavior of the gas this spinning up method is

[4] Note that the frequency of quadrupole mode oscillation ω_q depends on the rotation frequency of the gas via $\omega_q^2 = 2\omega_r^2 - \Omega^2$. This leads to a tiny shift of the maxima of ΔW^2 but does not affect our measurement of L_z within our experimental uncertainty.

[5] This is the largest magnetic field where absorption images can be taken with our current experimental setup.

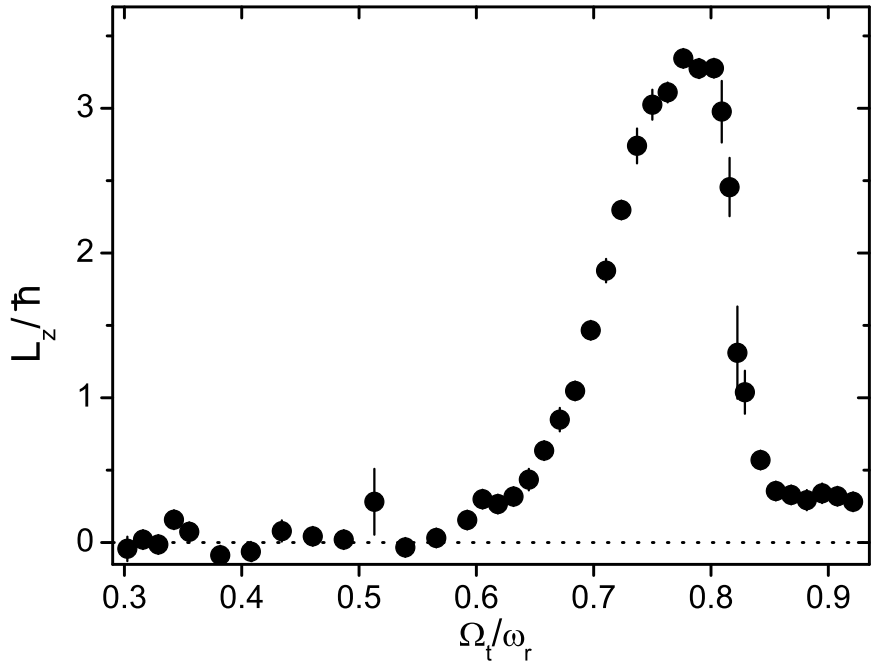

Fig. 6.3: The angular momentum L_z as a function of the rotation frequency Ω_t of the elliptic trap. Here we spin up the gas for $t_{\rm rot} = 60\,$ms. The temperature is $T/T_F \approx 0.2$. The gas is in the unitarity limit.

resonantly enhanced in a certain range of rotation frequencies; see Fig. 7.3. The reason for this behavior is the resonant excitation of quadrupolar flow which leads to a dynamic instability when Ω_t is close to half the oscillation frequency of the radial quadrupole mode $\omega_q/2 = 0.71\omega_r$. This effect was used to nucleate vortices in a BEC [Mad00] and was further studied in Refs. [Mad01, Hod02]. A signature of the resonant excitation is a strong elliptic deformation of the cloud shape which exceeds the ellipticity of the trap ϵ' during the spin-up process. We clearly see this effect when we spin up the gas. We also find that the rotation frequency where L_z starts to increase strongly depends on ϵ' and $t_{\rm rot}$ in a similar way as it was observed in Refs. [Mad01, Hod02]. Note that we cannot draw any conclusion concerning superfluidity from the resonant behavior of L_z in Fig. 7.3 because it is only a consequence of hydrodynamic behavior and the strongly interacting gas is hydrodynamic both below and above T_c. In fact, for temperatures clearly above T_c we a find similar behavior for L_z as a function of Ω_t.

For an atomic BEC, L_z was found to first increase abruptly from 0 to $1\hbar$ with Ω_t, caused by the appearance of a centered vortex [Che00]. As the formation of pairs is necessary for superfluidity in the BEC-BCS crossover regime, the angular momentum per atom of a single vortex in the center of the cloud amounts to $L_z = \hbar/2$. We do not observe such an abrupt increase in L_z. Nevertheless this does not exclude that vortices are created during our spin-up process; the abrupt change in L_z is not a necessary consequence of the creation of vortices as the

angular momentum of a vortex depends on its position in an inhomogeneous gas [Che00]. Furthermore our measurement of L_z cannot distinguish between the angular momentum carried by the superfluid and the normal part of the cloud. Also, we cannot directly observe vortices in our absorption images; we believe that the reason is the very elongated cloud which strongly decreases the contrast of the vortex core in the absorption images.

During our spin-up process we observe a significant heating of the gas depending on the rotation frequency and the rotation time. We keep these two parameters as small as possible. We find that a rotation frequency of $\Omega_t/\omega_r = 0.6$ and $t_{\mathrm{rot}} = 200\,\mathrm{ms}$ lead to an angular momentum of about $L_z = 2\hbar$. This is sufficient to perform the measurements, and at the same time does only moderately increase the temperature.

We determine the temperature of the gas after the spin-up process. To avoid complications in the temperature measurement, we wait until the rotation has completely decayed. To keep this wait time short, on the order of 100 ms, we speed up the decay by increasing the ellipticity of the trap; see discussion below. Note that the low initial angular momentum used in the experiments, always staying below $3\hbar$, does not lead to a significant increase in the temperature when the rotation energy is completely converted into heat[6].

6.4 Lifetime of the angular momentum

In an elliptic trap the angular momentum is not a conserved quantity and hence can decay. The dissipation of L_z is due to the friction of the gas caused by the trap anisotropy. Here we investigate the dependence of the decay of L_z on the static ellipticity for the case of unitarity-limited interactions. We compare our experimental results to the predicted behavior for a rotating Boltzmann gas [GO00]. Finally we study the dependence of the decay rate on the interaction strength in the BEC-BCS crossover regime.

The fact that the gas consists of two different components, the normal and the superfluid part, leads in general to a complex behavior for the decay of L_z. For example, in the case of a BEC an exponential decay is related to the corotation of the thermal cloud with the condensate [Zhu01, AS02]. When the thermal cloud is not rotating, theoretical [Zhu01] and experimental [Mad00] studies show nonexponetial behavior. For a gas completely in the hydrodynamic regime it is expected that the decrease in L_z has an exponential form [GO00].

To measure the decay rate of the angular momentum, we use the following procedure. After spinning up the gas as discussed in Sec. 6.3, we slowly increase the static ellipticity within 10 ms, wait for a certain hold time to let the angular momentum partially decay, and then we remove the ellipticity again within

[6] To estimate the increase of the temperature through the decay of the rotation we assume that the rotation energy is completely converted into heat. In the experiments L_z is well below $3\hbar$ which leads to a relative temperature increase of $\Delta T/T < 0.02$ in the relevant temperature range. This is clearly below the uncertainty of our temperature measurement.

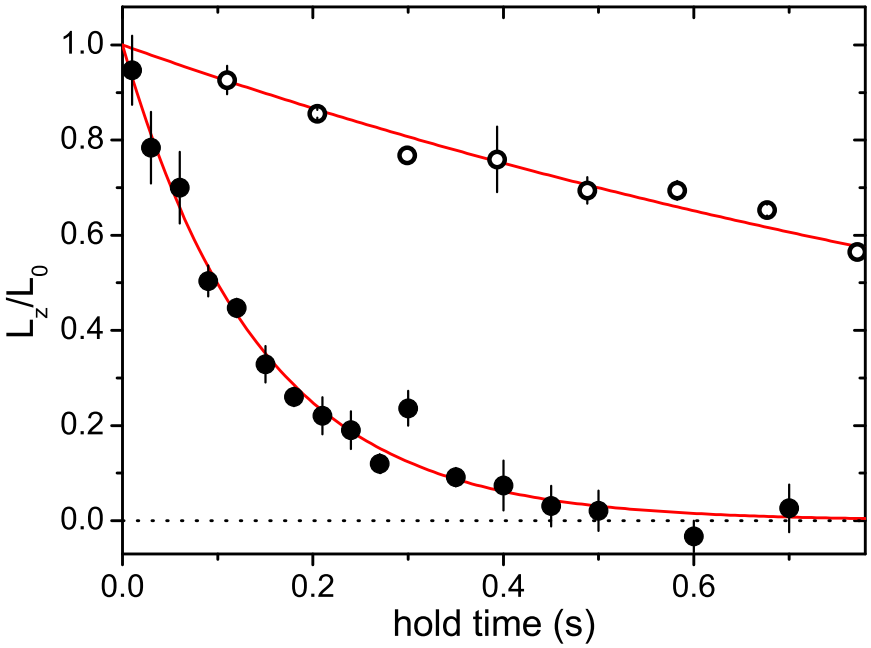

Fig. 6.4: Decay of the angular momentum L_z for a gas in the unitarity limit. The temperature is $T/T_F = 0.22(3)$. We fit an exponential decay behavior (solid lines) to the experimental data points. For low ellipticity $\epsilon = 0.009$ (open dots) the lifetime is 1.4 s, while at higher ellipticity $\epsilon = 0.1$ (filled dots) the lifetime is only 0.14 s. To better see the difference of the lifetime for the two ellipticities we normalized L_z by its initial value L_0. For the lower ellipticity $L_0 = 2.2\hbar$ and for the higher ellipticity $1.6\hbar$.

10 ms. Finally we excite the radial quadrupole mode and observe the precession to determine L_z using the simplified procedure discussed earlier.

In Fig. 6.4 we show two examples for the decay of L_z. We find that the decay of the angular momentum perfectly fits an exponential behavior for all the static ellipticities, temperatures, and interaction strengths we used. For the lowest temperatures obtained, the lifetime for a gas in the unitarity limit goes up to 1.4 s, presumably limited by a residual anisotropy of the trap. This lifetime is by more than a factor of thousand larger than the radial trap oscillation period. Furthermore the lifetime of the angular momentum is much larger than the lifetime of collective excitation modes. For example, the lifetime of the radial quadrupole mode under the same conditions is only 2 ms. A larger ellipticity of the trap significantly decreases the lifetime of L_z.

In the following we investigate quantitatively the dependence of the decay rate of the angular momentum, λ, on ellipticity and temperature. The experimental results are shown in Fig. 6.5 for two different temperatures. The full circles display the data for a temperature of $T/T_F = 0.22(3)$ and the open circles correspond to a temperature of $T/T_F = 0.35(2)$. For better comparison with theory, we plot the normalized decay rate λ/ω_r. A strong increase in the decay rate with increasing ellipticity shows the important role of the trap anisotropy

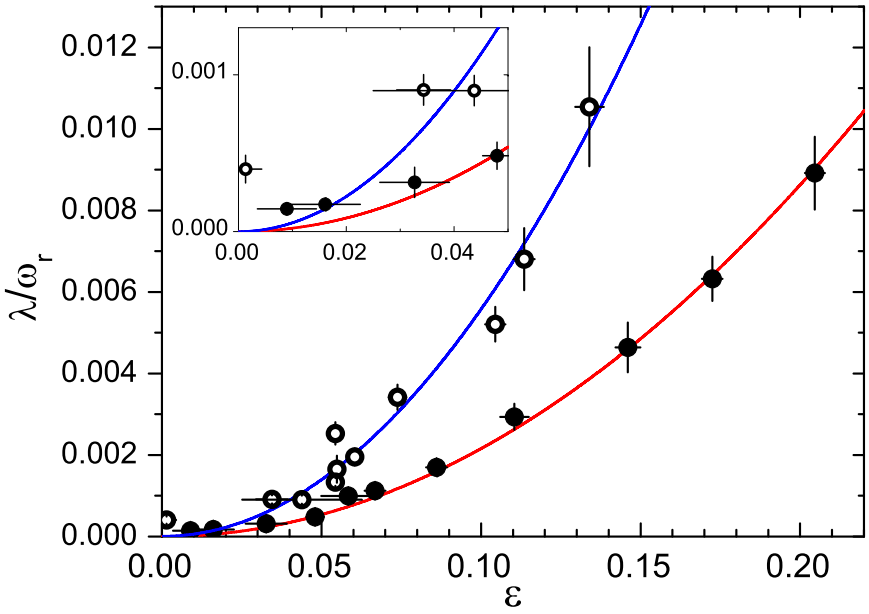

Fig. 6.5: Normalized decay rate of the angular momentum as a function of the ellipticity for a gas in the unitarity limit. The temperatures are $T/T_F = 0.22(3)$ (filled dots) and 0.35(2) (open dots). The solid lines are fits based on the expected behavior for a Boltzmann gas [GO00]. The inset shows the low ellipticity region.

on the lifetime of the angular momentum. For both temperatures the qualitative behavior of the decay rate is the same.

Next we compare the behavior of the decay rate with a theoretical prediction for a Boltzmann gas [GO00]. As we showed recently in Ref. [Rie08], a Boltzmann gas describes the behavior of a unitarity-limited gas in the normal state reasonably well. The predicted behavior of the decay rate is given by $\lambda/\omega_r = 2\epsilon^2\omega_r\tau$ under the assumption that $\epsilon \ll 1/(4\omega_r\tau)$ [7], where τ is the relaxation time or effective collision time [Rie08, Vic00, Hua87]. This condition is well fulfilled in our system because the gas is in the hydrodynamic regime where $\omega_r\tau \ll 1$. We compare this theoretical prediction, with τ as a free parameter, to our measurements. We find $\omega_r\tau = 0.108(5)$ for the lower temperature and $\omega_r\tau = 0.28(1)$ for the higher temperature data.

Note that at very low ellipticity, $\epsilon < 0.02´$, the observed decay rate for both temperatures lies significantly above the expected behavior; see inset of Fig. 6.5. We attribute this to an additional anisotropy of the trap beyond simple ellipticity. This weak anisotropy becomes relevant only at very low ϵ. Furthermore the finite linear heating rate of the trapped gas of $0.05T_F\,\mathrm{s}^{-1}$ becomes important when the decay rate is very low, which means that the lifetime of L_z is on the order of seconds. In this case the temperature cannot be assumed to be constant during the decay of L_z.

[7] For the temperatures used in the measurements $1/(4\omega_r\tau) > 0.9$ for a gas in the unitarity limit.

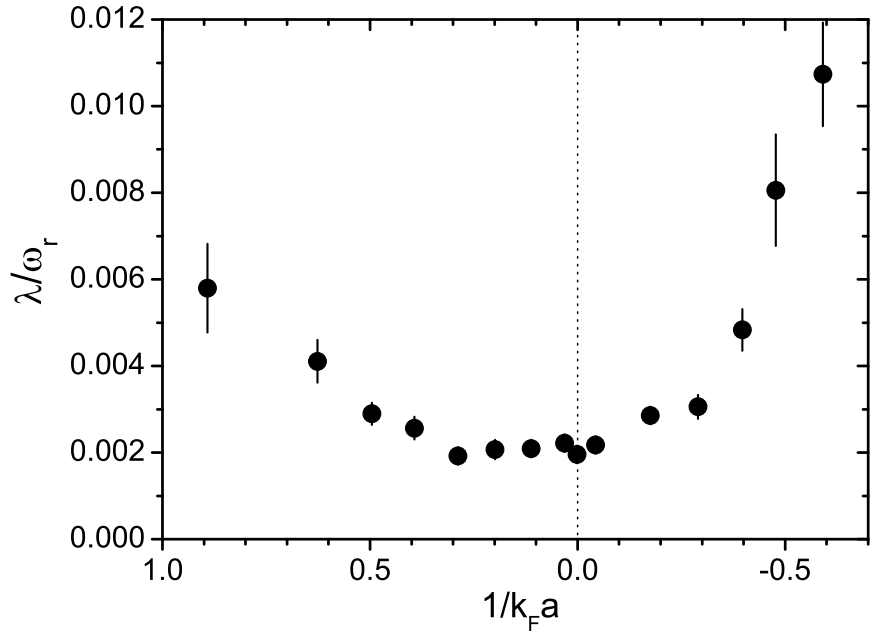

Fig. 6.6: Lifetime of the angular momentum versus interaction parameter $1/k_F a$ for $\epsilon = 0.09$. The temperature for $1/k_F a = 0$ is $T/T_F = 0.22(3)$.

A recent calculation of the relaxation time τ for a Fermi gas in the unitarity limit [Rie08] allows us to compare the experimental values for $\omega_r \tau$ to theory. For $T/T_F = 0.35$ the obtained relaxation time of $\omega_r \tau = 0.28$ is clearly larger than the calculated value of $\omega_r \tau = 0.13$. This means that the theory predicts that the gas is somewhat deeper in the hydrodynamic regime compared to the experimental findings. Similar deviations showed up when the theory was compared to the temperature dependence of collective oscillations [Rie08]. For the lower temperature the obtained value for $\omega_r \tau$ cannot be compared to the calculation of Ref. [Rie08] as the theory is restricted to higher temperatures.

Finally we study the decay of the angular momentum in the crossover region between the BEC and BCS regimes. We measure the decay rate for different interaction parameters $1/k_F a$. The experimental sequence is the same as for the decay rate in the unitarity limit beside ramping the magnetic field to the desired value in 100 ms before increasing the ellipticity and ramping back the magnetic field in 100 ms before exciting the quadrupole mode. Here the magnetic field is changed slowly such that the gas is not collectively excited. The ellipticity for all magnetic fields is set to be $\epsilon = 0.09$. This sizeable value of ϵ ensures that a small anisotropy beyond ellipticity does not affect the decay rate and makes the measurement less sensitive to heating while the angular momentum damps out as discussed above.

Figure 6.6 shows the decay rate of the angular momentum as a function of the interaction strength. The lifetime is largest where the interaction is strongest and accordingly the relaxation time is short. In addition to the two-body interaction strength, pairing effects play an important role for the relaxation time

[Rie08]. This might explain the higher decay rates for $1/k_F a < 0$, where the pairing is weak, compared to the decay rates for $1/k_F a > 0$, where the atoms are bound to molecules. Similar behavior has been seen in [Zwi05a] for the lifetime of a vortex lattice. Note that Ref. [Zwi05a] also reported a decrease in the lifetime in a narrow region around $1/k_F a = 0$, which we do not observe for our trap parameters.

In summary the hydrodynamic behavior in the crossover region leads to a very long lifetime of L_z.

6.5 Conclusion

In this work we have presented measurements on a strongly interacting Fermi gas carrying angular momentum. The angular momentum of the gas exhibits long lifetimes due to the deeply hydrodynamic behavior of the normal state in such a system. We investigated the decay rate of the angular momentum depending on the ellipticity of the trapping potential for two different temperatures. We find that the experimental results are in good agreement with the expected behavior for a simple Boltzmann gas. The dependence of the decay rate of the angular momentum on the interaction strength in the BEC-BCS crossover region confirms that the collective motion is very stable as long as the interaction strength is sufficiently large.

The long lifetime of the angular momentum in a rotating strongly interacting Fermi gas allows us to further investigate rotational properties both in the superfluid and normal phase in detail and with high precision. Currently we investigate the moment of inertia of the gas for different temperatures; see Chapter 7.

Acknowledgments
We acknowledge support by the Austrian Science Fund (FWF) within SFB 15 (project part 21) and SFB 40 (project part 4).

6.6 Appendix A

To calculate the precession angle and the oscillation of the width we assume that the frequency and damping rate for the $m = \pm 2$ excitations are independent. For the damping of each excitation we assume an exponential behavior. A superposition of the two excitations results in the fit function for the precession angle [Bre03]

$$\tan\left(2(\phi - \phi_e)\right) = \frac{e^{-(\Gamma_+ - \Gamma_-)t}\sin\left(\omega_+ t + 2\phi_0\right) - \sin\left(\omega_- t + 2\phi_0\right)}{e^{-(\Gamma_+ - \Gamma_-)t}\cos\left(\omega_+ t + 2\phi_0\right) + \cos\left(\omega_- t + 2\phi_0\right)} \tag{6.2}$$

Here $\omega_\pm$ are the frequencies, $\Gamma_\pm$ are the damping rates, ϕ_0 is the initial angle for the two excitations and ϕ_e is the precession angle resulting from the expansion

of the cloud. For the oscillation of the width difference ΔW we get

$$\begin{aligned} \Delta W^2 &= 4Ae^{-(\Gamma_+ + \Gamma_-)t}\cos^2\left(\frac{(\omega_+ + \omega_-)}{2}t + 2\phi_0\right) \\ &+ A(e^{-\Gamma_+ t} - e^{-\Gamma_- t})^2, \end{aligned} \tag{6.3}$$

where A is the amplitude of the oscillation.

6.7 Appendix B

Here we calculate the effect of the expansion of the cloud on the precession angle. Assuming conservation of angular momentum during the expansion, the rotation frequency Ω of the gas decreases as the size of the cloud is increasing. We introduce an effective precession time t_e which accounts for the changing precession angle ϕ during expansion. The total change in the precession angle resulting from the expansion is given by

$$\phi_e = \int_0^{t_{\mathrm{TOF}}} \dot{\phi}(t)dt = \dot{\phi}(0)t_e, \tag{6.4}$$

where $\dot{\phi}(0)$ is the precession frequency when the gas is still trapped and t_{TOF} is the expansion time. Assuming that also during the expansion $\dot{\phi}(t) = L_z/(2Mr^2_{\mathrm{rms}}(t))$ is still valid and inserting this into Eq. 6.4 we get

$$t_e = \int_0^{t_{\mathrm{TOF}}} r^2_{\mathrm{rms}}(0)/r^2_{\mathrm{rms}}(t)dt. \tag{6.5}$$

To calculate the relative increase of the cloud size during expansion, $r^2_{\mathrm{rms}}(t)/r^2_{\mathrm{rms}}(0)$, we use the scaling approach; see e.g. [Alt07c]. For our experimental parameters, $\omega_r = 800\,\mathrm{Hz}$ and $t_{\mathrm{TOF}} = 0.8\,\mathrm{ms}$, we get an effective precession time of $t_e = 0.26\,\mathrm{ms}$. This is shorter than the typical precession time in the trap of $0.75\,\mathrm{ms}$.

CHAPTER 7

Publication

Quenching of the moment of inertia in a strongly interacting Fermi gas[†]

manuscript in preparation

S. Riedl,[1,2] E. R. Sánchez Guajardo,[1,2] C. Kohstall,[1,2] J. Hecker Denschlag,[1] and R. Grimm[1,2]

[1] *Institut für Experimentalphysik und Zentrum für Quantenphysik, Universität Innsbruck, 6020 Innsbruck, Austria*

[2] *Institut für Quantenoptik und Quanteninformation, Österreichische Akademie der Wissenschaften, 6020 Innsbruck, Austria*

We report on the observation of a quenched moment of inertia as a consequence of superfluidity in a rotating, strongly interacting Fermi gas. To determine the moment of inertia of the trapped, rotating gas we measure the precession of the radial quadrupole mode. The measurements do not only provide evidence for superfluidity in the gas but also reveal the superfluid critical temperature.

A striking consequence of superfluidity is the reduction of the moment of inertia (MOI) with respect to its classical, rigid-body value. This so called quenching of the MOI is based on the fact that a superfluid cannot rotate like a rigid body and, as a result, the apparent MOI is smaller than that of a normal, rigid rotating system. Therefore the quenching of the MOI reveals superfluidity. Furthermore it contains information on the superfluid density distribution of the system. Quenching of the MOI was shown in liquid helium [Hes67] but also serves as a firm indicator for nucleon superfluidity [Rin80]. More recent

[†]The author of the present thesis developed the experimental procedure, performed the measurements and made the data analysis for this publication. Thereby he was supported by E.R.S.G. and C.K..

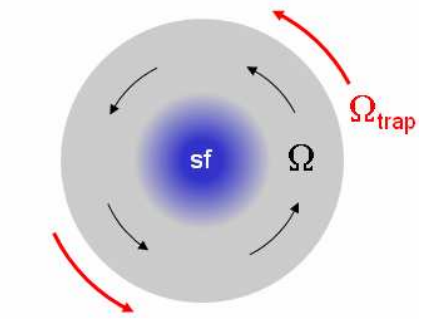

Fig. 7.1: Schematic illustration of a strongly interacting Fermi gas in a slowly rotating trap. The classical part in the outer trap region rotates with a frequency Ω, which in an equilibrium state corresponds to the rotation frequency Ω_{trap} imposed by the trap. The superfluid core cannot rotate and does not contribute to the MOI.

a nonclassical MOI in bulk solid helium was reported demonstrating superfluid behavior [Kim04a].

In this Letter, we report on the observation of a quenched MOI in a slowly rotating, strongly interacting Fermi gas [Ing08] and its application to study the superfluid phase transition. The basic experimental situation is illustrated in Fig. 7.1. Below T_c, the harmonically trapped cloud consists of a superfluid core and a surrounding classically hydrodynamic cloud. The slightly elliptic trap rotates with an angular velocity Ω_{trap}. The outer part of the cloud is subject to friction and thus follows the trap rotation with an internal angular velocity Ω. After a certain spin-up time, an equilibrium state of full rotation can be reached where $\Omega = \Omega_{\mathrm{trap}}$. The superfluid core cannot carry angular momentum, supposed that vortex nucleation is avoided.

Our measurements rely on the possibility to determine the total angular momentum L of a rotating hydrodynamic cloud by detecting the precession of a radial quadrupole excitation. This method is well established and has been extensively used in the context of atomic Bose-Einstein condensates [Che00, Hal01a, Lea02] and recently also with strongly interacting Fermi gases [Rie09]. The precession frequency can be written as $\Omega_{\mathrm{prec}} = L/(2\Theta_{\mathrm{rig}})$ [Zam98], where Θ_{rig} is the MOI under the assumption that the whole cloud is rotating rigidly, including the superfluid part. Expressing the angular momentum $L = \Theta\Omega$ in terms of the apparent MOI, Θ, and the internal rotation frequency, Ω, one arrives at the simple expression

$$\Omega_{\mathrm{prec}} = \frac{\Theta}{2\Theta_{\mathrm{rig}}}\,\Omega\,. \tag{7.1}$$

The maximum possible precession frequency of $\Omega_{\mathrm{prec}} = \Omega_{\mathrm{rot}}/2$ corresponds to a fully rotating ($\Omega = \Omega_{\mathrm{trap}}$), classically hydrodynamic gas above T_c ($\Theta = \Theta_{\mathrm{rig}}$). A lower precession frequency can be due to an incompletely rotating classical part, or to the quenching of the MOI. Consequently, to observe the quenching effect ($\Theta/\Theta_{\mathrm{rig}} < 1$), one has to make sure that the classical component is set into full

rotation.

To deduce superfluid behavior from the measurement of the MOI, one has to make sure that the velocity field of the normal component of the gas has a rigid form. If this is not the case, a reduced MOI can also be found above the superfluid transition temperature as has been shown by [Cla07]. Superfluidity in a strongly interacting Fermi gas has first been established by the observation of a vortex lattice [Zwi05a].

The starting point for our experiments is a strongly interacting Fermi gas consisting of an equal mixture of ^{6}Li atoms in the lowest two atomic states. We cool the gas until it is far in the degenerate regime using the techniques described in our previous work [Joc03a, Alt07c]. A broad Feshbach resonance centered at 834 G [Bar05b] allows us to tune the interaction strength. If not otherwise stated the measurements presented in this paper are performed at the center of the Feshbach resonance where the Fermi gas is unitarity-limited and therefore acquires universal properties [Gio08].

The atoms are confined in a combination of an optical dipole trap using a red-detuned, single focused laser beam and a magnetic trap. The optical dipole trap creates strong confinement perpendicular to the laser beam (x-y plane). The weaker confinement along the beam (z-direction) is dominated by the magnetic trap under the conditions of the present experiment. For the trap parameters used, the trap is well approximated by a harmonic potential with trap frequencies $\omega_x = \omega_y \approx 2\pi \times 680\,\mathrm{Hz}$ and $\omega_z = 2\pi \times 24\,\mathrm{Hz}$, leading to a cigar-shaped cloud. The Fermi energy of the noninteracting gas is given by $E_F = \hbar(3N\omega_x\omega_y\omega_z)^{1/3}$ where $N = 6 \times 10^5$ is the total atom number. The Fermi temperature is $T_F = E_F/k = 1.3\,\mu\mathrm{K}$, with k the Boltzmann constant.

To set the gas into rotation, with the rotation axis in z-direction, we use a rotating elliptic potential. To create this potential we employ a scanning system for the trapping laser beam which creates a time averaged optical dipole potential in the x-y plane [Alt07c]. Recently we successfully used this technique to spin up the strongly interacting Fermi gas [Rie09]. In contrast to the previous experiment, here we use a lower rotation frequency of $\Omega_{\mathrm{trap}} = 0.3\,\omega_x$ and a ellipticity of $\epsilon' = 0.1$ for our rotating elliptic potential[1]. The low value of Ω_{trap} avoids a resonant process which can lead to vortex creation[2].

In addition we use the scanning system to compensate residual ellipticity of the trapping laser beam to obtain an almost perfect cylindrical symmetry of the trapping potential. This leads to a very long lifetime of the rotation of the gas of about 1 s [Rie09], large enough to be able to perform the measurements on

[1] $\epsilon' = (\omega_x'^2 - \omega_y'^2)/(\omega_x'^2 + \omega_y'^2)$, where ω_x' and ω_y' are the trapfrequencies in the frame of the rotating potential.

[2] As it was shown in Refs. [Mad01, Hod02] vortices enter the gas via a resonant process which occurs when the rotation frequency of the elliptic potential is close to a critical frequency of $0.71\omega_x$. To verify that no vortices are created via this process, we make use of the fact that during the resonant process the aspect ratio of the cloud exceeds by far the aspect ratio of the rotating potential [Rie09]. For the parameters of the current spin-up we find that the aspect ratio of the cloud stays constant and consequently never exceeds the aspect ratio of the rotating potential.

the MOI.

To determine the MOI, we excite the radial quadrupole mode and measure the precession of the mode. The excitation scheme for the mode and the procedure to determine Ω_{prec} are given in Ref. [Rie09]. To determine the MOI from the measurement of Ω_{prec} we have to distinguish between the effect of Ω and $\Theta/\Theta_{\mathrm{rig}}$ on Ω_{prec}; see Eq. 7.1. This is possible because, on the one hand, Ω slowly increases when we spin up the gas until it saturates at its maximum value, which is set by Ω_{trap}. On the other hand $\Theta/\Theta_{\mathrm{rig}}$ only depends on temperature. Therefore we can determine $\Theta/\Theta_{\mathrm{rig}}$ after spinning the gas until Ω saturates.

To determine the temperature we follow the procedure described in Ref. [Rie09]. In brief, we determine the temperature of the gas after the spin-up process and after an adiabatic change of the magnetic field to 1132 G where the gas can be treated as a noninteracting one[3]. Different to the procedure described in Ref. [Rie09], here we give the temperature for the noninteracting gas T_i and do not convert to the temperature of a unitarity-limited gas, unless otherwise noted. The statistical uncertainty of the temperature measurement is about 5% for the relevant temperature range of the measurements.

The experimental sequence to measure the MOI for different temperatures is shown in Fig. 7.2. For the measurement to work it is important that the temperature is constant after spinning up the gas for a certain time t_{rot} as $\Theta/\Theta_{\mathrm{rig}}$ depends on temperature. But during the spin up we find that the temperature of the gas increase with a constant heating rate of about $\dot{T}_i/T_F = 0.13\,\mathrm{s}^{-1}$. To overcome this problem we preheat the gas before spinning it up such that the temperature is constant after spinning the gas for different t_{rot}.

The heating prior to spinning up the gas is again done by spinning the gas for a certain time. It takes advantage of the constant heating rate when we spin the gas. Furthermore we use the same parameters as for the main spin up process so we get the same heating rate. Before we start the actual spin-up we damp out the rotation in the gas. Damping out the rotation does only lead to a negligible increase of the temperature [Rie09]. To obtain a constant temperature after the spin-up, the rotation time to heat the gas t_{heat} is chosen such that the total rotation time $t_{\mathrm{tot}} = t_{\mathrm{heat}} + t_{\mathrm{rot}}$ is constant. To achieve different temperatures we simply change t_{tot}. From the constant heating rate during rotation we get an increase of T_i/T_F of about 0.026 for an increase of t_{tot} by 0.2 s. Note that the maximum value of t_{rot} is limited by t_{tot} and therefore Ω_{prec} might not saturate when t_{tot} is too small.

To check that the temperature for different t_{tot} is indeed constant we plot the average width of the cloud in the inset of Fig. 7.2. Note that if the gas has its maximum rotation frequency of $2\pi \times 200\,\mathrm{Hz}$ the width of the cloud is 1% smaller compared to the nonrotating case[4].

[3] This is the largest magnetic field where absorption images can be taken with our current experimental setup.

[4] The density of the rotating gas is described by a Thomas-Fermi profile with the centrifugal term added to the trapping potential. The centrifugal term leads to an increased width of the trapped gas compared to a nonrotating gas. On the other hand this decreases the expansion velocity leading to a small decrease of the cloud size after expansion for our

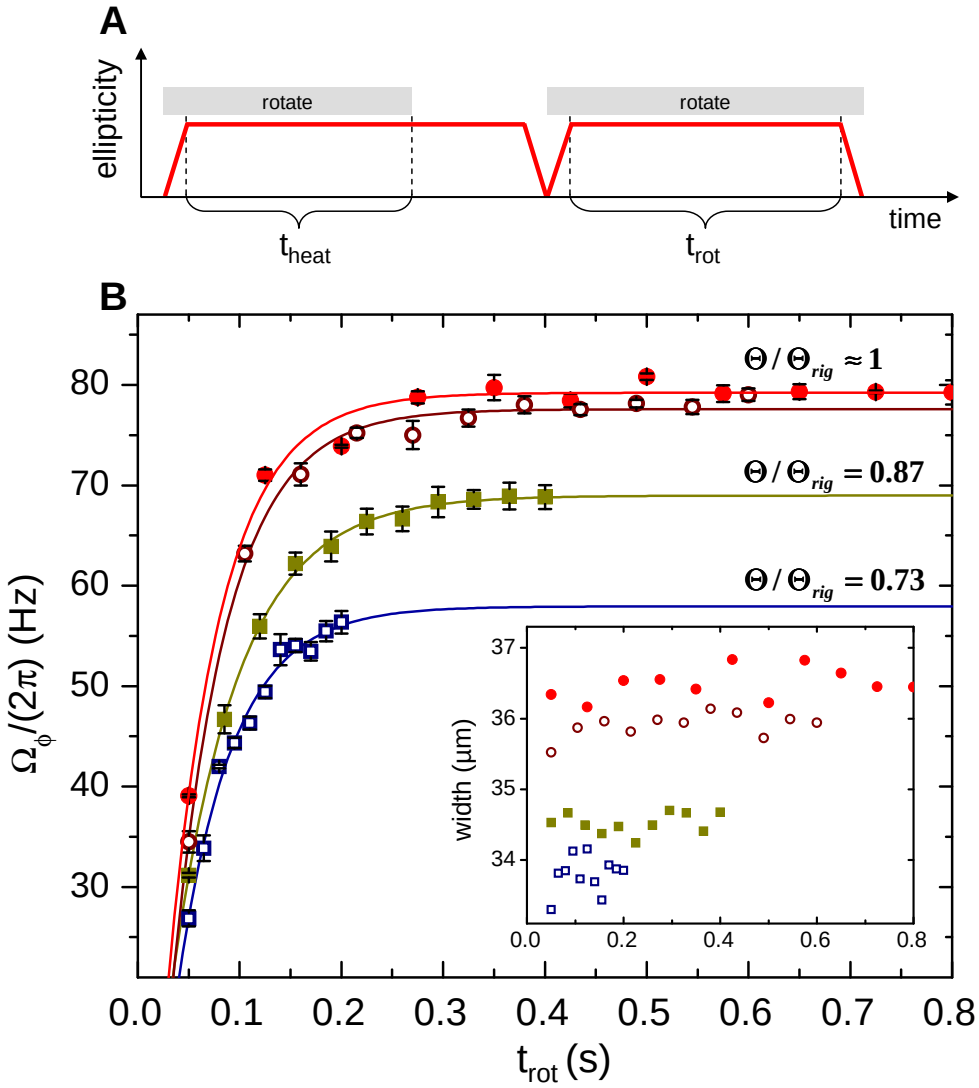

Fig. 7.2: The upper part, A, shows the spin up procedure leading to a constant temperature after spinning up the gas for different time t_{rot}. On the graph the ellipticity of the potential is drawn as a function of time. The gray bars indicate when the potential is rotating. To turn on the rotating potential adiabatically the ellipticity is increased and decreased in 50 ms. In the first part of the sequence we heat up the gas. Therefore we first spin the gas for a time t_{heat} and afterwards damp out the rotation of the gas by turning of the rotation of the potential but keeping the ellipticity for 200 ms. To increase the damping rate of the rotation we increase the magnetic field to 920 G [Rie09] in 110 ms and turn it back to the position of the Feshbach resonance in the same time before we start with the actual spin up. The times t_{heat} and t_{rot} do not include the time when we increase and decrease the ellipticity. The lower part, B, shows the precession frequency of the quadrupole mode as a function of t_{rot} using the experimental sequence shown in A. The different symbols correspond to t_{tot} of 0.2 s (open squares), 0.4 s (filled squares), 0.6 s (open circles), 0.8 s (filled circle). An increase of t_{tot} by 0.2 s corresponds to a temperature increase of $0.26T_F$. The lines fit the increase in Ω_{prec}. For lower temperature Ω_{prec} saturates at a lower value caused by the quenching of the moment of inertia due to superfluidity in the gas. The inset shows the average width of the cloud in the x-y plane. The constant width proofs that the temperature is indeed constant for different t_{rot}.

The experimental results for the measurement of the MOI for a strongly interacting Fermi gas at unitarity are shown in Fig. 7.2. The different symbols show Ω_{prec} as a function of t_{rot} for different t_{tot}. Each data point shown in the Figures is the average over three or more measurements. For the relatively high temperatures when $t_{\mathrm{tot}} = 0.6\,\mathrm{s}$ and $0.8\,\mathrm{s}$ the precession frequency saturates at almost the same value. We attribute this to the fact that the gas is in the normal regime or contains only a very small superfluid component. Thus the corresponding value of $\Theta/\Theta_{\mathrm{rig}}$ is about one. For $t_{\mathrm{tot}} = 0.4\,\mathrm{s}$ the precession frequency clearly saturates at a lower value which corresponds to $\Theta/\Theta_{\mathrm{rig}} = 0.87$ and hence the MOI is quenched. For the lowest temperature, when $t_{\mathrm{tot}} = 0.2\,\mathrm{s}$, the precession frequency hardly saturates as t_{tot} is to short to spin up the gas completely. Nevertheless the data suggest that $\Theta/\Theta_{\mathrm{rig}} = 0.73$.

When $\Theta/\Theta_{\mathrm{rig}} \approx 1$, the value of Ω_{prec} is slightly lower than $\Omega_{\mathrm{trap}}/2$ although the gas is in the normal regime. This can be explained by friction of the rotating gas caused by a small trap anisotropy [Rie09]. This reduces the maximum value of Ω during the spin-up and leads to a damping of Ω by about 10% after the spin-up before the quadrupole mode is excited. Note that this damping cannot lead to the observed decrease of the saturation value of Ω_{prec} with temperature as the damping rate is smaller at lower temperature [Rie09].

One assumption we made so far in our interpretation is that the superfluid part of the gas does not carry angular momentum. Nevertheless, this could be possible if the superfluid contains quantized vortices, which we cannot completely exclude. Although we spin up the gas very carefully, vortices could be created via the rotating normal part of the cloud [Hal01b]. These vortices can lead to an increase of the measured precession frequency but as the signature of quenching is a decrease of the maximum precession frequency, they can only quantitatively distort the measurement of the MOI. Note that we cannot directly see vortices in our absorption images [Rie09].

In the following measurement we determine the critical temperature for superfluidity based on the quenching of the MOI. The idea of the T_c measurement is to determine $\Theta/\Theta_{\mathrm{rig}}$ as a function of temperature and to identify the temperature where $\Theta/\Theta_{\mathrm{rig}}$ reaches one. As in the previous measurement we extract $\Theta/\Theta_{\mathrm{rig}}$ from the precession frequency of the quadrupole mode.

Here we simply spin the gas and determine Ω_{prec} after different rotation time. To determine the MOI it is again important that Ω is saturated. But while we spin the gas also the temperature and therefore $\Theta/\Theta_{\mathrm{rig}}$ increases. This means that the increase in Ω_{prec} can be due to an increase in Ω as well as an increase in $\Theta/\Theta_{\mathrm{rig}}$. Nevertheless it is possible to distinguish between the two effects when the change in Ω takes place on a much shorter timescale compared to the increase in $\Theta/\Theta_{\mathrm{rig}}$ while we rotate the gas. In this case the increase in Ω_{prec} is dominantly caused by $\Theta/\Theta_{\mathrm{rig}}$ after rotating the gas for a long time as Ω is already saturated then.

In the experiment, Fig. 7.3, we find that after a rotation time of about 850 ms the precession frequency saturates, meaning that both $\Theta/\Theta_{\mathrm{rig}}$ and Ω do not

experimental parameters.

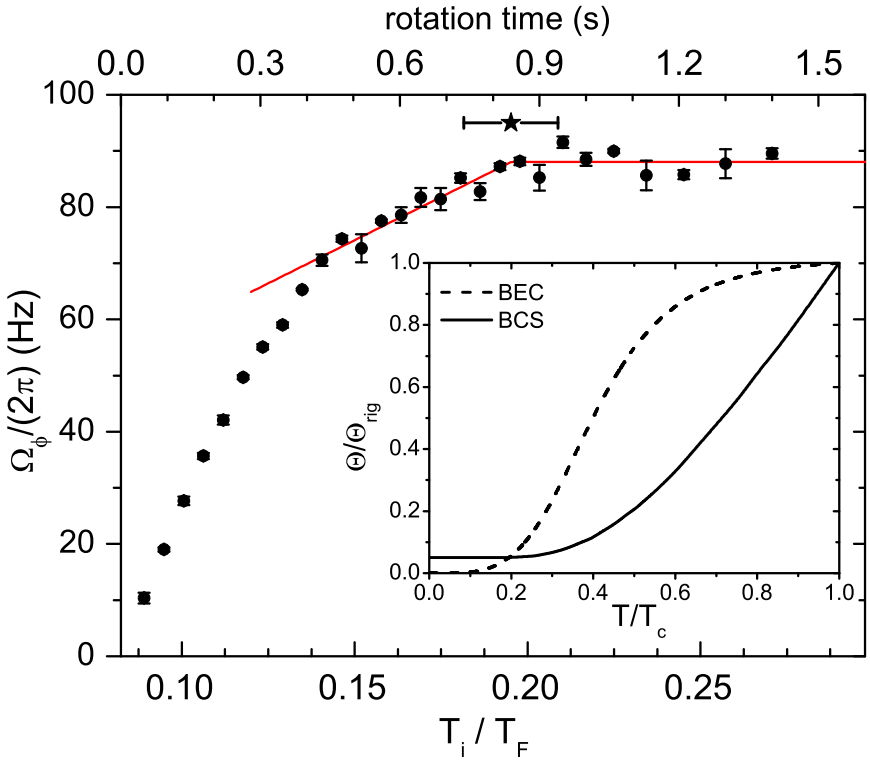

Fig. 7.3: The precession frequency of the quadrupole mode as a function of temperature and rotation time. For temperatures above $T_i/T_F = 0.15$ the increase of $\Omega_{\rm prec}$ is dominated by $\Theta/\Theta_{\rm rig}$ which allows to determine T_c from the point where $\Omega_{\rm prec}$ saturates (see main text). The solid line fits the data for temperatures above $T/T_F = 0.15$. It first increase linearly and stays constant afterwards. This is the expected behavior of $\Theta/\Theta_{\rm rig}$ for a gas in the BCS phase [Far00, Urb03] which is shown in the inset. Here the slope of $\Theta/\Theta_{\rm rig}$ suddenly changes at T_c. The star marks T_c. The horizontal errorbar shows the uncertainty of the temperature measurement. If $\Theta/\Theta_{\rm rig}$ approaches one very slowly, as for a BEC, the star marks the lower limit for T_c.

increase further. Note that $\Omega_{\rm prec}$ saturates again slightly below $\Omega_{\rm trap}/2$ due to damping of Ω. Next we check if close to the temperature where $\Omega_{\rm prec}$ saturates, the increase in $\Theta/\Theta_{\rm rig}$ dominates the increase in $\Omega_{\rm prec}$. Therefore we repeat the measurement, but this time we start to spin the gas at the temperature which corresponds to 850 ms of rotation in the previous measurement. As $\Theta/\Theta_{\rm rig}$ is already constant at that temperature this measurement reveals the time needed to spin up the gas. We find a spin up time on the order of 100 ms. For lower temperatures the spin up time is expected to be larger [GO00]. This means that for very short rotation times we cannot extract $\Theta/\Theta_{\rm rig}$. Therefore Fig. 7.3 can only reveal $\Theta/\Theta_{\rm rig}$ for temperatures close to the point where $\Omega_{\rm prec}$ saturates and above.

To set a limit to the region where the increase of $\Theta/\Theta_{\rm rig}$ is the dominating source for the increase in $\Omega_{\rm prec}$, we compare the data to the measurement of

$\Theta/\Theta_{\mathrm{rig}}$ shown in Fig. 7.2. Therefore we first determine the increase of $\Theta/\Theta_{\mathrm{rig}}$ with temperature from the data shown in figure Fig. 7.2. Using the lowest three temperatures we determine a linear increase of $\Theta/\Theta_{\mathrm{rig}}$ with temperature of $4.2(5)T_F/T_i$. If $\Theta/\Theta_{\mathrm{rig}}$ is the dominating source for the increase of Ω_{prec} in Fig. 7.3 we should find the same increase of $\Theta/\Theta_{\mathrm{rig}}$ there. Therefore we fit the solid line shown in Fig. 7.3 to the data points with $T_i/T_F > 0.15$. There Ω_{prec} increases almost linearly before it stays constant. The increase of $\Theta/\Theta_{\mathrm{rig}}$ with temperature is $3.5(4)T_F/T_i$ and agrees with the previous measurement. This makes us confident that for $T_i/T_F > 0.15$ the data shown in Fig. 7.3 reveals the change in $\Theta/\Theta_{\mathrm{rig}}$.

Finally we determine T_c from the point where Ω_{prec} saturates. Therefore we consider two different models for the temperature dependence of $\Theta/\Theta_{\mathrm{rig}}$. First we assume a linear increase of the MOI which stops right at T_c. Very similar behavior of $\Theta/\Theta_{\mathrm{rig}}$ is expected for a gas in the BCS phase [Far00, Urb03]; see inset of Fig. 7.3. The corresponding fit function is shown as the solid line. The star marks the critical temperature of $T_i/T_F = 0.195(14)$, where the main contribution for the uncertainty stems from the temperature measurement. Converting this temperature valid for the noninteracting gas to the actual temperature in the unitarity limit leads to $0.245\,T_F$ following the theory from Ref. [Che05a] and $0.20\,T_F$ using the conversion given in Ref. [Luo09]. The obtained value for T_c is close to previous experimental results [Reg04, Kin05b, Luo07, Ina08] and theory predictions [Gio08, Hau08]. Second we assume that $\Theta/\Theta_{\mathrm{rig}}$ approaches one very slowly as it is the case for a ideal Bose gas [Str96b]; see inset of Fig. 7.3. If this is the case it is not possible to determine T_c without the exact knowledge on how the MOI behaves as function of the temperature. In this case the value for T_c determined above serves as a lower limit.

In conclusion we showed quenching of the moment of inertia of a strongly interacting Fermi gas, which is a direct consequence of superfluidity. Furthermore we determined T_c from the point where the moment of inertia reaches its classical value.

We acknowledge support by the Austrian Science Fund (FWF) within SFB 15 (project part 21) and SFB 40 (project part 4).

CHAPTER 8

Outlook

Second sound

An interesting dynamic effect in a superfluid gas is the appearance of second sound [Lan41, Kha65]. Second sound is theoretically predicted by the two-fluid hydrodynamic equations, first derived by Landau. In contrast to a density wave, second sound shows up as a temperature modulation of a gas containing both a superfluid and normal part. In superfluid ^{4}He Peshkov was the first to excite and measure the speed of second sound by producing a local heat pulse [Pes46]. A first experiment that studied second sound in ultracold gases has been performed in a dilute Bose gas [SK98]. The rather weak interactions in such a system makes a systematic investigation of second sound rather difficult. In particular hydrodynamic behavior of the normal part of the gas and sufficiently strong interactions between the superfluid and normal part cannot be achieved easily. In a strongly interacting gas both of these conditions are naturally satisfied making it an ideal candidate to investigate second sound. Nevertheless the excitation and detection of second sound in an ultracold gas is a challenging task. In a recent article [Tay09] the coupling between collective modes and entropy oscillations was studied theoretically revealing a promising way of exciting and detecting second sound.

Interference between molecular condensates

A striking property of a superfluid quantum gas is the existence of a macroscopic wavefunction. In dilute atomic quantum gases coherence and the existence of a macroscopic wavefunction can be demonstrated by directly interfering two condensates [And97]. In a recent experiment we demonstrate coherence of a molecular BEC by observing interference fringes when overlapping two condensates. Therefore we load the gas into a double well potential which is created by our acousto-optical modulation system. The interference fringes are detected when the two condensates overlap after release from the double well potential, see Fig. 8.1. This experiment is a first step towards the investigation of matter wave coherence in a strongly interacting Fermi gas. Furthermore the possibility

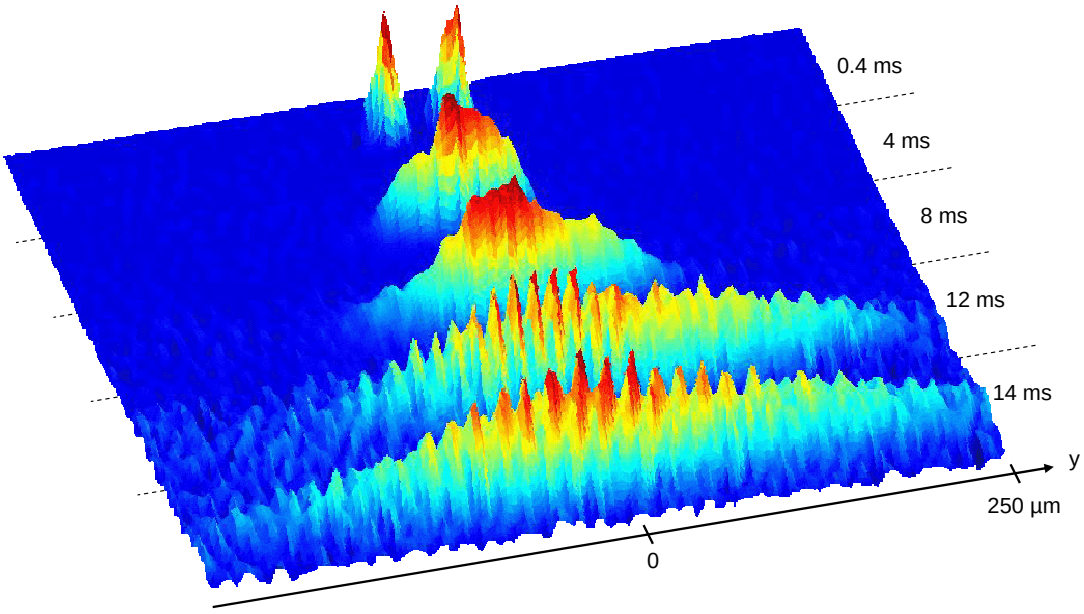

Fig. 8.1: The Figure shows the expansion of two separated molecular Bose-Einstein condensates ($B = 700$ G) after release from a double well potential. During the expansion the two condensates overlap and thereby develop interference fringes. The expansion time is indicated on the right. The anisotropic shape of the cloud mainly results from a magnetic potential that is present during the expansion.

to determine the relative phase between two separated condensates is important in future experiments which study the Josephson effect in the BEC-BCS crossover regime [Spu07, Sal09].

BIBLIOGRAPHY

[Abe66] W. R. Abel, A. C. Anderson, and J. C. Wheatley, *Propagation of Zero Sound in Liquid He3 at Low Temperatures*, Phys. Rev. Lett. **17**, 74 (1966).

[Alt06] A. Altmeyer, S. Riedl, C. Kohstall, M. Wright, J. Hecker Denschlag, and R. Grimm, *Note on "Collecitive Excitations of a Degenerate gas at the BEC-BCS Crossover",Phys. Rev. Lett. 92, 203201 (2004)*, cond-mat/0611285 (2006).

[Alt07a] A. Altmeyer, *Collective oscillations of an ultracold quantum gas in the BEC-BCS crossover regime*, Ph.D. thesis, Innsbruck University (2007).

[Alt07b] A. Altmeyer, S. Riedl, C. Kohstall, M. J. Wright, R. Geursen, M. Bartenstein, C. Chin, J. Hecker Denschlag, and R. Grimm, *Precision Measurements of Collective Oscillations in the BEC-BCS Crossover*, Phys. Rev. Lett. **98**, 040401 (2007).

[Alt07c] A. Altmeyer, S. Riedl, M. J. Wright, C. Kohstall, J. Hecker Denschlag, and R. Grimm, *Dynamics of a strongly interacting Fermi gas: The radial quadrupole mode*, Phys. Rev. A **76**, 033610 (2007).

[And97] M. R. Andrews, C. G. Townsend, H.-J. Miesner, D. S. Durfee, D. M. Kurn, and W. Ketterle, *Observation of Interference Between Two Bose Condensates*, Science **275**, 637 (1997).

[AS02] J. R. Abo-Shaeer, C. Raman, and W. Ketterle, *Formation and Decay of Vortex Lattices in Bose-Einstein Condensates at Finite Temperatures*, Phys. Rev. Lett. **88**, 070409 (2002).

[Ast04] G. E. Astrakharchik, J. Boronat, J. Casulleras, and S. Giorgini, *Equation of State of a Fermi Gas in the BEC-BCS crossover: A Quantum Monte Carlo Study*, Phys. Rev. Lett. **93**, 200404 (2004).

[Ast05] G. E. Astrakharchik, R. Combescot, X. Leyronas, and S. Stringari, *Equation of State and Collective Frequencies of a Trapped Fermi Gas Along the BEC-Unitarity Crossover*, Phys. Rev. Lett. **95**, 030404 (2005).

[Bar57a] J. Bardeen, L. N. Cooper, and J. R. Schrieffer, *Microscopic Theory of Superconductivity*, Phys. Rev. **106**, 162 (1957).

[Bar57b] J. Bardeen, L. N. Cooper, and J. R. Schrieffer, *Theory of Superconductivity*, Phys. Rev. **108**, 1175 (1957).

[Bar04a] M. Bartenstein, A. Altmeyer, S. Riedl, S. Jochim, C. Chin, J. Hecker Denschlag, and R. Grimm, *Collective Excitations of a Degenerate Gas at the BEC-BCS Crossover*, Phys. Rev. Lett. **92**, 203201 (2004).

[Bar04b] M. Bartenstein, A. Altmeyer, S. Riedl, S. Jochim, C. Chin, J. Hecker Denschlag, and R. Grimm, *Crossover from a Molecular Bose-Einstein Condensate to a Degenerate Fermi Gas*, Phys. Rev. Lett. **92**, 120401 (2004).

[Bar05a] M. Bartenstein, *From Molecules to Cooper Pairs: Experiments in the BEC-BCS Crossover*, Ph.D. thesis, Innsbruck University (2005).

[Bar05b] M. Bartenstein, A. Altmeyer, S. Riedl, R. Geursen, S. Jochim, C. Chin, J. Hecker Denschlag, R. Grimm, A. Simoni, E. Tiesinga, C. J. Williams, and P. S. Julienne, *Precise determination of ^{6}Li cold collision parameters by radio-frequency spectroscopy on weakly bound molecules*, Phys. Rev. Lett. **94**, 103201 (2005).

[Bou03] T. Bourdel, J. Cubizolles, L. Khaykovich, K. M. F. Magalhães, S. J. J. M. F. Kokkelmans, G. V. Shlyapnikov, and C. Salomon, *Measurement of the Interaction Energy near a Feshbach Resonance in a ^{6}Li Fermi Gas*, Phys. Rev. Lett. **91**, 020402 (2003).

[Bou04] T. Bourdel, L. Khaykovich, J. Cubizolles, J. Zhang, F. Chevy, M. Teichmann, L. Tarruell, S. J. J. M. F. Kokkelmans, and C. Salomon, *Experimental Study of the BEC-BCS Crossover Region in Lithium 6*, Phys. Rev. Lett. **93**, 050401 (2004).

[Bre03] V. Bretin, P. Rosenbusch, F. Chevy, G. V. Shlyapnikov, and J. Dalibard, *Quadrupole Oscillation of a Single-Vortex Bose-Einstein Condensate: Evidence for Kelvin Modes*, Phys. Rev. Lett. **90**, 100403 (2003).

[Bru00] G. M. Bruun and C. W. Clark, *Ideal gases in time-dependent traps*, Phys. Rev. A **61**, 061601 (2000).

[Bru05] G. M. Bruun and H. Smith, *Viscosity and thermal relaxation for a resonantly interacting Fermi gas*, Phys. Rev. A **72**, 043605 (2005).

[Bru07] G. M. Bruun and H. Smith, *Frequency and damping of the scissors mode of a Fermi gas*, Phys. Rev. A **76**, 045602 (2007).

[Bug05] C. Buggle, P. Pedri, W. von Klitzing, and J. T. M. Walraven, *Shape oscillations in nondegenerate Bose gases: Transition from the collisionless to the hydrodynamic regime*, Phys. Rev. A **72**, 043610 (2005).

[Bul05] A. Bulgac and G. F. Bertsch, *Collective Oscillations of a Trapped Fermi Gas near the Unitary Limit*, Phys. Rev. Lett. **94**, 070401 (2005).

[Che00] F. Chevy, K. M. Madison, and J. Dalibard, *Measurement of the Angular Momentum of a Rotating Bose-Einstein Condensate*, Phys. Rev. Lett. **85**, 2223 (2000).

[Che02] F. Chevy, V. Bretin, P. Rosenbusch, K. W. Madison, and J. Dalibard, *Transverse Breathing Mode of an Elongated Bose-Einstein Condensate*, Phys. Rev. Lett. **88**, 250402 (2002).

[Che03] F. Chevy and S. Stringari, *Kelvin modes of a fast rotating Bose-Einstein condensate*, Phys. Rev. A **68**, 053601 (2003).

[Che05a] Q. Chen, J. Stajic, and K. Levin, *Thermodynamics of Interacting Fermions in Atomic Traps*, Phys. Rev. Lett. **95** (2005).

[Che05b] Q. Chen, J. Stajic, S. Tan, and K. Levin, *BCS-BEC Crossover: From High Temperature Superconductors to Ultracold Superfluids*, Phys. Rep. **412**, 1 (2005).

[Che06] Q. Chen, C. A. Regal, D. S. Jin, and K. Levin, *Finite-temperature momentum distribution of a trapped Fermi gas*, Phys. Rev. A **74**, 011601 (2006).

[Chi04] C. Chin, M. Bartenstein, A. Altmeyer, S. Riedl, S. Jochim, J. Hecker Denschlag, and R. Grimm, *Observation of the Pairing Gap in a Strongly Interacting Fermi Gas*, Science **305**, 1128 (2004).

[Chi08] C. Chin, R. Grimm, P. Julienne, and E. Tiesinga (2008), submitted to Rev. Mod. Phys., arXiv:0812.1496.

[Cla07] B. Clancy, L. Luo, and J. E. Thomas, *Observation of Nearly Perfect Irrotational Flow in Normal and Superfluid Strongly Interacting Fermi Gases*, Phys. Rev. Lett. **99**, 140401 (2007).

[Com04] R. Combescot and X. Leyronas, *Comment on "Collective Excitations of a Degenerate Gas at the BEC-BCS Crossover"*, Phys. Rev. Lett. **93** (2004).

[Com06] R. Combescot, M. Y. Kagan, and S. Stringari, *Collective mode of homogeneous superfluid Fermi gases in the BEC-BCS crossover*, Phys. Rev. A **74** (2006).

[Coo56] L. N. Cooper, *Bound Electron Pairs in a Degenerate Fermi Gas*, Phys. Rev. **104**, 1189 (1956).

[Cub03] J. Cubizolles, T. Bourdel, S. J. J. M. F. Kokkelmans, G. V. Shlyapnikov, and C. Salomon, *Production of Long-Lived Ultracold Li_2 Molecules from a Fermi Gas*, Phys. Rev. Lett. **91**, 240401 (2003).

[Dod97] R. J. Dodd, K. Burnett, M. Edwards, and C. Clark, *Excitation spectroscopy of vortex states in dilute Bose-Einstein condensed gases*, Phys. Rev. A **56**, 587 (1997).

[Eag69] D. M. Eagles, *Possible pairing without superconductivity at low carrier concentrations in bulk and thin-film superconducting semiconductors*, Phys. Rev. **186**, 456 (1969).

[Eng97] J. R. Engelbrecht, M. Randeria, and C. A. R. Sá de Melo, *BCS to Bose Crossover: Broken-Symmetry State*, Phys. Rev. B **55**, 15153 (1997).

[Far00] M. Farine, P. Schuck, and X. Viñas, *Moment of inertia of a trapped superfluid gas of atomic fermions*, Phys. Rev. A **62**, 013608 (2000).

[Fri01] N. Friedman, A. Kaplan, D. Carasso, and N. Davidson, *Observation of Chaotic and Regular Dynamics in Atom-Optics Billiards*, Phys. Rev. Lett. **86**, 1518 (2001).

[Gen01] S. D. Gensemer and D. S. Jin, *Transition from Collisionless to Hydrodynamic Behavior in an Ultracold Fermi Gas*, Phys. Rev. Lett. **87**, 173201 (2001).

[Gio00] S. Giorgini, *Collisionless dynamics of dilute Bose gases: Role of quantum and thermal fluctuations*, Phys. Rev. A **61**, 063615 (2000).

[Gio08] S. Giorgini, L. P. Pitaevskii, and S. Stringari, *Theory of ultracold atomic Fermi gases*, Rev. Mod. Phys. **80**, 1215 (2008).

[GO99a] D. Guéry-Odelin and S. Stringari, *Scissors Mode and Superfluidity of a Trapped Bose-Einstein Condensed Gas*, Phys. Rev. Lett. **83**, 4452 (1999).

[GO99b] D. Guéry-Odelin, F. Zambelli, J. Dalibard, and S. Stringari, *Collective oscillations of a classical gas confined in harmonic traps*, Phys. Rev. A **60**, 4851 (1999).

[GO00] D. Guèry-Odelin, *Spinning up and down a Boltzmann gas*, Phys. Rev. A **62**, 033607 (2000).

[Gre03] M. Greiner, C. A. Regal, and D. S. Jin, *Emergence of a Molecular Bose-Einstein Condensate from a Fermi Gas*, Nature **426**, 537 (2003).

[Gre05] M. Greiner, C. A. Regal, and D. S. Jin, *Probing the Excitation Spectrum of a Fermi Gas in the BCS-BEC Crossover Regime*, Phys. Rev. Lett. **94**, 070403 (2005).

[Hal01a] P. C. Haljan, B. P. Anderson, I. Coddington, and E. A. Cornell, *Use of Surface-Wave Spectroscopy to Characterize Tilt Modes of a Vortex in a Bose-Einstein Condensate*, Phys. Rev. Lett. **86**, 2922 (2001).

[Hal01b] P. C. Haljan, I. Coddington, P. Engels, and E. A. Cornell, *Driving Bose-Einstein-Condensate Vorticity with a Rotating Normal Cloud*, Phys. Rev. Lett. **87**, 210403 (2001).

[Hau08] R. Haussmann and W. Zwerger, *Thermodynamics of a trapped unitary Fermi gas*, Phys. Rev. A **78**, 063602 (2008).

[Hei04] H. Heiselberg, *Collective Modes of Trapped Gases at the BEC-BCS Crossover*, Phys. Rev. Lett. **93**, 040402 (2004).

[Hen03] G. Hendl, *Atom - Atom Wechselwirkung in einem ultrakalten, fermionischen Gas*, Ph.D. thesis, Innsbruck University (2003).

[Hes67] G. B. Hess and W. M. Fairbank, *Measurements of Angular Momentum in Superfluid Helium*, Phys. Rev. Lett. **19**, 216 (1967).

[Hod02] E. Hodby, G. Hechenblaikner, S. A. Hopkins, O. M. Maragò, and C. J. Foot, *Vortex Nucleation in Bose-Einstein Condensates in an Oblate, Purely Magnetic Potential*, Phys. Rev. Lett. **88**, 010405 (2002).

[Hou98] M. Houbiers, H. T. C. Stoof, W. I. McAlexander, and R. G. Hulet, *Elastic and inelastic collisions of ^6Li atoms in magnetic and optical traps*, Phys. Rev. A **57**, R1497 (1998).

[Hu04] H. Hu, A. Minguzzi, X.-J. Liu, and M. P. Tosi, *Collective Modes and Ballistic Expansion of a Fermi Gas in the BCS-BEC Crossover*, Phys. Rev. Lett. **93**, 190403 (2004).

[Hua87] K. Huang (Ed.), *Statistical Mechanics*, John Wiley & Sons, New York, 1987, page 104.

[Huc09] J. H. Huckans, J. R. Williams, E. L. Hazlett, R. W. Stites, and K. M. O'Hara, *Three-Body Recombination in a Three-State Fermi Gas with Widely Tunable Interactions*, Phys. Rev. Lett. **102**, 165302 (2009).

[Ina08] Y. Inada, M. Horikoshi, S. Nakajima, M. Kuwata-Gonokami, M. Ueda, and T. Mukaiyama, *Critical Temperature and Condensate Fraction of a Fermion Pair Condensate*, Phys. Rev. Lett. **101**, 180406 (2008).

[Ing08] M. Inguscio, W. Ketterle, and C. Salomon (Eds.), *Ultracold Fermi Gases*, IOS Press, Amsterdam, 2008, Proceedings of the International School of Physics "Enrico Fermi", Course CLXIV, Varenna, 20-30 June 2006.

[Jin96] D. S. Jin, J. R. Ensher, M. R. Matthews, C. E. Wieman, and E. A. Cornell, *Collective Excitations of a Bose-Einstein Condensate in a Dilute Gas*, Phys. Rev. Lett. **77**, 420 (1996).

[Jin97] D. S. Jin, M. R. Matthews, J. R. Ensher, C. E. Wieman, and E. A. Cornell, *Temperature-Dependent Damping and Frequency Shifts in Collective Excitations of a Dilute Bose-Einstein Condensate*, Phys. Rev. Lett. **78**, 764 (1997).

[Joc03a] S. Jochim, M. Bartenstein, A. Altmeyer, G. Hendl, S. Riedl, C. Chin, J. Hecker Denschlag, and R. Grimm, *Bose-Einstein Condensation of Molecules*, Science **302**, 2101 (2003).

[Joc03b] S. Jochim, M. Bartenstein, A. Altmeyer, G. Hendl, C. Chin, J. Hecker Denschlag, and R. Grimm, *Pure Gas of Optically Trapped Molecules Created from Fermionic Atoms*, Phys. Rev. Lett **91**, 240402 (2003).

[Joc04] S. Jochim, *Bose-Einstein Condensation of Molecules*, Ph.D. thesis, Innsbruck University (2004).

[Jos07] J. Joseph, B. Clancy, L. Luo, J. Kinast, A. Turlapov, and J. E. Thomas, *Measurement of Sound Velocity in a Fermi Gas near a Feshbach Resonance*, Phys. Rev. Lett. **98**, 170401 (2007).

[Kha65] I. Khalatnikov, *An Introdcution to the Theory of Superfluidity*, Westview Press, 1965.

[Kim04a] E. Kim and M. H. W. Chan, *Observation of Superflow in Solid Helium*, Science **305**, 1941 (2004).

[Kim04b] Y. E. Kim and A. L. Zubarev, *Time-dependent density-functional theory for trapped strongly interacting fermionic atoms*, Phys. Rev. A **70**, 033612 (2004).

[Kin04a] J. Kinast, S. L. Hemmer, M. E. Gehm, A. Turlapov, and J. E. Thomas, *Evidence for Superfluidity in a Resonantly Interacting Fermi Gas*, Phys. Rev. Lett. **92**, 150402 (2004).

[Kin04b] J. Kinast, A. Turlapov, and J. E. Thomas, *Breakdown of Hydrodynamics in the Radial Breathing Mode of a Strongly Interacting Fermi Gas*, Phys. Rev. A **70**, 051401(R) (2004).

[Kin05a] J. Kinast, A. Turlapov, and J. E. Thomas, *Damping of a Unitary Fermi Gas*, Phys. Rev. Lett. **94**, 170404 (2005).

[Kin05b] J. Kinast, A. Turlapov, J. E. Thomas, Q. Chen, J. Stajic, and K. Levin, *Heat Capacity of a Strongly Interacting Fermi Gas*, Science **307**, 1296 (2005).

[Kin06] J. Kinast, *Thermodynamics and Superfluidity of a Strongly Interacting Fermi Gas*, Ph.D. thesis, Duke University (2006).

[Koh07] C. Kohstall, *A New Toolbox for Experiments with Ultracold Li6*, Ph.D. thesis, Innsbruck University (2007).

[Lan41] L. Landau, *Theory of superfluidity of He II*, J. Phys. U.S.S.R **5**, 71 (1941).

[Lea02] A. E. Leanhardt, A. Görlitz, A. P. Chikkatur, D. Kielpinski, Y. Shin, D. E. Pritchard, and W. Ketterle, *Imprinting Vortices in a Bose-Einstein Condensate using Topological Phases*, Phys. Rev. Lett. **89**, 190403 (2002).

[Lee57a] T. D. Lee, K. Huang, and C. N. Yang, *Eigenvalues and Eigenfunctions of a Bose System of Hard Spheres and its Low-Temperature Properties*, Phys. Rev. **106**, 1135 (1957).

[Lee57b] T. D. Lee and C. N. Yang, *Many-Body Problem in Quantum Mechanics and Quantum Statistical Mechanics*, Phys. Rev. **105**, 1119 (1957).

[Leg80] A. J. Leggett, in: A. Pekalski and R. Przystawa (Eds.), *Modern Trends in the Theory of Condensed Matter*, vol. 115 of *Lecture Notes in Physics*, 13, Springer Verlag, Berlin, 1980.

[Luo07] L. Luo, B. Clancy, J. Joseph, J. Kinast, and J. E. Thomas, *Measurement of the Entropy and Critical Temperature of a Strongly Interacting Fermi Gas*, Phys. Rev. Lett. **98**, 080402 (2007).

[Luo09] L. Luo and J. E. Thomas, *Thermodynamic Measurements in a Strongly Interacting Fermi Gas*, J. Low Temp. Phys. **154**, 1 (2009).

[Mad00] K. W. Madison, F. Chevy, W. Wohlleben, and J. Dalibard, *Vortex Formation in a Stirred Bose-Einstein Condensate*, Phys. Rev. Lett. **84**, 806 (2000).

[Mad01] K. W. Madison, F. Chevy, V. Bretin, and J. Dalibard, *Stationary States of a Rotating Bose-Einstein Condensate: Routes to Vortex Nucleation*, Phys. Rev. Lett. **86**, 4443 (2001).

[Man05] N. Manini and L. Salasnich, *Bulk and Collective Properties of a Dilute Fermi Gas in the BCS-BEC crossover*, Phys. Rev. A **71**, 033625 (2005).

[Mar00] O. M. Maragò, S. A. Hopkins, J. Arlt, E. Hodby, G. Hechenblaikner, and C. J. Foot, *Observation of the Scissors Mode and Evidence for Superfluidity of a Trapped Bose-Einstein Condensed Gas*, Phys. Rev. Lett. **84**, 2056 (2000).

[Mar01] O. Maragò, G. Hechenblaikner, E. Hodby, and C. Foot, *Temperature Dependence of Damping and Frequency Shifts of the Scissors Mode of a Trapped Bose-Einstein Condensate*, Phys. Rev. Lett. **86**, 3938 (2001).

[Mas05] P. Massignan, G. M. Bruun, and H. Smith, *Viscous relaxation and collective oscillations in a trapped Fermi gas near the unitarity limit*, Phys. Rev. A **71**, 033607 (2005).

[Men02] C. Menotti, P. Pedri, and S. Stringari, *Expansion of an Interacting Fermi Gas*, Phys. Rev. Lett. **89**, 250402 (2002).

[Mew96] M.-O. Mewes, M. R. Andrews, N. J. van Druten, D. M. Kurn, D. S. Durfee, C. G. Townsend, and W. Ketterle, *Collective Excitations of a Bose-Einstein Condensate in a Magnetic Trap*, Phys. Rev. Lett. **77**, 988 (1996).

[Mil01] V. Milner, J. L. Hanssen, W. C. Campbell, and M. G. Raizen, *Optical Billiards for Atoms*, Phys. Rev. Lett. **86**, 1514 (2001).

[Mil07] D. E. Miller, J. K. Chin, C. A. Stan, Y. Liu, W. Setiawan, C. Sanner, and W. Ketterle, *Critical Velocity for Superfluid Flow across the BEC-BCS Crossover*, Phys. Rev. Lett. **99** (2007).

[Min01] A. Minguzzi and M. P. Tosi, *Scissors mode in a superfluid Fermi gas*, Phys. Rev. A **63**, 023609 (2001).

[Mod03] M. Modugno, G. Modugno, G. Roati, C. Fort, and M. Inguscio, *Scissors mode of an expanding Bose-Einstein condensate*, Phys. Rev. A **67** (2003).

[Noz85] P. Nozières and S. Schmitt-Rink, J. Low Temp. Phys. **59**, 195 (1985).

[O'H02] K. M. O'Hara, S. L. Hemmer, M. E. Gehm, S. R. Granade, and J. E. Thomas, *Observation of a Strongly Interacting Degenerate Fermi Gas*, Science **298**, 2179 (2002).

[Ono00] R. Onofrio, D. S. Durfee, C. Raman, M. Köhl, C. E. Kuklewicz, and W. Ketterle, *Surface Excitations of a Bose-Einstein Condensate*, Phys. Rev. Lett. **84**, 810 (2000).

[Ott08] T. B. Ottenstein, T. Lompe, M. Kohnen, A. N. Wenz, and S. Jochim, *Collisional Stability of a Three-Component Degenerate Fermi Gas*, Phys. Rev. Lett. **101**, 203202 (2008).

[Par05] G. B. Partridge, K. E. Strecker, R. I. Kamar, M. W. Jack, and R. G. Hulet, *Molecular Probe of Pairing in the BEC-BCS Crossover*, Phys. Rev. Lett. **95**, 020404 (2005).

[Par06a] G. B. Partridge, W. Li, R. I. Kamar, Y. Liao, and R. G. Hulet, *Pairing and Phase Separation in a Polarized Fermi Gas*, Science **311**, 503 (2006).

[Par06b] G. B. Partridge, W. Li, Y. A. Liao, R. G. Hulet, M. Haque, and H. T. C. Stoof, *Deformation of a Trapped Fermi Gas with Unequal Spin Populations*, Phys. Rev. Lett. **97**, 190407 (2006).

[Ped03] P. Pedri, D. Guéry-Odelin, and S. Stringari, *Dynamics of a classical gas including dissipative and mean-field effects*, Phys. Rev. A **68**, 043608 (2003).

[Per04] A. Perali, P. Pieri, L. Pisani, and G. C. Strinati, *BCS-BEC Crossover at Finite Temperature for Superfluid Trapped Fermi Atoms*, Phys. Rev. Lett. **92** (2004).

[Pes46] V. P. Peshkov, *Determination of the velocity of propagation of the second sound in helium II*, J. Phys. U.S.S.R **10**, 389 (1946).

[Pie05] P. Pieri, L. Pisani, and G. C. Strinati, *Comparison between a diagrammatic theory for the BCS-BEC crossover and quantum Monte Carlo results*, Phys. Rev. B **72**, 012506 (2005).

[Pit98] L. Pitaevskii and S. Stringari, *Elementary Excitations in Trapped Bose-Einstein Condensed Gases Beyond the Mean-Field Approximation*, Phys. Rev. Lett. **81**, 4541 (1998).

[Reg04] C. A. Regal, M. Greiner, and D. S. Jin, *Observation of Resonance Condensation of Fermionic Atom Pairs*, Phys. Rev. Lett. **92**, 040403 (2004).

[Reg05] C. A. Regal, M. Greiner, S. Giorgini, M. Holland, and D. S. Jin, *Momentum Distribution of a Fermi Gas of Atoms in the BCS-BEC Crossover*, Phys. Rev. Lett. **95**, 250404 (2005).

[Rie04] S. Riedl, *Untersuchung stark wechselwirkender fermionischer Quantengase mittels Absorptionsabbildung*, Ph.D. thesis, Innsbruck University (2004).

[Rie08] S. Riedl, E. R. Sánchez Guajardo, C. Kohstall, A. Altmeyer, M. J. Wright, J. Hecker Denschlag, R. Grimm, G. M. Bruun, and H. Smith, *Collective oscillations of a Fermi gas in the unitarity limit: Temperature effects and the role of pair correlations*, Phys. Rev. A **78**, 053609 (2008).

[Rie09] S. Riedl, E. R. Sánchez Guajardo, C. Kohstall, J. Hecker Denschlag, and R. Grimm, *Lifetime of angular momentum in a rotating strongly interacting Fermi gas*, Phys. Rev. A **79**, 053628 (2009).

[Rin80] P. Ring and P. Schuck, *The Nuclear Many Body Problem*, Springer, Berlin, 1980.

[Sal09] L. Salasnich, F. Ancilotto, N. Manini, and F. Toigo, *DC and AC Josephson effects with superfluid Fermi atoms across a Feshbach resonance*, Laser Phys. **19**, 636 (2009).

[Sch07a] C. H. Schunck, Y. Shin, A. Schirotzek, M. W. Zwierlein, and W. Ketterle, *Pairing Without Superfluidity: The Ground State of an Imbalanced Fermi Mixture*, Science **316**, 867 (2007).

[Sch07b] C. H. Schunck, M. W. Zwierlein, A. Schirotzek, and W. Ketterle, *Superfluid Expansion of a Rotating Fermi Gas*, Phys. Rev. Lett. **98**, 050404 (2007).

[Sch08a] A. Schirotzek, Y. Shin, C. H. Schunck, and W. Ketterle, *Determination of the Superfluid Gap in Atomic Fermi Gases by Quasiparticle Spectroscopy*, Phys. Rev. Lett. **101**, 140403 (2008).

[Sch08b] C. H. Schunck, Y. Shin, A. Schirotzek, and W. Ketterle, *Determination of the fermion pair size in a resonantly interacting superfluid*, Nature **454**, 739 (2008).

[Shi06] Y. Shin, M. W. Zwierlein, C. H. Schunck, A. Schirotzek, and W. Ketterle, *Observation of Phase Separation in a Strongly Interacting Imbalanced Fermi Gas*, Phys. Rev. Lett. **97** (2006).

[Shi07] Y. Shin, C. H. Schunck, A. Schirotzek, and W. Ketterle, *Tomographic rf Spectroscopy of a Trapped Fermi Gas at Unitarity*, Phys. Rev. Lett. **99**, 090403 (2007).

[Shi08a] Y. Shin, *Determination of the equation of state of a polarized Fermi gas at unitarity*, Phy. Rev. A **77**, 041603 (2008).

[Shi08b] Y. Shin, C. H. Schunck, A. Schirotzek, and W. Ketterle, *Phase diagram of a two-component Fermi gas with resonant interactions*, Nature **451**, 689 (2008).

[Sin97] S. Sinha, *Semiclassical analysis of collective excitations in Bose-Einstein condensate*, Phys. Rev. A **55**, 4325 (1997).

[SK98] D. M. Stamper-Kurn, H.-J. Miesner, S. Inouye, M. R. Andrews, and W. Ketterle, *Collisionless and Hydrodynamic Excitations of a Bose-Einstein Condensate*, Phys. Rev. Lett. **81**, 500 (1998).

[Spu07] A. Spuntarelli, P. Pieri, and G. C. Strinati, *Josephson Effect throughout the BCS-BEC Crossover*, Phys. Rev. Lett. **99**, 040401 (2007).

[Sta05] J. Stajic, Q. Chen, and K. Levin, *Density Profiles of Strongly Interacting Trapped Fermi Gases*, Phys. Rev. Lett. **94** (2005).

[Ste06] J. T. Stewart, J. P. Gaebler, C. A. Regal, and D. S. Jin, *Potential Energy of a [sup 40]K Fermi Gas in the BCS-BEC Crossover*, Phys. Rev. Lett. **97** (2006).

[Ste08] J. T. Stewart, J. P. Gaebler, and D. S. Jin, *Using photoemission spectroscopy to probe a strongly interacting Fermi gas*, Nature **454**, 744 (2008).

[Str] S. Stringari, private communication.

[Str96a] S. Stringari, *Collective Excitations of a Trapped Bose-Condensed Gas*, Phys. Rev. Lett. **77**, 2360 (1996).

[Str96b] S. Stringari, *Moment of Inertia and Superfluidity of a Trapped Bose Gas*, Phys. Rev. Lett. **76**, 1405 (1996).

[Str04] S. Stringari, *Collective Oscillations of a Trapped Superfluid Fermi Gas near a Feshbach Resonance*, Europhys. Lett. **65**, 749 (2004).

[Svi98] A. A. Svidzinsky and A. L. Fetter, *Normal modes of a vortex in a trapped Bose-Einstein condensate*, Phys. Rev. A **58**, 3168 (1998).

[Tay09] E. Taylor, H. Hu, X.-J. Liu, L. P. Pitaevskii, A. Griffin, and S. Stringari, *Hybridization and excitation of second sound in a trapped Fermi gas at unitarity* (2009), arXiv:0905.0257.

[Urb03] M. Urban and P. Schuck, *Slow rotation of a superfluid trapped Fermi gas*, Phys. Rev. A **67**, 033611 (2003).

[Urb07] M. Urban, *Coupling of hydrodynamics and quasiparticle motion in collective modes of superfluid trapped Fermi gases*, Phys. Rev. A **75**, 053607 (2007).

[Vara] R. Grimm, in [Ing08]; cond-mat/0703091.

[Varb] S. Stringari, in [Ing08]; cond-mat/0702526.

[Vee08] G. Veeravalli, E. Kuhnle, P. Dyke, and C. J. Vale, *Bragg Spectroscopy of a Strongly Interacting Fermi Gas*, Phys. Rev. Lett. **101**, 250403 (2008).

[Vic00] L. Vichi, *Collisional Damping of the Collective Oscillations of a Trapped Fermi Gas*, J. Low. Temp. Phys. **121**, 177 (2000).

[Wil02] J. E. Williams, E. Zaremba, B. Jackson, T. Nikuni, and A. Griffin, *Dynamical Instability of a Condensate Induced by a Rotating Thermal Gas*, Phys. Rev. Lett. **88**, 070401 (2002).

[Wri07] M. J. Wright, S. Riedl, A. Altmeyer, C. Kohstall, E. R. S. Guajardo, J. H. Denschlag, and R. Grimm, *Finite-Temperature Collective Dynamics of a Fermi Gas in the BEC-BCS Crossover*, Phys. Rev. Lett. **99** (2007).

[Zam98] F. Zambelli and S. Stringari, *Quantized Vortices and Collective Oscillations of a Trapped Bose-Einstein Condensate*, Phys. Rev. Lett. **81**, 1754 (1998).

[Zhu01] O. N. Zhuravlev, A. E. Muryshev, and P. O. Fedichev, *Dissipative dynamics of vortex arrays in anisotropic traps*, Phys. Rev. A **64**, 053601 (2001).

[Zwi03] M. W. Zwierlein, C. A. Stan, C. H. Schunck, S. M. F. Raupach, S. Gupta, Z. Hadzibabic, and W. Ketterle, *Observation of Bose-Einstein Condensation of Molecules*, Phys. Rev. Lett. **91**, 250401 (2003).

[Zwi04] M. W. Zwierlein, C. A. Stan, C. H. Schunck, S. M. F. Raupach, A. J. Kerman, and W. Ketterle, *Condensation of Pairs of Fermionic Atoms near a Feshbach Resonance*, Phys. Rev. Lett. **92**, 120403 (2004).

[Zwi05a] M. W. Zwierlein, J. R. Abo-Shaeer, A. Schirotzek, C. H. Schunck, and W. Ketterle, *Vortices and Superfluidity in a Strongly Interacting Fermi Gas*, Nature **435**, 1047 (2005).

[Zwi05b] M. W. Zwierlein, C. H. Schunck, C. A. Stan, S. M. F. Raupach, and W. Ketterle, *Formation Dynamics of a Fermion Pair Condensate*, Phys. Rev. Lett. **94**, 180401 (2005).

[Zwi06a] M. W. Zwierlein, A. Schirotzek, C. H. Schunck, and W. Ketterle, *Direct observation of the superfluid phase transition in ultracold Fermi gases*, Nature **442**, 54 (2006).

[Zwi06b] M. W. Zwierlein, A. Schirotzek, C. H. Schunck, and W. Ketterle, *Fermionic Superfluidity with Imbalanced Spin Populations*, Science **311**, 492 (2006).

Acknowledgments

In this final chapter of my thesis I want to thank all the people I worked with and who supported me during my time as a Ph.D. student. Without my advisor Rudolf Grimm and a whole team working on the experiments the results presented in this thesis would not have been possible.

I started on the experiment already during my master thesis where I had the opportunity to work with Selim Jochim, Markus Bartenstein. They did not only build most of the apparatus, with great help of Gerhard Hendl, but together with Alexander Altmeyer, Cheng Chin, Johannes Hecker Denschlag and of course Rudi we obtained the first important experimental results. During the first years of my thesis Alexander was my lab mate and together with Reece Geursen and Matthew Wright, who joined the team for one year as postdocs, we worked hard to improve the experiment. Johannes was an advisor for our experiment. He was always available for questions and discussions on the experiments. In the second half of my time as a Ph.D. student, Christoph Kohstall and Edmundo Sánchez Guajardo joined the team. They both never stopped asking me about the experiment and from our discussions I learned a lot myself. I also want to thank all the other members of the Grimm group who shared their knowledge with me and made the group an interesting place to be. I also want to thank the non-scientific members of the institute, who helped us to keep things running.

I also thank all the people who made me leave the lab and enjoy the wonderful mountains. Together with Mattias I had a lot of fun riding up the mountains with my mountainbike, although for some reason he did not like the downhills to much (see Ph.D. thesis of Mattias Gustavsson for details). Also with Christoph I enjoyed lots of mountainbiking and skiing. Thanks for that and all the other fun things and trips we did together. Whenever Trese joined, it was truly an adventure. Thanks to her my life became even more exciting and enjoyable.

Finally I would like to thank my family. They consistently supported and encouraged me during all my studies. Thanks.